UNIVERSITY OF CRETE
DEPARTMENT OF MATERIALS SCIENCE AND TECHNOLOGY

Viscoelastic properties of supramolecular gels based on hydrogen bonding

Master's Thesis

Emmanouil Vereroudakis

Heraklion, July 2020

Acknowledgements

First of all, I'd like to thank Dimitris Vlassopoulos for all of the support that he has provided these last three years, for all that he has taught me, for all the chances that he has given me to improve and to gain new experiences, one of them being helping me get introduced to the world of computer simulations ultimately leading to my decision to follow a PhD in simulations and of course for all the helpful talks and inspiration he provided me with. I am very grateful to Bert Meijer and his post docs Rene Lafleur, Nathan Van Zee and Nicholas Matsumoto for the excellent collaboration, insightful discussions over the years and for providing the materials used in this thesis. Without their contribution this thesis would not have been possible. On the same note I'm also very grateful for getting to know and working with Emanuela Del Gado and her student Minaspi Bantawa. Both of them have taught me a lot and their contribution was crucial for this thesis. I'd also like to thank Benoit Loppinet because his door was always open even for the slightest question I had. He always patiently tried to help me learn and understand the gist of every method, every experiment, every formula, every concept we discussed. I will be eternally grateful to George Fytas for introducing me to the world of polymer physics and specifically of supramolecular polymers. By chance, during my last 6 months or so in the lab I started collaborating with George Petekidis on a completely new project regarding molecular dynamics simulations of colloidal gels. I would really like to thank him for this collaboration and for the chance I had to start simulating a system from scratch. This wouldn't really be possible if I hadn't had the great joy of visiting Christos Likos' group in Vienna where I was introduced to MD simulations by Emanuele Locatelli and Christos who both were excellent and patient teachers, as well as a short two weeks visit in Emanuela Del Gado's group being introduced to the specifics of simulating a colloidal system by her and her amazing PhD student Minaspi Bantawa.

I would also like to thank Antonis for all the advice, help and the fun we've had over the years. The same goes for Antje, both of them were always there when I needed them either for a word of advice or having a laugh. Moving on to fellow students and past members of the lab….I have to start from Danielakis who has taught me most of what I know about rheometry and was always there (and still is) whenever I needed him. Esmaeel with whom I have shared a lot of laughs and who has taught me every necessary Iranian word. Katerina R. my lunch and smoking buddy. DF and Kalaf (I could definitely write more about the star of the lab but I would need a second thesis..) who joined the lab the second year of my Master's and Katerina P. a bit later who suddenly made every day in the lab as fun as it was back in our first year of University. Captain Thanasis for his very interesting and insightful questions but even more for his…educational stories. Nikos B. for being the first friend I made when I joined the lab and for all the fun we've had ever since. Stelios ,the second guy supporting Olympiakos in the lab

so I wouldn't be alone and a great cooking buddy and food enthusiast, but most of all for always trying to push me out of my comfort zone! Consiglia for her "Kaaaaalimera" and singing that somehow made the day much better than it had started out. Christina for always tolerating my jokes and for always giving a solemn word of advice, Mohan with his always (very) honest compliments that I will always remember, Andrei with his infinite amount of jokes…

I could really go on and on, however what sticks to mind while writing these lines is that on a more personal level, I feel like these two paragraphs could be one; both of them talk about friends, and how each one, in his own way, shaped these last wonderful three years.

I'd like to thank from the bottom of my heart, my best friends, Nikos, Aspasia, Evaggelos, Vaggos and Stratos for tolerating me, when the pressure was turned up, trying to balance courses, experiments and preparing for the exams needed for my PhD application as well as for all the love they've given me throughout the years. I would have never made it this far without them.

Last but not least, I can't thank enough my mother Efi, my father Kostas and my sister Amalia, for all their support during all those years, and for how easy it was for them to make me "decompress" even in the most stressful of times. Their being there, is invaluable to me.

Table of Contents

Chapter 1. Supramolecular assemblies: associating and living polymers

1. Introduction

Secondary associations are ubiquitous in nature. They are commonly used in natural biomaterials to acquire the necessary properties for a particular function[1]. A common example is the formation of beta-sheets through van der Waals interactions and hydrogen bonding[2]. Specifically, spider silk obtains its extraordinary mechanical properties through the connectivity of these crystalline beta-sheets in the form of an amorphous macromolecular network [3–5]. These associations are also relevant for synthetic materials and have been utilized to "bequeath" them with some of the extraordinary properties found in natural biomaterials[6–8]. The different types of associations are illustrated in Figure 1.1, where the ranges of binding energies for different bonds are presented as along with the respecting probability of breaking, where associations with lower binding energies are more probable to break. There are two large categories of polymeric materials which are based on reversible associations, the associating polymers and the living polymers. Whereas sometimes there is some overlap, macromolecular assemblies exhibit distinct properties which render their grouping necessary. The following presentation focuses on understanding the main mechanisms and differences behind the dynamics and stress relaxation in associating and living polymers. The common central feature is the lifetime of associations which controls their dynamics.

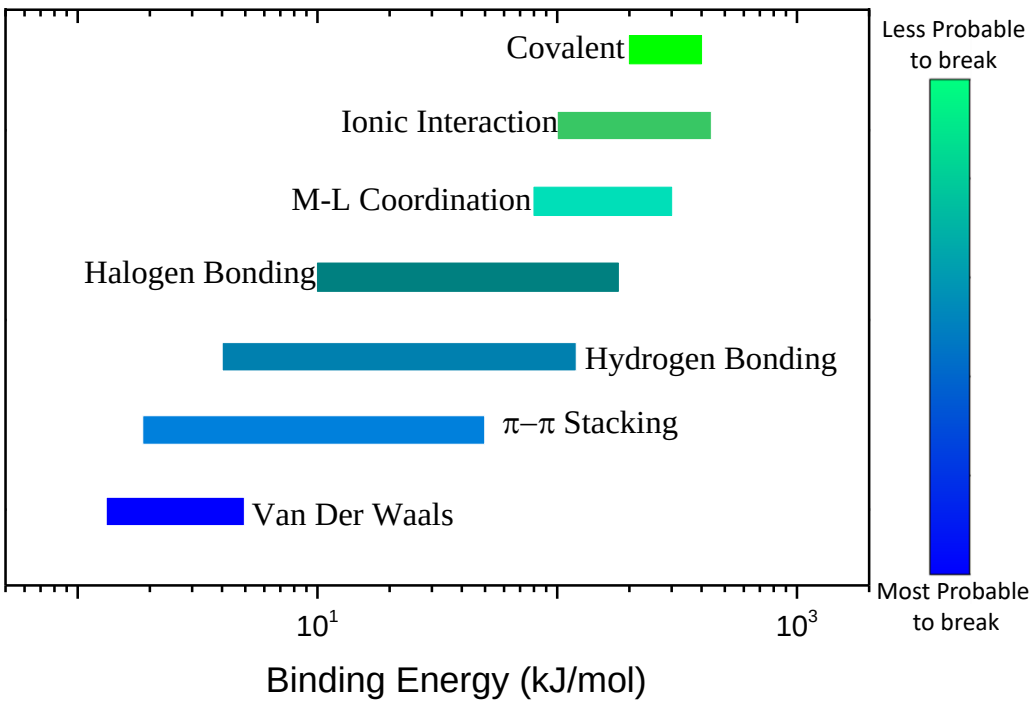

Figure 1.1. Binding energy ranges of different types of secondary interactions, in kJ/mol (about 0.4 kT at room temperature). The color bar represents the probability of a bond breaking spontaneously due to thermal fluctuations. Adapted from Mendes et al.[1]

Associating polymers tend to have sites for reversible bonding perpendicular to the main backbone (Figure 1.2), while along the backbone they possess covalent links[9]. Often they tend to aggregate and form supramolecular networks and their properties have been studied extensively, with main representatives being polyelectrolytes and ionomers[10–12] as well as linear or branched polymers linked through metal-ligand coordination[13,14] , hydrogen bonding units[15] , solvophobic interactions[16,17] leading to possible local associations or weaker π-π links[18,19]. Of interest in this review is their stress-relaxation and mechanical properties such as self-healing have been explored with the goal to use them as recyclable elastomers with tunable mechanical properties [20,21].

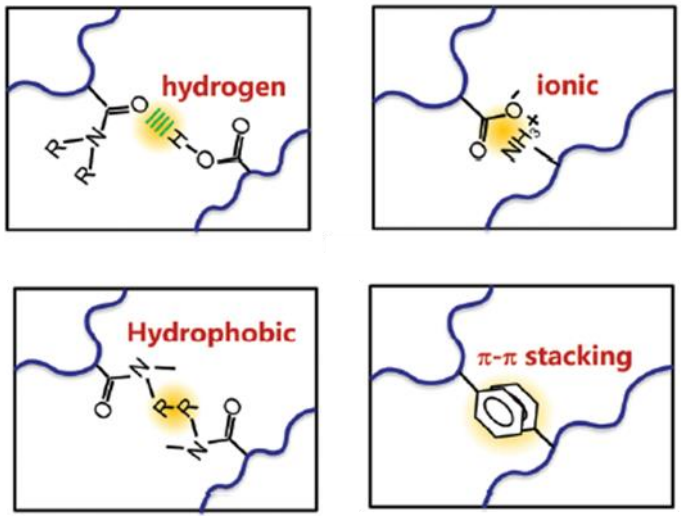

Figure 1.2. Schematic representation of associative polymers with different associating groups on the side chains. Inspired from [9].

Living polymers are supramolecular assemblies made by building units connected by means of non-covalent interactions mostly along the backbone[22–24] (Figure 1.3). The bonds can break spontaneously at a given (often room) temperature, making these supramolecular polymers quite dynamic (usually called living polymers),in contrast to traditional linear polymers. The most common secondary bonds in supramolecular polymers are π-π stacking[25], hydrogen bonds[26,27] and metal-ligand coordination[28]. These bonds are directional and additive. For example, the combination of hydrogen bonds with a π-π stacking moiety yields more stable supramolecular polymers compared single interactions of one type only[22,29]. By using combinations of these interactions one can tailor the binding energy, hence the properties of the formed networks[30,31]. There are different kinds of living polymers with wormlike micelles being the best known and more widely investigated. Their amphiphilic nature leads to an effective attractive interaction between the solvophobic parts of the associating molecules (typically surfactants) , which leads to the self-assembly into larger structures while the solvophilic parts interact with the solvent and protect the system from complete phase separation[26]. Telechelic polymer chains constitute another building block, where the ends consist of units that can associate through attractive interactions which can also be directional such as hydrogen bonds, leading to long supramolecular polymers (like semiflexible filaments) that can form topological entanglements[22]. However, in this case there cyclic molecules may form as well and

strongly affect the viscoelasticity of the system[32]. In general, in such a situation the resulting structure involves loops and bridges whose ratio depends primarily on fraction and strength of attractive groups as well as the concentration to telechelic polymers in the case of solutions[16,33–36]. Also, small organic molecules can start self-assembling into larger 1D assemblies resembling polymer chains[26].

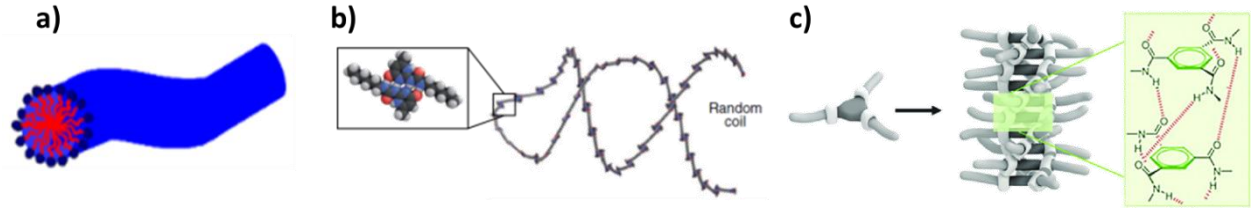

Figure 1.3. Different types of living polymers. **a)** Wormlike micelle: red tails represent solvophobic part while blue heads represent the solvophilic part. **b)** Telechelic polymer chains functionalized with a quadruple hydrogen-bonding motif leading primarily to a large living polymer that has a random-coil like conformation[7] .**c)** Small organic molecules (Benzene tricarboxylamide based) self-assembled into a 1-D polymer-like array[37].

Applications of supramolecular assemblies based on reversible secondary interactions include self-healing and shape memory materials which are easily processable and recyclable[7,38], since at high temperatures they become liquids of molecularly dissolved organic molecules. Furthermore, their dynamic nature and similarites with biopolymers make them strong candidates for understanding and/or synthesizing complex bio materials[8,39–42].

In general, when the supramolecular interactions yield one dimensional wormilike self-assembled structures, their dynamics are described by the model of Cates [43–45] for stress relaxation in living polymers. This model predicts a single-exponential decay even though the wormike living chains are polydisperse and has been confirmed, in part, experimentally and also formed the basis for further developments in modeling associating polymers[23,46,47]. The key idea was that living polymers can reversibly break or exchange monomers while reptating out of their effective tube. On the other hand, depending of the type of association and structures formed, there are different models that

describe their stress relaxation, such as the sticky Rouse[10,48] or sticky reptation[49]. For more complex associating polymers such as hydrophobically modified ethylene-oxide urethane block copolymers (HEUR)[16], which is a telechelic PEO forming loops and bridges, other models have been proposed to describe their longest relaxation such as the Tanaka-Edwards[50,51] model or the free path model of Ianniruberto and Marucci[52,53].

In this review we focus on the dynamics governing stress relaxation and non-linear flow of supramolecular polymers, and more specifically on supramolecular polymers in solution based on hydrogen bonding. We do not address associating polymers which have been recently reviewed extensively by Colby and coworkers[9]. Moreover, the process of self-assembly will only be discussed in the context of how it affects the structure and dynamics or how it can be affected by the environment, while supramolecular chemistry shall not be reviewed[26,30,54–56]. Low molar mass gelators are of interest in several industrial applications such as coatings, lubricants or cosmetics, and here we shall attempt to establish a connection between the structure and dynamics at the scale of the unimers and assess the rheological properties of the resulting materials.

2. Supramolecular living polymerics

A wide range of low molecular weight compounds used in supramolecular polymerizations, both in water and in organic solvents, yielding very long 1-D structures akin to polymers. Some characteristic examples are presented here with emphasis on the role of small changes in the molecular structure in the final self-assembled product. In general, highly directional associations with large association energies are necessary to form long polymer-like supramolecular structures.

Figure 1.4 illustrates four typical units used for such self-assembly. In the following paragraphs, we discuss applications using these four motifs in the formation of supramolecular living polymers with versatile properties and great sensitivity to slight changes in their environment or structure.

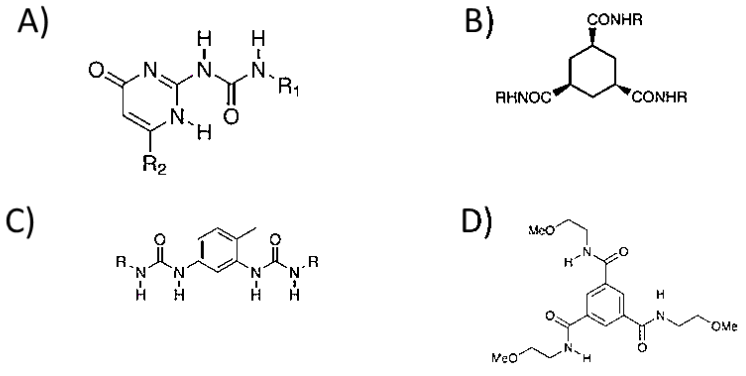

Figure 1.4. Motifs for supramolecular self-assembly via different types of bonding interactions: A) Ureidopyrimidinone (UPy) with quadruple hydrogen bonding[57,58] ; B) Cyclohexane-Tricarboxamide (CTC)[59] with triple hydrogen bonding ; C) Bisurea group with hydrogen bonding and pi-pi stacking[60] ; D) 1,3,5-Benzene Tricarboxamide (BTA) group[61,62] with triple hydrogen bonding and pi-pi stacking.

Sijbesma et al.[22] have used UPy to functionalize small alkyl spacers (component 1 in Figure 1.5A) at both ends (bifunctional), which when dissolved in trichloromethane ($CHCl_3$) lead to viscous solutions with the viscosity being highly concentration- and temperature-dependent. Specifically, supramolecular solutions based on UPy motifs with the compound 1a (H) exhibit a power-law concentration dependence of the viscosity with exponent of 3.6 (Figure 1.5B), in agreement with the predicted value from the model of Cates for living polymers[43]. On the other hand, the different compound 1b (CH_3) leads to different assemblies with a more peculiar behavior of the viscosity, characterized by linear dependence at lower concentrations and a much stronger dependence at higher concentrations (with a power-law exponent of about 6). This is attributed to the fact that there seems to be a predominance of cyclic structures with compound 1b at smaller concentrations but will eventually form elongated objects at higher concentrations. The former act essentially as small particles contributing to the viscosity of the solution according to the Einstein-Batchelor equation. The unidirectionality of the associations was confirmed by mixing the mono-functional compound 2 in solutions of 1. As shown in figure 1.5C, the specific viscosity as a function of molar fraction of the mono-functional components decreases by an order of magnitude with addition of very small amounts of the end-capper. Addition of component 2 (Fig. 1.5A) leads to the termination of the supramolecular

polymerization by capping active ends, and thus to much shorter self-assembled structures (provided that there is no uncontrollable gelation or branching taking place).

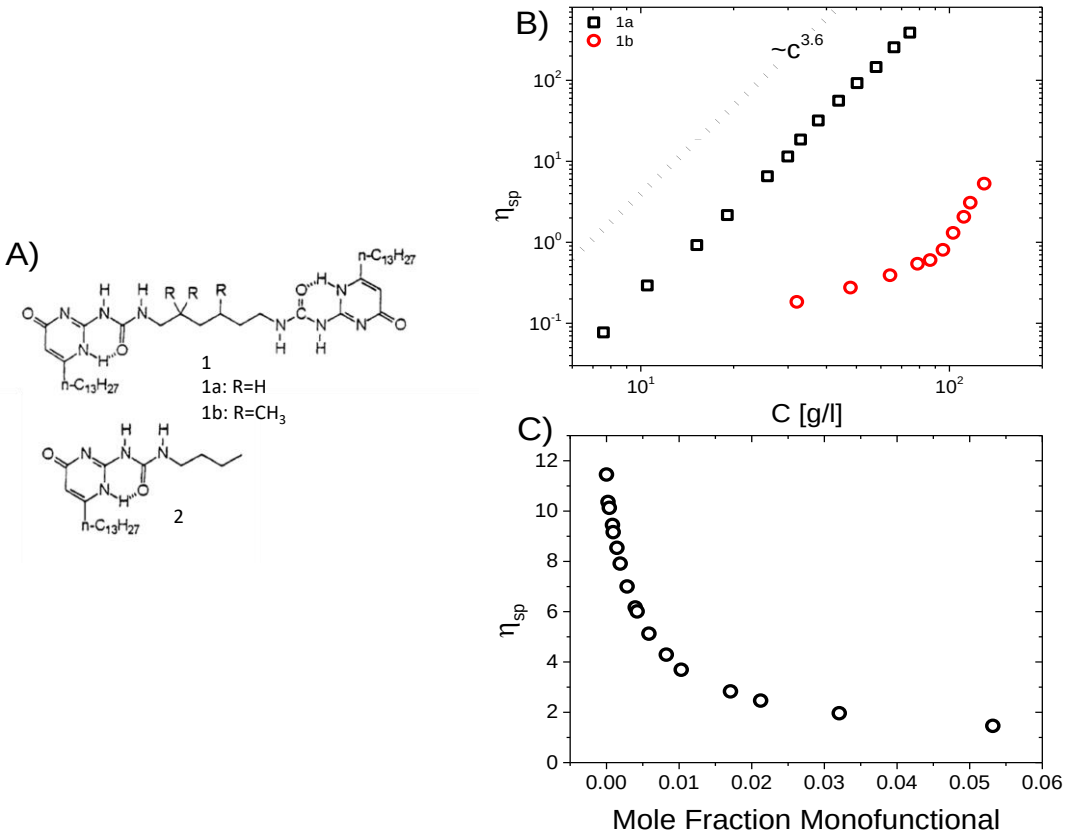

Figure 1.5. A) Structure of the bi-functional and mono-functional compounds For UPy-based supramolecular assemblies. B) Specific viscosity of solutions of assemblies based on 1 in $CHCl_3$ as a function of concentration for the two different bi-functional compounds. Black squares correspond to compound 1a while red circles to compound 1b. The dotted line shows the slope 3.6. C) Specific viscosity of mixtures based on difunctional component 1 and monofunctional component 2 in $CHCl_3$ as a function of mole fraction of compound 2. Data were taken from [18]

It is important to note that the self-assembly of supramolecular polymers depends on the solvent due to the fact that secondary associations are in general dipolar and can be easily affected by the polarity of the solvent[63] as well as specific solvophobic effects that might occur. For example, Hirschberg et al.[64] explored the role of the solvent on the self-assembly of supramolecular polymers based on UPy group (Figure 1.6A) and reported that the same unit may form small flexible-coil

assemblies in $CHCl_3$ or long helical columnar stacks in dodecane, due to the solvophobic stacking of the aromatic parts of the molecules (Figure 1.6B).

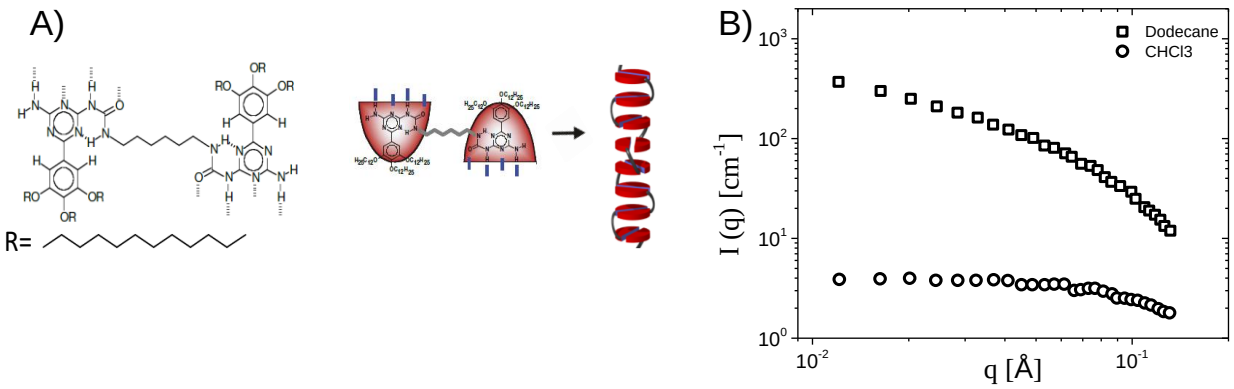

Figure 1.6. A) Chemical structure of unimer and schematic illustration of the proposed self-assembly. B) Neutron scattering intensities in deuterated dodecane and choloroform. Data were taken from [58]

A strong solvent effect has been also observed during the self-assembly of bisurea-based moieties and in particular the 2,4(Ethyl Hexyl Ureido)Toluene (EHUT), which is depicted in Figure 1.7A. EHUT is known to self-assemble into thin thread-like structures at larger temperatures in apolar solvent toluene and tube-like structures at lower temperatures. This was evidenced by SANS experiments (Figure 1.7B) and validated by molecular dynamics simulations[65,66]. In figure 1.7B, the transition with temperature leads to a marked difference in the scattering intensity I(q), where q is the scattering wave vector. However, the fact that I(q) decays as q^{-1} (see the flat curves in the Holtzer plot of qI versus q) signifies that both structures formed are rigid and seem to have a finite cross-section since the intensity decreases sharply with increasing q values. Since the structure formed is a hollow tube, to be stable it needs to be filled with solvent and thus if one changes the solvent size without changing the dielectric properties of the solvent, the tubular structure would become unstable[67], leading to the two different pseudo-phase diagrams shown in Figures 1.7C and 1.7D corresponding to the diagrams in phases in toluene and trimethylbenzene (TBM) respectively. The fact that the transition from the monomer to the thin filament is the same reflects the very similar dielectric properties of TBM and toluene.

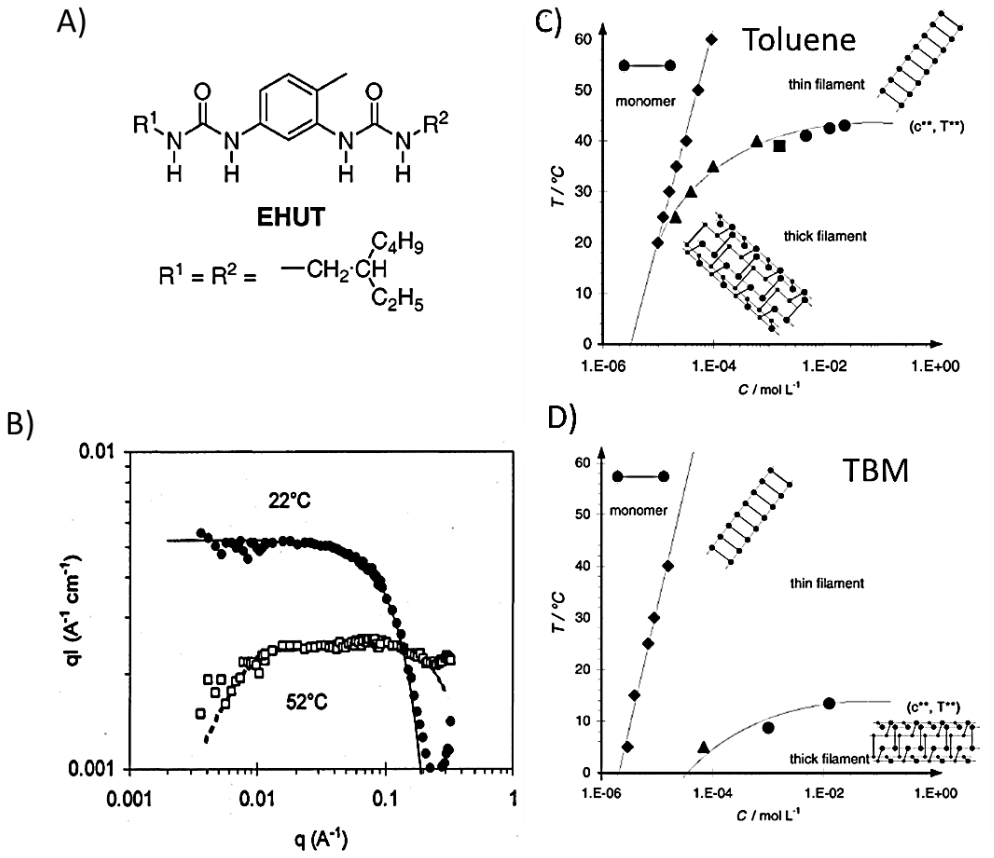

Figure 1.7. A) Chemical Structure of bisurea-based moiety 2,4(Ethyl Hexyl Ureido)Toluene (EHUT). B) Holtzer plot of qI versus q for EHUT in toluene at two different temperatures. The plateau indicates the rigid structure formed by EHUT at both temperatures, whereas the difference in aggregation number is evident since at 52^{o}C the intensity is much lower. C) Pseudo-phase diagram of EHUT in toluene. D) Pseudo-phase diagram of EHUT in TBM. Data were taken from [59] and [61].

Recently, Van Zee et al.[68] have demonstrated that the structure and helicity of a novel self-assembling moiety based on BTA, BPTA (Figure 1.8), in organic solvent methylcyclohexane change significanlty in the presence of trace amounts of water which interacts with the hydrogen bonding moieties. In a nutshell, at low temperatures the water molecules in the monomeric state immersed in an organic oil, interact with BPTA and saturate the supramolecular structure, which has a right-handed helical conformation. By increasing the temperature, water molecules leave the structure

which eventually becomes completely "dry" and turns into a left-handed helix. These are the three structures reported in figure 1.8B along with the ratio (v) of water molecules per BPTA unimer.

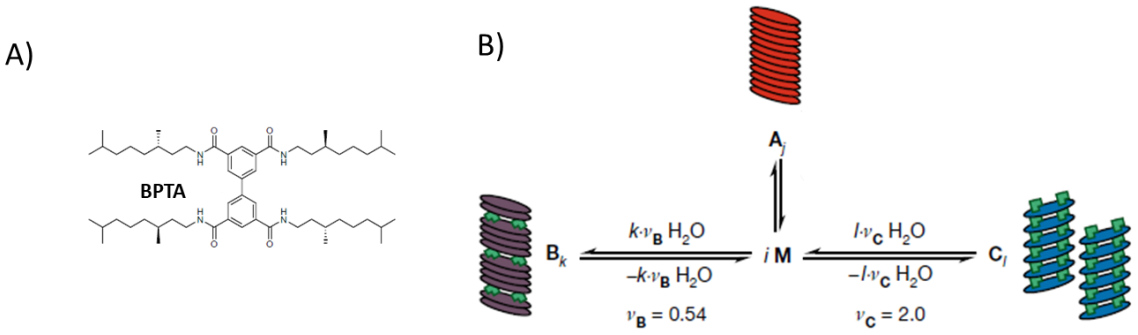

Figure 1.8. A)Chemical structure of BPTA self-assembling motif B)Schematic of the three-component thermodynamic model used in [68]. Discs represent the BPTA unimer, whereas v_B and v_c are the ratio of water molecules to BPTA unimers found in the two wet states **B** and **C**.

This transition have been monitored with circular dichroism (CD). Characteristic CD spectra are shown in Figure 1.9A for increasing concentration of BPTA and Figure 1.9B for increasing water content. It is described by a thermodynamic model involving three competing, cooperative polymerization, which provides the free energy of deformation for the different states. By measuring the enthalpy of deformation (through Van't Hoff analysis) of the dry and two different wet states (depending on the water content) by DSC and inputting this information in the model, it is possible to predict the CD spectra which are in full agreement with the experimental spectra (Figures 1.9).

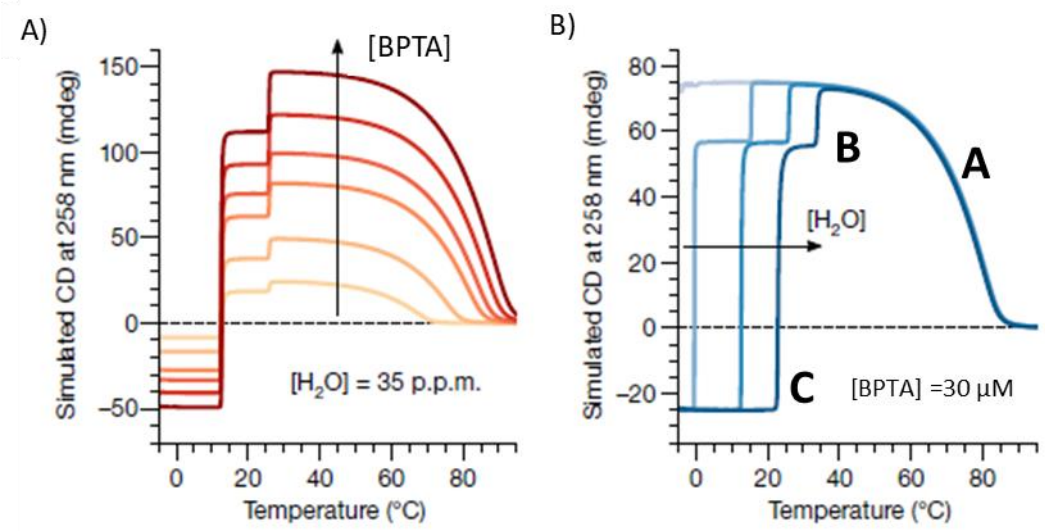

Figure 9 A) Experimental data of the evolution of the CD spectra with temperature at different concentrations of BPTA and constant concentration of water B) Respective predictions of the thermodynamic model.

To complete this section we mention that similar units to those discussed so far can self-assemble in water to yield hydrogels that have been proposed for use as biomaterials[8,39,41]. The self-assembly of a rationally designed BTA derivative has been studied extensively in water by Meijer and coworkers[26,27,30,69,70]. The outer part of the molecule includes a tetraethylene glycol moiety to ensure solubility in water, whereas the inner section comprises an alkyl chain that create a hydrophobic core shielded from water molecules. Leenders et al.[26] have shown that the self-assembly of BTA (Figure 1.10A) in water leads to 1D fibrillar structures probed by cryo-TEM (figure 1.10B). They exhibit a periodic change in contrast along their backbone (darker and lighter spots) which is usually found in helical bundles or twisted ribbons. Furthermore, this system has distinct signatures in the UV-Vis spectra that hint toward a possible supramolecular polymerization mechanism. Specifically, Figure 1.9C depicts the evolution of the UV-Vis spectra of a BTA sample originally dissolved in methanol (unimers) and subsequently injected in water. The UV-Vis spectrum of BTA in methanol shows a maximum at 209 nm which is consistent with the molecularly dissolved state. However, immediately after injection in water the absorption spectrum displays a strong peak at 192 nm (blue curve in Figure 1.10C), suggesting that initially the BTAs self-assemble into helical columnar stacks which decays

over time and evolves two bands at 213 nm and 230 nm (in figure 1.10C), and turns into the structure observed in cryo-TEM. This scenario was later confirmed by molecular dynamics simulations of the self-assembly of the same BTA derivative in water using a coarse-grained model which suggests that BTAs first assemble into disordered aggregates which evolve into ordered stacked BTA oligomers and eventually polymerize to form longer fibers[71]. All supramolecular structures described here are based on reversible interactions, therefore the dynamics breaking and reformation are central to the design of living polymers with desired function. For example, the copolymerization with a BTA derivative with branched outer chains leads to reduced monomer dynamics compared to the same without branches, due to the stabilization of the assembly by increasing the order in the fibers[69]. In another situation, by slightly changing the length of the aliphatic chain in BTA from 12 carbons (Figure 1.9A) to 11 and 13 carbons, Lou et al.[25] have shown a progressive slow-down of the dynamics (Figure 1.9D).

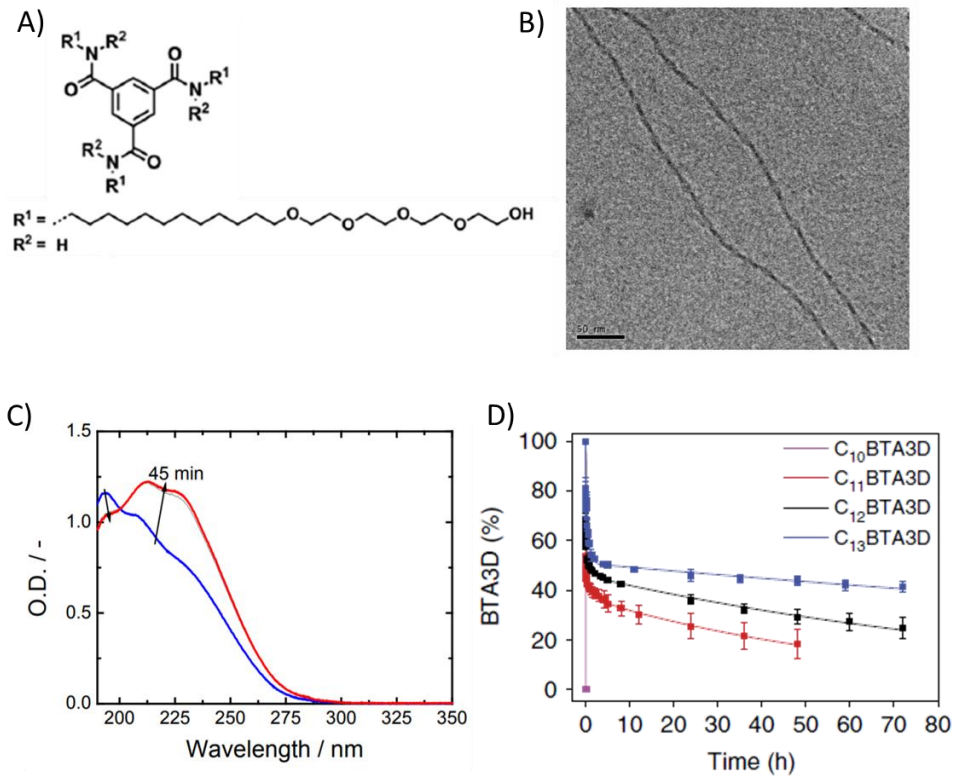

Figure 1.10. A) Chemical structure of BTA derivative for aqueous systems. B) Cryo-TEM image of the structure created by the BTA in water. The periodically varying contrast suggests a helical bundle structure. Scale bar is 50nm[26] C) Time evolution of UV-Vis spectra of BTA in water. The system in methanol was

molecularly dissolved and injected into water at t=0. Arrows indicate how curves change over time[26]. The two peaks shown in the red curve are peaks at 213 nm and 230 nm. Grey line is the spectra after 15 minutes. Note that the y axis is optical density, a quantity proportional to the absorption. D) Hydrogen-Deuterium exchange is used to examine the dynamics of systems of BTA with varying alkyl spacer length. The fraction of BTA with only the outer labile hydrogens in the –OH groups is monitored. Over time, the BTA3D changes into BTA6D since once a unimer leaves the fiber the hydrogens in the –NH groups near the core become deuterated as well. The time when the percentage of BTA3D drops is indicative of the unimer dynamics[30].

3. Bridging monomer dynamics to rheological properties

Given the various intricacies of the self-assemby process of unimers into 1-D living polymeric structures, in particular with respect to the role of the environment or the chemical structure, establishing the link between unimer dynamics and bulk properties of these polymers is an extraordinary albeit necessary challenge to address. The model of Cates model for wormlike micelles[43] represents the basis. In this model, the living polymers are polydisperse with a length distribution that can be determined from free energy arguments and is directly related to the scission energy per micelle. The stress relaxation is predicted and experimentally found to be almost Maxwellian[24,72,73], due to the reversible nature of these living polymers, which break and reform spontaneously while relaxing stresses through the reptation mechanism. In linear entangled polymers, the tube has completely relaxed once the chain has passed through. However, in living polymers, due to breaking and reformation there are different tubes formed depending on the dynamics of this process. In particular, that if the breaking time, τ_b, is much larger or comparable to the overall polymer relaxation (reptation) time, τ_{rep}, a polymeric response with characteristic time τ_{rep} is observed. On the other hand, if the breaking time is smaller than the reptation time the living polymer relaxes its stress with a time shorter than τ_{rep}, following a Maxwellian terminal process despite its polydispersity[44,74]. A more detailed description of the Cates model is presented in the Appendix. This rheological behavior has been observed in supramolecular living polymers[46,47,60,75,76]. Indicative linear

viscoelastic (LVE) data are shown in Figure 1.11. Specifically, in figure 1.11A the LVE spectra for an associating BTA derivative in decane are presented at various concentrations. The behavior is clearly Maxwellian as shown by the almost perfect semi-circular Cole-Cole plot of loss versus storage modulus in Figure 1.11C. The same holds for EHUT in dodecane, as shown in Figures 1.11B, D. The deviation from the semi-circular shape at higher frequencies (or larger storage moduli) reflects the presence of faster modes, such as Rouse-modes or breathing modes which are of course not present in a Maxwell element. This is the reason for distinguishing different regions, I, II and III, in Figure 1.11D. In region I, the data follow the semi-circular evolution expected from a mono-exponential relaxation, but in region II they start to deviate from and eventually exhibit a minimum in region III. The latter is related to the number of entanglements living polymer solution[45] and has been proposed to provide information about its average length [77,78]. A compilation of the moduli and relaxation times as functions of concentration is presented in Figures 1.12A and B, respectively. The modulus follows the predicted power law , whereas this is not the case for the terminal relaxation time, which remains more ambiguous[45,47,77,78].

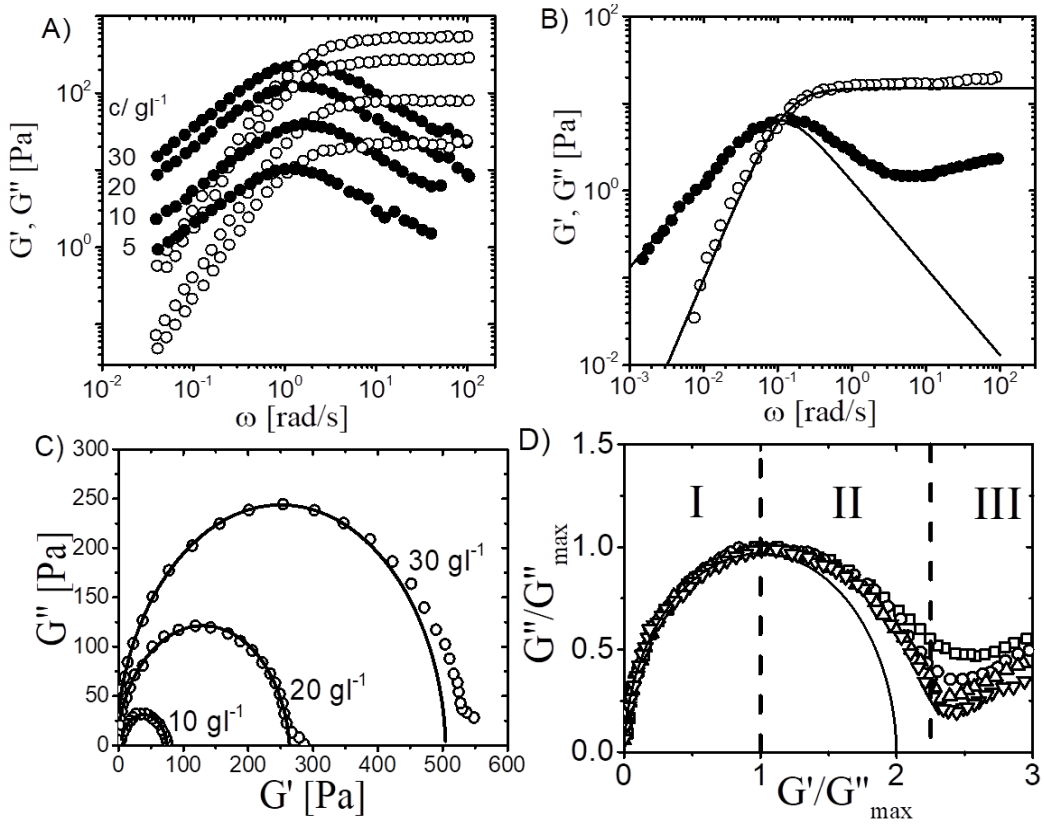

Figure 1.11. A) Linear viscoelastic spectra of a self-assembled BTA derivative in decane at various concentrations. Data are taken from [75]. B) Respective spectra for EHUT in dodecane. Lines represent the fit of the terminal regime with a Maxwell model. Data are taken from [76]. C) Cole-Cole representation of the data in A. The lines are the fits of the data with a semi-circle. D) Cole-Cole representation of the data from B for various concentrations ranging from 2.9 g/L to 10 g/L. The line is the fit of the data with a semi-circle. Data are taken from [75,76]

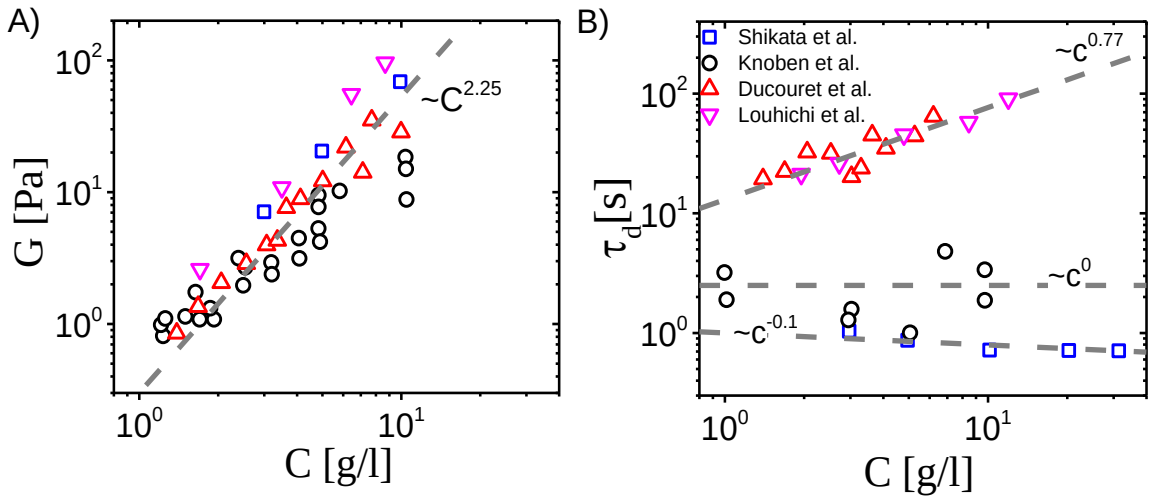

Figure 1.12. A) Compilation of plateau moduli, as obtained from the minimum of G'', for different supramolecular living polymers. Dashed lines indicate the power law predicted from Cates works[23,47,75,76] B) Compilation of terminal relaxation times as obtained from the inverse cross-over frequency for different systems. Symbols are the same as in (A). Dashed line indicates scaling laws found in each study. Data are taken from [23,47,75,76]

Recently, Louhichi et al. [47] investigated the properties of EHUT solutions under controlled humidity conditions and reported that the level of environmental humidity can affect the terminal relaxation time. In Figure 1.13A, the LVE spectra of the same EHUT solution in dodecane are depicted. The black circles correspond to the sample measured under dry conditions while the blue stars under ambient humidity conditions. The terminal relaxation time changes by a factor of three while the plateau modulus is virtually unchanged, suggesting that the strength of the entanglement network is not affected by humidity. There is also a slight shift of the frequency where G'' exhibits a minimum, which is related to the breaking time of the assembly, however the change in the terminal relaxation time is more substantial (Figure 1.13A). The change of the terminal relaxation time is attributed to the change in the average length of the EHUT self-assembled structures. Indeed, it has been shown that by adding impurities or monofunctional unimers in a solution of EHUT may result in chain scission, yielding shorter polymers[23,79]. It is also possible that the water molecules do not just end-cap the supramolecular assemblies but can get incorporated between unimers as suggested by van Zee et al.[68]

and essentially “plasticize” the associations which have a slightly lower binding energy. This will lead to both shorter assemblies and faster breaking time. Therefore, even tiny amounts of water in apolar solvents (even less than 0.1wt%) can interfere with the hydrogen-bonded self-assembly and influence the macroscopic properties of the solution. In this respect, an outstanding challenge is to understand why some living polymer systems (organogels under dry conditions) exhibit a much weaker concentration dependence of their terminal relaxation than that predicted by Cates.(see Figure 1.12B).[80]. It has been suggested that this might be related to the dependence of the average contour length predicted by the model since both the breaking and reptation times depend on the contour length. Note that the model considers the most probable length distribution . Furthermore, constraint release should play a role in the terminal relaxation and depend on concentration, but it has not been considered in the model[81]. We should also note that the great sensitivity of such measurements to humidity may be an additional reason for the different power laws of figure 1.12F (the data reported are taken without humidity control, with the exception of [47]). Louhichi et al. have also reported some transient shear stress data of the supramolecular living polymer solutions. An unusual strong transient strain-hardening and a steady shear thinning were observed (Figure 1.14B). The former is reminiscent of the strain hardening observed for biological systems such as F-actin and is attributed to the semi-flexible character of this kind of systems[82]. Interestingly, the effect of humidity is apparent also in the nonlinear viscoelastic regime since the steady state as well as the peak viscosities of the sample measured in ambient conditions are always smaller than those measured under dry conditions (Figure 1.14B). This might be related to the difference in terminal relaxation times since the two samples are essentially measured at different Weissenberg numbers. For the same shear rate, the humid sample is actually measured at smaller Weissenberg number and does not stretch as much, leading to less pronounced overshoots. This observation does not exclude a possible more subtle effect that the humidity might have on the supramolecular assembly, such as the weakening of associations making the scission under shear easier and leading to less pronounced peaks. The shear-scission has been observed for such systems and recently found to be associated with an unexpected non-monotonic stress relaxation was (Figure 1.14C). In fact, upon flow cessation (where some scission takes place), the stress relaxation can become non-monotonic because bonds between broken

species can reform and the energy released from this process can lead to the formation of locally deformed domains with increased elastic energy and some local anisotropy, leading to a transient stress increase [83]. Furthermore, the EHUT living polymer solution is known to shear-band [76], i.e., the flow curve exhibits a stress plateau with shear rate (Figure 1.14D). This behavior is typical of living polymers as it has been widely observed in wormlike surfactant micelles systems[74,77,84] and in living polymers based on metal-ligand coordination[85]. It is also predicted by constitutive models incorporating the idea of changing shear rate associated with heterogeneities in the system and described by different mechanisms (stress diffusion, stress-concentration coupling) [86–94] (see also Appendix). Corroborating evidence has been provided by birefringence measurements under flow and particle tracking velocimetry[95,96].

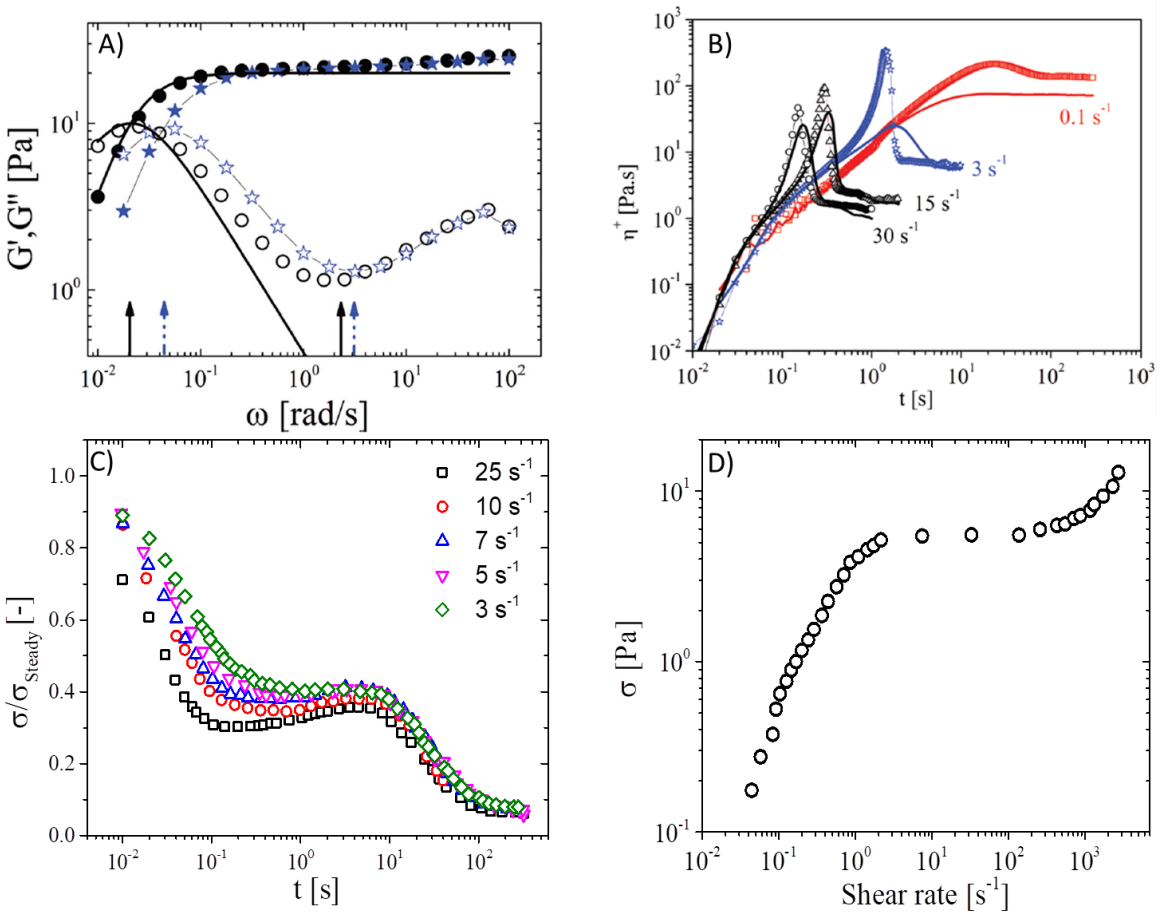

Figure 1.14. A) Linear viscoelastic spectra for EHUT in dodecane under dry conditions (black circles) and ambient humidity conditions (blue stars). Arrows indicate the cross-over frequency associated with the terminal

relaxation time and the frequency of the minimum in G'' associated with the breaking time of the living polymer. B) Transient viscosity versus time at different shear rates for a sample measured under ambient humidity conditions and for a sample at the same concentration but measured under dry conditions (linear and symbols, respectively). C) Stress relaxation after cessation of flow for EHUT in dodecane. At intermediate times the stress exhibits an overshoot. D) Flow curve for EHUT in dodecane. The stress plateau is characteristic of shear banding.

4. Future Perspectives and conclusions

Associating supramolecular living polymers such as those described here exist both in organic solvents and in water, the latter case being primarily represented by wormlike surfactant micelles. To date, low molecular weight hydrogelators have been studied only in terms of how effective they are in forming hydrogels[27,97] for materials with potential use in biomedical engineering. The common central theme of these works is the combination of a hydrogelator with a telechelic polymer chain functionalized at its ends. The hydrogelator forms hydrogels due to entanglements of the long fibrillar sturctures and the telechelic chain forms hydrogels due to the bridging of small micellar aggregates that are created by its closed-loop structure, similar to what has been observed in the past for amphiphilic block copolymers[33,98]. These complex hydrogelators have been considered as potential candidates for tissue engineering [40] .[99]. Moreover, their mixtures exhibit an intriguing non-monotonic dependence of the mechanical properties with mixing ratio of the two components. These promising results render a more detailed rheological study including the stress relaxation dynamics necessary in order to understand the interplay of different bonding energies and possibly directionalities on the macroscopic properties of hydrogel mixtures. This will be the subject of chapter 3. Chapter 4 will focus on the linear viscoelasticity of the organogelators described in section 2 (by van Zee et al.[68]) and finally the effects of environment (humidity) on the nonlinear viscoelasticity of this system will be presented in chapter 5.

Recently, supramolecular organogels with thermo-thickening properties have been prepared. It is hypothesized that the origin of this behavior is a phase transition from a quasi-ordered phase to an amorphous phase leads to an increase in viscosity due to the creation of more entanglements in the system[100]. Evidently, further investigations of the viscoelastic properties of these materials will deepen our understanding of their function and broaden the range of their potential applications.

In conclusion, supramolecular polymers represent a well-established class of materials with unique properties and promising applications, but also with outstanding challenges centered one the effects of slight changes in their chemical structure or the environment.

References

(1) Mendes, A. C.; Baran, E. T.; Reis, R. L.; Azevedo, H. S. Self-Assembly in Nature: Using the Principles of Nature to Create Complex Nanobiomaterials: Self-Assembling in Nature. *Wiley Interdiscip. Rev. Nanomed. Nanobiotechnol.* **2013**, *5* (6), 582–612. https://doi.org/10.1002/wnan.1238.

(2) Cheng, P.-N.; Pham, J. D.; Nowick, J. S. The Supramolecular Chemistry of β-Sheets. *J. Am. Chem. Soc.* **2013**, *135* (15), 5477–5492. https://doi.org/10.1021/ja3088407.

(3) Grubb, D. T.; Jelinski, L. W. Fiber Morphology of Spider Silk: The Effects of Tensile Deformation. *Macromolecules* **1997**, *30* (10), 2860–2867. https://doi.org/10.1021/ma961293c.

(4) Riekel, C.; Vollrath, F. Spider Silk Fibre Extrusion: Combined Wide- and Small-Angle X-Ray Microdiffraction Experiments. *Int. J. Biol. Macromol.* **2001**, *29* (3), 203–210. https://doi.org/10.1016/S0141-8130(01)00166-0.

(5) Vollrath, F.; Porter, D. Spider Silk as Archetypal Protein Elastomer. *Soft Matter* **2006**, *2* (5), 377. https://doi.org/10.1039/b600098n.

(6) Yan, X.; Wang, F.; Zheng, B.; Huang, F. Stimuli-Responsive Supramolecular Polymeric Materials. *Chem. Soc. Rev.* **2012**, *41* (18), 6042. https://doi.org/10.1039/c2cs35091b.

(7) Aida, T.; Meijer, E. W.; Stupp, S. I. Functional Supramolecular Polymers. *Science* **2012**, *335* (6070), 813–817. https://doi.org/10.1126/science.1205962.

(8) Webber, M. J.; Appel, E. A.; Meijer, E. W.; Langer, R. Supramolecular Biomaterials. *Nat. Mater.* **2016**, *15* (1), 13–26. https://doi.org/10.1038/nmat4474.

(9) Zhang, Z.; Chen, Q.; Colby, R. H. Dynamics of Associative Polymers. *Soft Matter* **2018**, *14* (16), 2961–2977. https://doi.org/10.1039/C8SM00044A.

(10) Chen, Q.; Tudryn, G. J.; Colby, R. H. Ionomer Dynamics and the Sticky Rouse Model. *J. Rheol.* **2013**, *57* (5), 1441–1462. https://doi.org/10.1122/1.4818868.

(11) Chen, Q.; Bao, N.; Wang, J.-H. H.; Tunic, T.; Liang, S.; Colby, R. H. Linear Viscoelasticity and Dielectric Spectroscopy of Ionomer/Plasticizer Mixtures: A Transition from Ionomer to Polyelectrolyte. *Macromolecules* **2015**, *48* (22), 8240–8252. https://doi.org/10.1021/acs.macromol.5b01958.

(12) Zhang, Z.; Liu, C.; Cao, X.; Wang, J.-H. H.; Chen, Q.; Colby, R. H. Morphological Evolution of Ionomer/Plasticizer Mixtures during a Transition from Ionomer to Polyelectrolyte. *Macromolecules* **2017**, *50* (3), 963–971. https://doi.org/10.1021/acs.macromol.6b02225.

(13) Zhuge, F.; Hawke, L. G. D.; Fustin, C.-A.; Gohy, J.-F.; van Ruymbeke, E. Decoding the Linear Viscoelastic Properties of Model Telechelic Metallo-Supramolecular Polymers. *J. Rheol.* **2017**, *61* (6), 1245–1262. https://doi.org/10.1122/1.4997593.
(14) Filippidi, E.; Cristiani, T. R.; Eisenbach, C. D.; Waite, J. H.; Israelachvili, J. N.; Ahn, B. K.; Valentine, M. T. Toughening Elastomers Using Mussel-Inspired Iron-Catechol Complexes. *Science* **2017**, *358* (6362), 502–505. https://doi.org/10.1126/science.aao0350.
(15) Feldman, K. E.; Kade, M. J.; Meijer, E. W.; Hawker, C. J.; Kramer, E. J. Model Transient Networks from Strongly Hydrogen-Bonded Polymers. *Macromolecules* **2009**, *42* (22), 9072–9081. https://doi.org/10.1021/ma901668w.
(16) Annable, T.; Buscall, R.; Ettelaie, R.; Whittlestone, D. The Rheology of Solutions of Associating Polymers: Comparison of Experimental Behavior with Transient Network Theory. *J. Rheol.* **1993**, *37* (4), 695–726. https://doi.org/10.1122/1.550391.
(17) Volpert, E.; Selb, J.; Candau, F. Influence of the Hydrophobe Structure on Composition, Microstructure, and Rheology in Associating Polyacrylamides Prepared by Micellar Copolymerization. *Macromolecules* **1996**, *29* (5), 1452–1463. https://doi.org/10.1021/ma951178m.
(18) Pasquino, R.; Zhang, B.; Sigel, R.; Yu, H.; Ottiger, M.; Bertran, O.; Aleman, C.; Schlüter, A. D.; Vlassopoulos, D. Linear Viscoelastic Response of Dendronized Polymers. *Macromolecules* **2012**, *45* (21), 8813–8823. https://doi.org/10.1021/ma301029t.
(19) Costanzo, S.; Scherz, L. F.; Schweizer, T.; Kröger, M.; Floudas, G.; Schlüter, A. D.; Vlassopoulos, D. Rheology and Packing of Dendronized Polymers. *Macromolecules* **2016**, *49* (18), 7054–7068. https://doi.org/10.1021/acs.macromol.6b01311.
(20) Cordier, P.; Tournilhac, F.; Soulié-Ziakovic, C.; Leibler, L. Self-Healing and Thermoreversible Rubber from Supramolecular Assembly. *Nature* **2008**, *451* (7181), 977–980. https://doi.org/10.1038/nature06669.
(21) Zhang, G.; Zhao, Q.; Zou, W.; Luo, Y.; Xie, T. Unusual Aspects of Supramolecular Networks: Plasticity to Elasticity, Ultrasoft Shape Memory, and Dynamic Mechanical Properties. *Adv. Funct. Mater.* **2016**, *26* (6), 931–937. https://doi.org/10.1002/adfm.201504028.
(22) Sijbesma, R. P.; Beijer, F. H.; Brunsveld, L.; Folmer, B. J. B.; Hirschberg, J. H. J. K.; Lange, R. F. M.; Lowe, J. K. L.; Meijer, E. W. Reversible Polymers Formed from Self-Complementary Monomers Using Quadruple Hydrogen Bonding. *Science* **1997**, *278* (5343), 1601–1604.
(23) Knoben, W.; Besseling, N. A. M.; Bouteiller, L.; Cohen Stuart, M. A. Dynamics of Reversible Supramolecular Polymers: Independent Determination of the Dependence of Linear Viscoelasticity on Concentration and Chain Length by Using Chain Stoppers. *Phys. Chem. Chem. Phys.* **2005**, *7* (11), 2390. https://doi.org/10.1039/b503463a.
(24) Berret, J. F.; Appell, J.; Porte, G. Linear Rheology of Entangled Wormlike Micelles. *Langmuir* **1993**, *9* (11), 2851–2854. https://doi.org/10.1021/la00035a021.
(25) Burattini, S.; Greenland, B. W.; Hayes, W.; Mackay, M. E.; Rowan, S. J.; Colquhoun, H. M. A Supramolecular Polymer Based on Tweezer-Type Π−π Stacking Interactions: Molecular Design for Healability and Enhanced Toughness. *Chem. Mater.* **2011**, *23* (1), 6–8. https://doi.org/10.1021/cm102963k.
(26) Leenders, C. M. A.; Albertazzi, L.; Mes, T.; Koenigs, M. M. E.; Palmans, A. R. A.; Meijer, E. W. Supramolecular Polymerization in Water Harnessing Both Hydrophobic Effects and Hydrogen Bond Formation. *Chem. Commun.* **2013**, *49* (19), 1963. https://doi.org/10.1039/c3cc38949a.
(27) Leenders, C. M. A.; Mes, T.; Baker, M. B.; Koenigs, Marcel. M. E.; Besenius, P.; Palmans, A. R. A.; Meijer, E. W. From Supramolecular Polymers to Hydrogel Materials. *Mater Horiz* **2014**, *1* (1), 116–120. https://doi.org/10.1039/C3MH00103B.
(28) Zhuge, F.; Brassinne, J.; Fustin, C.-A.; van Ruymbeke, E.; Gohy, J.-F. Synthesis and Rheology of Bulk Metallo-Supramolecular Polymers from Telechelic Entangled Precursors. *Macromolecules* **2017**, *50* (13), 5165–5175. https://doi.org/10.1021/acs.macromol.7b00646.

(29) Murray, T. J.; Zimmerman, S. C. New Triply Hydrogen Bonded Complexes with Highly Variable Stabilities. *J. Am. Chem. Soc.* **1992**, *114* (10), 4010–4011. https://doi.org/10.1021/ja00036a079.
(30) Lou, X.; Lafleur, R. P. M.; Leenders, C. M. A.; Schoenmakers, S. M. C.; Matsumoto, N. M.; Baker, M. B.; van Dongen, J. L. J.; Palmans, A. R. A.; Meijer, E. W. Dynamic Diversity of Synthetic Supramolecular Polymers in Water as Revealed by Hydrogen/Deuterium Exchange. *Nat. Commun.* **2017**, *8* (1), 15420. https://doi.org/10.1038/ncomms15420.
(31) Hendrikse, S. I. S.; Wijnands, S. P. W.; Lafleur, R. P. M.; Pouderoijen, M. J.; Janssen, H. M.; Dankers, P. Y. W.; Meijer, E. W. Controlling and Tuning the Dynamic Nature of Supramolecular Polymers in Aqueous Solutions. *Chem Commun* **2017**, *53* (14), 2279–2282. https://doi.org/10.1039/C6CC10046E.
(32) Parisi, D.; Ahn, J.; Chang, T.; Vlassopoulos, D.; Rubinstein, M. Stress Relaxation in Symmetric Ring-Linear Polymer Blends at Low Ring Fractions. *Macromolecules* **2020**, *53* (5), 1685–1693. https://doi.org/10.1021/acs.macromol.9b02536.
(33) Watanabe, H.; Sato, T.; Osaki, K.; Yao, M.-L.; Yamagishi, A. Rheological and Dielectric Behavior of a Styrene−Isoprene−Styrene Triblock Copolymer in Selective Solvents. 2. Contribution of Loop-Type Middle Blocks to Elasticity and Plasticity. *Macromolecules* **1997**, *30* (19), 5877–5892. https://doi.org/10.1021/ma9617577.
(34) Watanabe, H.; Matsumiya, Y.; Sawada, T.; Iwamoto, T. Rheological and Dielectric Behavior of Dipole-Inverted (SIS) $_p$ -Type Multiblock Copolymers: Estimates of Bridge/Loop Fractions for Respective I Blocks and Effect of Loops on High Extensibility of Bridges. *Macromolecules* **2007**, *40* (19), 6885–6897. https://doi.org/10.1021/ma0712495.
(35) Balsara, N. P.; Tirrell, M.; Lodge, T. P. Micelle Formation of BAB Triblock Copolymers in Solvents That Preferentially Dissolve the A Block. *Macromolecules* **1991**, *24* (8), 1975–1986. https://doi.org/10.1021/ma00008a040.
(36) Lang, C.; LaNasa, J. A.; Utomo, N.; Xu, Y.; Nelson, M. J.; Song, W.; Hickner, M. A.; Colby, R. H.; Kumar, M.; Hickey, R. J. Solvent-Non-Solvent Rapid-Injection for Preparing Nanostructured Materials from Micelles to Hydrogels. *Nat. Commun.* **2019**, *10* (1), 3855. https://doi.org/10.1038/s41467-019-11804-7.
(37) Gerth, M.; Voets, I. K. Molecular Control over Colloidal Assembly. *Chem Commun* **2017**, *53* (32), 4414–4428. https://doi.org/10.1039/C6CC09985H.
(38) Bosman, A. W.; Sijbesma, R. P.; Meijer, E. W. Supramolecular Polymers at Work. *Mater. Today* **2004**, *7* (4), 34–39. https://doi.org/10.1016/S1369-7021(04)00187-7.
(39) Goor, O. J. G. M.; Hendrikse, S. I. S.; Dankers, P. Y. W.; Meijer, E. W. From Supramolecular Polymers to Multi-Component Biomaterials. *Chem Soc Rev* **2017**, *46* (21), 6621–6637. https://doi.org/10.1039/C7CS00564D.
(40) Cheng, J.; Amin, D.; Latona, J.; Heber-Katz, E.; Messersmith, P. B. Supramolecular Polymer Hydrogels for Drug-Induced Tissue Regeneration. *ACS Nano* **2019**, *13* (5), 5493–5501. https://doi.org/10.1021/acsnano.9b00281.
(41) Dankers, P. Y. W.; van Luyn, M. J. A.; Huizinga-van der Vlag, A.; Petersen, A. H.; Koerts, J. A.; Bosman, A. W.; Popa, E. R. Convenient Formulation and Application of a Supramolecular Ureido-Pyrimidinone Modified Poly(Ethylene Glycol) Carrier for Intrarenal Growth Factor Delivery. *Eur. Polym. J.* **2015**, *72*, 484–493. https://doi.org/10.1016/j.eurpolymj.2015.07.010.
(42) Bakker, M. H.; Lee, C. C.; Meijer, E. W.; Dankers, P. Y. W.; Albertazzi, L. Multicomponent Supramolecular Polymers as a Modular Platform for Intracellular Delivery. *ACS Nano* **2016**, *10* (2), 1845–1852. https://doi.org/10.1021/acsnano.5b05383.
(43) Cates, M. E. Reptation of Living Polymers: Dynamics of Entangled Polymers in the Presence of Reversible Chain-Scission Reactions. *Macromolecules* **1987**, *20* (9), 2289–2296. https://doi.org/10.1021/ma00175a038.
(44) Cates, M. E.; Candau, S. J. Statics and Dynamics of Worm-like Surfactant Micelles. *J. Phys. Condens. Matter* **1990**, *2* (33), 6869–6892. https://doi.org/10.1088/0953-8984/2/33/001.
(45) Granek, R.; Cates, M. E. Stress Relaxation in Living Polymers: Results from a Poisson Renewal Model. *J. Chem. Phys.* **1992**, *96* (6), 4758–4767. https://doi.org/10.1063/1.462787.

(46) Jacob, A. R.; Deshpande, A. P.; Bouteiller, L. Large Amplitude Oscillatory Shear of Supramolecular Materials. *J. Non-Newton. Fluid Mech.* **2014**, *206*, 40–56. https://doi.org/10.1016/j.jnnfm.2014.03.001.
(47) Louhichi, A.; Jacob, A. R.; Bouteiller, L.; Vlassopoulos, D. Humidity Affects the Viscoelastic Properties of Supramolecular Living Polymers. *J. Rheol.* **2017**, *61* (6), 1173–1182. https://doi.org/10.1122/1.4997600.
(48) Rubinstein, M.; Semenov, A. N. Thermoreversible Gelation in Solutions of Associating Polymers. 2. Linear Dynamics. **1998**, *31* (4), 12.
(49) Leibler, L.; Rubinstein, M.; Colby, R. H. Dynamics of Reversible Networks. *Macromolecules* **1991**, *24* (16), 4701–4707. https://doi.org/10.1021/ma00016a034.
(50) Tanaka, F.; Edwards, S. F. Viscoelastic Properties of Physically Crosslinked Networks. 1. Transient Network Theory. *Macromolecules* **1992**, *25* (5), 1516–1523. https://doi.org/10.1021/ma00031a024.
(51) Tanaka, F.; Edwards, S. F. Viscoelastic Properties of Physically Crosslinked Networks Part 2. Dynamic Mechanical Moduli. *J. Non-Newton. Fluid Mech.* **1992**, *43*, 16.
(52) Marrucci, G.; Bhargava, S.; Cooper, S. L. Models of Shear-Thickening Behavior in Physically Crosslinked Networks. *Macromolecules* **1993**, *26* (24), 6483–6488. https://doi.org/10.1021/ma00076a027.
(53) Ianniruberto, G.; Marrucci, G. New Interpretation of Shear Thickening in Telechelic Associating Polymers. *Macromolecules* **2015**, *48* (15), 5439–5449. https://doi.org/10.1021/acs.macromol.5b01048.
(54) Bochicchio, D.; Pavan, G. M. Effect of Concentration on the Supramolecular Polymerization Mechanism via Implicit-Solvent Coarse-Grained Simulations of Water-Soluble 1,3,5-Benzenetricarboxamide. *J. Phys. Chem. Lett.* **2017**, *8* (16), 3813–3819. https://doi.org/10.1021/acs.jpclett.7b01649.
(55) Zhao, D.; Moore, J. S. Nucleation–Elongation: A Mechanism for Cooperative Supramolecular Polymerization. *Org Biomol Chem* **2003**, *1* (20), 3471–3491. https://doi.org/10.1039/B308788C.
(56) De Greef, T. F. A.; Smulders, M. M. J.; Wolffs, M.; Schenning, A. P. H. J.; Sijbesma, R. P.; Meijer, E. W. Supramolecular Polymerization. *Chem. Rev.* **2009**, *109* (11), 5687–5754. https://doi.org/10.1021/cr900181u.
(57) Beijer, F. H.; Sijbesma, R. P.; Kooijman, H.; Spek, A. L.; Meijer, E. W. Strong Dimerization of Ureidopyrimidones via Quadruple Hydrogen Bonding. *J. Am. Chem. Soc.* **1998**, *120* (27), 6761–6769. https://doi.org/10.1021/ja974112a.
(58) Söntjens, S. H. M.; Sijbesma, R. P.; van Genderen, M. H. P.; Meijer, E. W. Stability and Lifetime of Quadruply Hydrogen Bonded 2-Ureido-4[1 *H*]-Pyrimidinone Dimers. *J. Am. Chem. Soc.* **2000**, *122* (31), 7487–7493. https://doi.org/10.1021/ja000435m.
(59) Hanabusa, K.; Koto, C.; Kimura, M.; Shirai, H.; Kakehi, A. Remarkable Viscoelasticity of Organic Solvents Containing Triakyl-1,3,5-Benzenetricarboxamides and Their Intermolecular Hydrogen Bonding. *Chem. Lett.* **1997**, *26* (5), 429–430.
(60) Lortie, F.; Boileau, S.; Bouteiller, L.; Chassenieux, C.; Demé, B.; Ducouret, G.; Jalabert, M.; Lauprêtre, F.; Terech, P. Structural and Rheological Study of a Bis-Urea Based Reversible Polymer in an Apolar Solvent †. *Langmuir* **2002**, *18* (19), 7218–7222. https://doi.org/10.1021/la0255166.
(61) Yasuda, Y.; Iishi, E.; Inada, H.; Shirota, Y. Novel Low-Molecular-Weight Organic Gels: N',N',N''-Tristearyltrimesamid/Organic Solvent System. *Chem. Lett.* **1996**, *25* (7), 575–576.
(62) Lightfoot, M. P.; Mair, F. S.; Pritchard, R. G.; Warren, J. E. New Supramolecular Packing Motifs: P-Stacked Rods Encased in Triply-Helical Hydrogen Bonded Amide Strands. 2.
(63) Smithrud, D. B.; Diederich, F. Strength of Molecular Complexation of Apolar Solutes in Water and in Organic Solvents Is Predictable by Linear Free Energy Relationships: A General Model for Solvation Effects on Apolar Binding. *J. Am. Chem. Soc.* **1990**, *112* (1), 339–343. https://doi.org/10.1021/ja00157a052.
(64) Hirschberg, J. H. K. K.; Brunsveld, L.; Ramzi, A.; Vekemans, J. A. J. M.; Sijbesma, R. P.; Meijer, E. W. Helical Self-Assembled Polymers from Cooperative Stacking of Hydrogen-Bonded Pairs. *Nature* **2000**, *407* (6801), 167–170. https://doi.org/10.1038/35025027.

(65) Bouteiller, L.; Colombani, O.; Lortie, F.; Terech, P. Thickness Transition of a Rigid Supramolecular Polymer. *J. Am. Chem. Soc.* **2005**, *127* (24), 8893–8898. https://doi.org/10.1021/ja0511016.
(66) Alvarenga, B. G.; Bernardino, K.; de Moura, A. F.; Sabadini, E. Two Different Pathways for Assembling Bis-Urea in Benzene and Toluene. *J. Mol. Model.* **2018**, *24* (7), 154. https://doi.org/10.1007/s00894-018-3688-6.
(67) Pinault, T.; Isare, B.; Bouteiller, L. Solvents with Similar Bulk Properties Induce Distinct Supramolecular Architectures. *ChemPhysChem* **2006**, *7* (4), 816–819. https://doi.org/10.1002/cphc.200500636.
(68) Van Zee, N. J.; Adelizzi, B.; Mabesoone, M. F. J.; Meng, X.; Aloi, A.; Zha, R. H.; Lutz, M.; Filot, I. A. W.; Palmans, A. R. A.; Meijer, E. W. Potential Enthalpic Energy of Water in Oils Exploited to Control Supramolecular Structure. *Nature* **2018**, *558* (7708), 100–103. https://doi.org/10.1038/s41586-018-0169-0.
(69) Thota, B. N. S.; Lou, X.; Bochicchio, D.; Paffen, T. F. E.; Lafleur, R. P. M.; van Dongen, J. L. J.; Ehrmann, S.; Haag, R.; Pavan, G. M.; Palmans, A. R. A.; Meijer, E. W. Supramolecular Copolymerization as a Strategy to Control the Stability of Self-Assembled Nanofibers. *Angew. Chem. Int. Ed.* **2018**, *57* (23), 6843–6847. https://doi.org/10.1002/anie.201802238.
(70) Garzoni, M.; Baker, M. B.; Leenders, C. M. A.; Voets, I. K.; Albertazzi, L.; Palmans, A. R. A.; Meijer, E. W.; Pavan, G. M. Effect of H-Bonding on Order Amplification in the Growth of a Supramolecular Polymer in Water. *J. Am. Chem. Soc.* **2016**, *138* (42), 13985–13995. https://doi.org/10.1021/jacs.6b07530.
(71) Bochicchio, D.; Pavan, G. M. From Cooperative Self-Assembly to Water-Soluble Supramolecular Polymers Using Coarse-Grained Simulations. *ACS Nano* **2017**, *11* (1), 1000–1011. https://doi.org/10.1021/acsnano.6b07628.
(72) Gaudino, D.; Pasquino, R.; Grizzuti, N. Adding Salt to a Surfactant Solution: Linear Rheological Response of the Resulting Morphologies. *J. Rheol.* **2015**, *59* (6), 1363–1375. https://doi.org/10.1122/1.4931114.
(73) Zou, W.; Tang, X.; Weaver, M.; Koenig, P.; Larson, R. G. Determination of Characteristic Lengths and Times for Wormlike Micelle Solutions from Rheology Using a Mesoscopic Simulation Method. *J. Rheol.* **2015**, *59* (4), 903–934. https://doi.org/10.1122/1.4919403.
(74) Rehage, H.; Hoffmann, H. Rheological Properties of Viscoelastic Surfactant Systems. *J. Phys. Chem.* **1988**, *92* (16), 4712–4719. https://doi.org/10.1021/j100327a031.
(75) Shikata, T.; Ogata, D.; Hanabusa, K. Viscoelastic Behavior of Supramolecular Polymeric Systems Consisting of *N* , *N* ‘ , *N* ‘ ‘ -Tris(3,7-Dimethyloctyl)Benzene-1,3,5-Tricarboxamide and *n* -Alkanes. *J. Phys. Chem. B* **2004**, *108* (2), 508–514. https://doi.org/10.1021/jp030510q.
(76) Ducouret, G.; Chassenieux, C.; Martins, S.; Lequeux, F.; Bouteiller, L. Rheological Characterisation of Bis-Urea Based Viscoelastic Solutions in an Apolar Solvent. *J. Colloid Interface Sci.* **2007**, *310* (2), 624–629. https://doi.org/10.1016/j.jcis.2007.01.059.
(77) Khatory, A.; Lequeux, F.; Kern, F.; Candau, S. J. Linear and Nonlinear Viscoelasticity of Semidilute Solutions of Wormlike Micelles at High Salt Content. *Langmuir* **1993**, *9* (6), 1456–1464. https://doi.org/10.1021/la00030a005.
(78) Kern, F.; Lequeux, F.; Zana, R.; Candau, S. J. Dynamic Properties of Salt-Free Viscoelastic Micellar Solutions. *Langmuir* **1994**, *10* (6), 1714–1723. https://doi.org/10.1021/la00018a018.
(79) Knoben, W.; Besseling, N. A. M.; Cohen Stuart, M. A. Chain Stoppers in Reversible Supramolecular Polymer Solutions Studied by Static and Dynamic Light Scattering and Osmometry. *Macromolecules* **2006**, *39* (7), 2643–2653. https://doi.org/10.1021/ma0518914.
(80) Berret, J.-F. RHEOLOGY OF WORMLIKE MICELLES : EQUILIBRIUM PROPERTIES AND SHEAR BANDING TRANSITION. In *Molecular Gels*; Springer: Netherlands, 2006; Vol. 19, pp 667–720.
(81) Dealy, J. M.; Read, Daniel. J.; Larson, R. G. *Structure and Rheology of Molten Polymers*, 2nd ed.; Hanser, 2018.
(82) Broedersz, C. P.; MacKintosh, F. C. Modeling Semiflexible Polymer Networks. *Rev. Mod. Phys.* **2014**, *86* (3), 995–1036. https://doi.org/10.1103/RevModPhys.86.995.
(83) Hendricks, J.; Louhichi, A.; Metri, V.; Fournier, R.; Reddy, N.; Bouteiller, L.; Cloitre, M.; Clasen, C.; Vlassopoulos, D.; Briels, W. J. Nonmonotonic Stress Relaxation after Cessation

of Steady Shear Flow in Supramolecular Assemblies. *Phys. Rev. Lett.* **2019**, *123* (21), 218003. https://doi.org/10.1103/PhysRevLett.123.218003.
(84) Olmsted, P. D. Dynamics and Flow-Induced Phase Separation in Polymeric Fluids. *Curr. Opin. Colloid Interface Sci.* **1999**, *4*, 95.
(85) Terech, P.; Coutin, A. Organic Solutions of Monomolecular Organometallic Threads. Nonlinear Rheology and Effects of End-Capping Species. *J. Phys. Chem. B* 7.
(86) Cates, M. E. Nonlinear Viscoelasticity of Wormlike Micelles (and Other Reversibly Breakable Polymers). *J. Phys. Chem.* **1990**, *94* (1), 371–375. https://doi.org/10.1021/j100364a063.
(87) Spenley, N. A.; Cates, M. E.; McLeish, T. C. B. Nonlinear Rheology of Wormlike Micelles. *Phys. Rev. Lett.* **1993**, *71* (6), 939–942. https://doi.org/10.1103/PhysRevLett.71.939.
(88) Cates, M. E.; Fielding, S. M. Rheology of Giant Micelles. *Adv. Phys.* **2006**, *55* (7–8), 799–879. https://doi.org/10.1080/00018730601082029.
(89) Vasquez, P. A.; McKinley, G. H.; Pamela Cook, L. A Network Scission Model for Wormlike Micellar Solutions. *J. Non-Newton. Fluid Mech.* **2007**, *144* (2–3), 122–139. https://doi.org/10.1016/j.jnnfm.2007.03.007.
(90) Dhont, J. K. G.; Briels, W. J. Gradient and Vorticity Banding. *Rheol. Acta* **2008**, *47* (3), 257–281. https://doi.org/10.1007/s00397-007-0245-0.
(91) Dhont, J., K. G.; Kang, K.; Letting, M. P.; Briels, W. J. Shear Banding Instabilities. *Korea-Aust. Rheol. J.* **2010**, *22* (4).
(92) Olmsted, P. D. Perspectives on Shear Banding in Complex Fluids. *Rheol. Acta* **2008**, *47* (3), 283–300. https://doi.org/10.1007/s00397-008-0260-9.
(93) Germann, N.; Cook, L. P.; Beris, A. N. A Differential Velocities-Based Study of Diffusion Effects in Shear Banding Micellar Solutions. *J. Non-Newton. Fluid Mech.* **2016**, *232*, 43–54. https://doi.org/10.1016/j.jnnfm.2016.03.011.
(94) Lerouge, S.; Olmsted, P. D. Non-Local Effects in Shear Banding of Polymeric Flows. *Front. Phys.* **2020**, *7*, 246. https://doi.org/10.3389/fphy.2019.00246.
(95) Cappelaere, E.; Cressely, R.; Decruppe, J. P. Linear and Non-Linear Rheological Behaviour of Salt-Free Aqueous CTAB Solutions. *Colloids Surf. Physicochem. Eng. Asp.* **1995**, *104* (2–3), 353–374. https://doi.org/10.1016/0927-7757(95)03332-2.
(96) Boukany, P. E.; Wang, S.-Q. Use of Particle-Tracking Velocimetry and Flow Birefringence To Study Nonlinear Flow Behavior of Entangled Wormlike Micellar Solution: From Wall Slip, Bulk Disentanglement to Chain Scission. *Macromolecules* **2008**, *41* (4), 1455–1464. https://doi.org/10.1021/ma702527s.
(97) Pape, A.; Bastings, M.; Kieltyka, R.; Wyss, H.; Voets, I.; Meijer, E.; Dankers, P. Mesoscale Characterization of Supramolecular Transient Networks Using SAXS and Rheology. *Int. J. Mol. Sci.* **2014**, *15* (1), 1096–1111. https://doi.org/10.3390/ijms15011096.
(98) Lundberg, D. J.; Glass, J. E.; Eley, R. R. Viscoelastic Behavior among HEUR Thickeners. *J. Rheol.* **1991**, *35* (6), 1255–1274. https://doi.org/10.1122/1.550174.
(99) Noteborn, W. E. M.; Zwagerman, D. N. H.; Talens, V. S.; Maity, C.; van der Mee, L.; Poolman, J. M.; Mytnyk, S.; van Esch, J. H.; Kros, A.; Eelkema, R.; Kieltyka, R. E. Crosslinker-Induced Effects on the Gelation Pathway of a Low Molecular Weight Hydrogel. *Adv. Mater.* **2017**, *29* (12), 1603769. https://doi.org/10.1002/adma.201603769.
(100) Ayzac, V.; Sallembien, Q.; Raynal, M.; Isare, B.; Jestin, J.; Bouteiller, L. A Competing Hydrogen Bonding Pattern to Yield a Thermo-Thickening Supramolecular Polymer. *Angew. Chem. Int. Ed.* **2019**, *58* (39), 13849–13853. https://doi.org/10.1002/anie.201908954.

Chapter 2 Competitive supramolecular associations mediate the viscoelasticity of binary hydrogels

1. Introduction

Ever since their discovery[1,2], supramolecular polymers have received a great deal of attention because of the reversibility and dynamic nature of the secondary bonds that govern their self-organization. These dynamic bonds dictate the macroscopic properties and enable applications in various fields ranging from biomaterials to electronics[3–5]. Supramolecular chemists have worked for years on fine-tuning the molecular structure to obtain macroscopic properties that for long were reserved for macromolecules only[6]. On the other hand, a grand challenge from the standpoint of materials design is the fundamental understanding of the dynamic assembly of supramolecular gelators and the role of competitive associations which may often be present.

In conventional synthetic or biological polymers, where monomeric constituents are connected through covalent bonds, their physical properties such as viscoelasticity can be tuned by blending different polymers, adding molecular solvents or by the copolymerization of two or more different monomers. An additional possibility with ample implications in tailoring their properties is introducing physical interactions (e.g. hydrogen bonds) which lead to the formation of dynamic networks. For example, interacting polymer blends or copolymers typically exhibit a non-monotonic dependence of segmental dynamics and viscosity on composition[7–11]. This has important consequences on the tunability of the mechanical[12–14] and thermal properties (e.g. gelation temperature)[15]. For materials based on supramolecular polymers, the additional challenge and at the same time design parameter, is the fact that the viscoelasticity of their transient networks depends on the average lifetime of the secondary interactions associated with their self-assembly. The most widely explored

example of this category of molecules is wormlike micelles where the relaxation time of the material is related to the breaking time of the associating units[16]. Thus, the relaxation time of the materials can be tuned by controlling the length of the polymer as well as the association strength. A mixture comprising an entangled aqueous solution of wormlike micelles and hydrophobically modified polymers was also found to exhibit a non-monotonic dependence of plateau modulus and terminal relaxation time on composition, due to the synergistic interactions of the two components[17,18]. Along the same lines, entangled wormlike micelles mixed with short telechelic chains formed a transient network with instead monotonic dependence of viscoelastic properties on composition[19]. It should be noted however that in these surfactant micelle composites the motifs for self-assembly are different (surfactant molecule and hydrophobic unit in a covalently-bonded chain in the presence of salt ions[17] or telechelic polymer bridging the surfactant micelles[19]).

Recent advances in the chemistry of supramolecular polymers have led to the use of supramolecular copolymerization as a means to tailor the properties of the supramolecular polymers by carefully balancing the secondary interactions, inspired by the approaches in covalent polymer synthesis[20]. In an attempt to control the dynamics of the monomers, Thota *et al.*[21] copolymerized 1,3,5-benzene-tricarboxamide (BTA) derivatives with linear and dendritic ethylene glycol side-chains. The sterically hindered dendritic monomers stabilized the supramolecular polymers by slowing-down the dynamics of the BTA monomers. Using the concept of sterically hindered monomers copolymerized with monomers forming long polymers, Appel *et al.*[22] achieved control over the length of 1D fibrillar assemblies. Others have successfully studied how the properties of amphiphilic block copolymers affect the gelation of supramolecular compounds and the mechanical properties of the resultant materials. Using telechelic polymer chains having one or both ends functionalized with the same supramolecular motif, the hydrogels exhibited an unusual viscoelastic behaviour that

varied non-monotonically with the fraction of the moiety[23–25]. However, there is a strong need to obtain a molecular-level understanding on how such properties can arise in supramolecular binary hydrogels.

Here we address the formidable challenge to rationally combine two different supramolecular compounds, which are based on the same hydrogen bonding motif BTA, to produce responsive materials with tunable properties. We approach this bioinspired challenge by focusing on synthetic hydrogels. In particular, we prepare self-assembled 1D fibers based on two compounds, BTA[26–28] and a telechelic poly(ethylene glycol) (PEG) with both ends functionalized with BTA (BTA-PEG-BTA), and explore the viscoelastic properties of their mixtures at different ratios. These mixtures form stable hydrogels whose viscoelastic properties and structure are investigated by means of shear rheology and cryogenic transmission electron microscopy (cryo-TEM). Complementary coarse-grained molecular dynamics (MD) simulations elucidate the interplay of two different interactions between the compounds and its implications on the dynamics of the mixed networks. We find a non-monotonic dependence of viscoelasticity on the composition of the mixture, which points to the importance of competitive supramolecular associations as a molecular design tool for making hydrogels with desired and tunable properties.

2. Methods

Sample Preparation. The concentration of all hydrogels, pure components and mixtures, was always kept at 5 wt%. The dry monomers and the appropriate amount water were placed in a vial along with a Teflon-coated magnetic stirring bar and were shaken until a hazy suspension started to form. The vial was then immersed in a water bath at 80^{o}C sitting on a hot plate with magnetic stirring mechanism. The vials were sealed with Teflon tape to ensure that no water

from the bath entered the vial while the preparation protocol was ongoing. The vials remained in the bath for 15 mins with short intervals (~ 10s) of vortexing and were then left to equilibrate overnight at room temperature. The next day a strong gel was formed that could sustain its weight (vial inversion test).

Rheology. We performed rheological measurements in an Anton-Paar (Austria) Physica MCR-501 rheometer, operating in the strain-controlled mode, equipped with a Peltier unit for temperature control at 37^{o}C, which also constitutes the bottom plate, and a cone geometry. All metallic components were stainless steel. We used three different cones, 8 (α=1°) mm, 12.5 (α=1°) mm, and 25 mm (α=2°) to increase the torque signal when needed. Samples were loaded at 15^{o}C to avoid evaporation during the loading procedure. An aluminium sealing ring was placed around the sample to create a silicon oil (PDMS) bath, covering the lateral surface of the sample exposed to air to prevent evaporation. Several measurements were conducted a priori in order to ensure the non-diffusivity of the stagnant oil into the hydrogels and the negligible extra-friction due to the presence of the sealing fluid. After successful loading and thermal equilibration, we performed a mechanical rejuvenation test to erase the mechanical history of the sample due to the hydrogel preparation and loading in the measuring stage (see SI and Figure S22). We have used two different rejuvenation protocols. One consists of a fixed high strain (nonlinear regime) and fixed oscillatory frequency (1 rad/s) for a given time until full liquid-like behavior of the system is reached (typically 300 s). The second protocol consists of a fixed oscillatory frequency (10 rad/s) applied on the material while the strain amplitude is varied from small to large values, well into the nonlinear regime. Afterwards, the aging kinetics were observed and measurements were done after the sample has reached its mechanical steady-state (Figure S22). Creep measurements are step-stress experiments, typically used to study materials with solid-like or very slow flow response. When the applied stress is within the linear viscoelastic regime, then the creep

response (compliance) can be converted into dynamic moduli through the relaxation/retardation spectra[51]. Here, the creep compliance J(t) was converted to G'(ω) and G"(ω) by means of the NLReg software, based on a generalization of the Tikhonov regularization method[52].

Simulations. We have studied the properties of the binary hydrogel mixture by means of coarse-grained Molecular Dynamics (MD) simulations for N particles with position vectors $\{\boldsymbol{r}_i\}$, $i = 1 \ldots N$, and total potential energy $\boldsymbol{U}(\boldsymbol{r}_i)$ involving two- and three-body terms. The two-body term is a Lennard-Jones like potential which consists of a repulsive core and a narrow attractive well, controlling the bond strength. The three body term limits the coordination number and confers angular rigidity to the inter-particle bonds[41,42,46,53] (see Figure S21) All simulations have been performed using a version of LAMMPS [54] suitably modified by us to include this interactions potential. Here we considered two distinct types of particles (associating units) whose interactions have the same form but differ for the value of the parameter that determines the relative strength of the attractive potential well. The latter is important as by changing it one can mimic the association respectively in the pure BTA and BTA-PEG-BTA experimental systems, as described in the Results section. Further details can be found in the SI (section VIII and VIII A).[41–43,46,53]The starting point for all calculations is always a configuration of $N = N_1 + N_2$ particles (N_1 with interactions corresponding to component (I) and $N_2$for the component (II)) initially prepared at $\frac{k_B T}{\varepsilon} = 5 \cdot 10^{-3}$ (where ε is the energy unit used in all simulations) leading to stable self-assembled structures that depend on the interaction parameters. Each configuration is carefully equilibrated using an optimized protocol. All the data refer to mixtures consisting of $N = 32000 - 64000$ particles in a cubic simulation box of size $L = 54\ d$. For each data point, we have run simulations over 5 independently generated samples and used sample-to-sample fluctuations to obtain error bars. In all plots, error bars are smaller than the symbol size used.

The self-assembled structures are then quenched to $\frac{k_B T}{\varepsilon} \simeq 0$ by means of dissipative dynamics to perform the rheological tests, which use a shearing protocol based on non-equilibrium molecular dynamics and a computational scheme, inspired by a recently developed experimental technique[58], to obtain the full linear viscoelastic spectrum by applying an optimally windowed chirp (OWCh) signal[55] . Further information can be found in the SI (section VIII B).

3. Results and discussion

The synthesis of the BTA that assembles into large aspect ratio supramolecular polymers is based on strategies reported previously[26] (see details in the Supporting Information, SI). This small molecule contains three aliphatic chains with tetra(ethylene glycol) at their periphery (Scheme 1). We designed a new supramolecular telechelic compound that features the same BTA motif attached to the two ends of a linear PEG (Mn = 20 kDa). To synthesize BTA-PEG-BTA, the small molecule BTA was first tosylated and subsequently azidated. The mono-azide product was isolated from the resulting mixture by column chromatography. The reaction with dialkyne functionalized PEG yielded the telechelic BTA-PEG-BTA on multigram scale (Scheme 2.1, Figures S1-S10 of the SI).

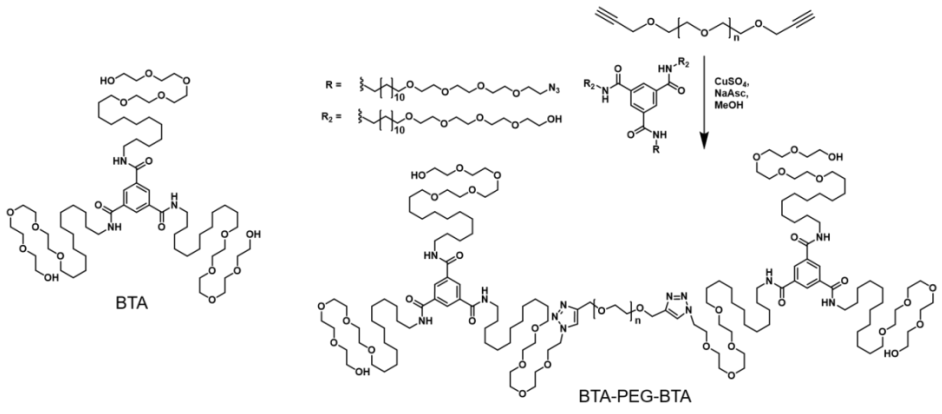

Scheme 2.1: Chemical structures of BTA (left) and the synthetic scheme for BTA-PEG-BTA (right).

Using oscillatory shear rheology, we have characterized the mechanical properties of the two pure components (here described as BTA and BTA-PEG-BTA) and their mixtures at several mixing ratios. The concentration of the hydrogels, for both pure components and mixtures, was always kept at 5 wt%. We observe that the linear viscoelastic spectra of these materials depend non-monotonically on the mixing ratio. The frequency-dependent storage (G') and loss (G'') moduli, obtained over a large range of frequencies for the pure components as well as the mixtures, are shown in Figure 2.1 and in Figures S11-S13, and the respective complex viscosities in Figure S14. The viscoelastic spectrum of the pure BTA self-assembled network is characterized by an extended entanglement-like plateau region followed by an almost Maxwellian relaxation, reminiscent to that of living polymers (blue symbols and lines in Figure 2.1a, Figure S11)[16,29–31]. The plateau modulus (G_p) has a low value (10 Pa) and extends over almost 7 decades, indicating a persistent network made by highly entangled supramolecular polymers. On the other hand, the pure BTA-PEG-BTA telechelic system exhibits a more complex viscoelastic response (red symbols and lines in Figure 2.1a, Figure S12). The high-frequency plateau modulus exceeds that of pure BTA hydrogel by almost three decades and there is a fast moduli crossover, with G'' > G' ever since. This BTA-PEG-BTA system exhibits a slow relaxation process before eventually reaching terminal flow below 0.01 rad/s, much before that of the BTA-based network. By estimating the volume fraction occupied by the PEG only, we consider an equivalent solution of pure PEG linear chains that has a molar mass of 20 kg/mol. The dilution effect is so marked that no entanglements would be formed for such a solution. However, the molecular weight needed for a pure PEG network (at the same volume fraction) to exhibit the same high-frequency plateau modulus as the BTA-PEG-BTA system and relaxation time, is calculated to be 1100 kg/mol (see SI for details, Figure S12). Clearly, the PEG chain by itself

is not long enough to produce the viscoelastic spectrum of BTA-PEG-BTA as displayed in Figure 2.1a. The mesh size calculated from the high frequency modulus using the theory of rubber elasticity is 8 nm, a value very close to the radius of gyration of 20 kg/mol PEG in water (about 9 nm). Based on this, we attribute this mode to the relaxation of the PEG strands in the system. Furthermore, we have conducted Dynamic Light Scattering measurements (Figures S15, S16) in the dilute regime (0.3 wt %), i.e. very different from the concentration regime where the properties of the networks were investigated (Figs. 2.1,2.2), to show that the BTA-PEG-BTA self-assembles in the dilute regime. The distribution of relaxation times obtained from the Laplace transformation of the intermediate scattering function, using the CONTIN routine[32], shows a unimodal distribution with an apparent hydrodynamic radius of approximately 50 nm, which is larger than the size of the single PEG chain of20 kg/mol as mentioned above, or a unimer of BTA-PEG-BTA (or spherical micelle as discussed below). The presence of the latter cannot be excluded but they are certainly very few since they are not resolved by DLS. Therefore, self-assembly is confirmed and the supramolecular interactions are responsible for the observed behavior and the two hydrogels exhibit markedly distinct viscoelastic signatures.

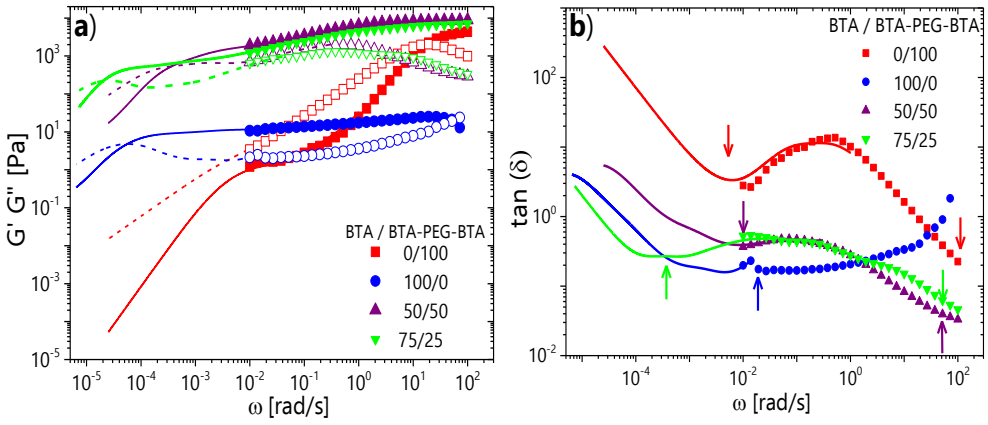

Figure 2.1: a) Linear viscoelastic spectra of the pure components, BTA (blue) and BTA-PEG-BTA (red) and two characteristic compositions of their mixtures, BTA/BTA-PEG-BTA 50/50 (purple) and BTA/BTA-PEG-BTA 75/25 (green) at 5 wt%. Closed circles correspond to the storage moduli while open squares correspond to loss moduli. The lines represent the dynamic moduli obtained from creep measurements, which are inverted to

yield the storage (solid lines) and loss (dashed lines) moduli (see methods). b) Loss factor (tan(δ)) as a function of the frequency. The relaxation processes are shown with arrows. Solid lines represent tan(δ) from creep measurements.

The binary hydrogels formed from BTA and BTA-PEG-BTA (see methods for details) show the emergence of two different modes of relaxation (Figure 2.1 and Figure S13) which ultimately yield two plateau moduli. The two relaxation processes are clearly visible in Figure 2.1b, as minima in the loss factor as a function of frequency. Interestingly, the longest relaxation time, crudely obtained from the low-frequency moduli crossover or the onset of terminal slopes of moduli with frequency, varies with composition. This affects the viscosity in an unexpected manner, because the viscosities of the mixtures are much higher than those of the two pure components, disobeying normal mixing rules[33] (Figure S14). The nonlinear response of the two hydrogels and their mixtures to large-amplitude oscillatory shear confirms their dramatically different dynamics. The BTA-based network exhibits a two-step yielding process and thixotropic response, in contrast to the BTA-PEG-BTA system that is reversible with one yielding process. Interestingly, the mixtures exhibit only one yielding process, reversibility and a much lower yield strain than either of the pure components. Both the yield stress and yield strain exhibit a non-monotonic dependence on composition. Details are provided in the SI (Figure S17). We note however that the nonlinear response requires a separate dedicated study which is beyond the scope of the present investigation.

We now discuss the non-monotonic dependence of the plateau modulus on the composition of the mixture (here represented by the weight fraction of the telechelic component BTA-PEG-BTA), as shown in Figure 2.2. Similar findings have been observed by the group of Messersmith[34], who used similar materials for tissue engineering. In their work they observe the non-monotonicity of mechanical properties with mixing ratio but do not

elucidate its origin. Here, we try to shed light as to why this non-monotonicity is observed in such systems[23,25,34].

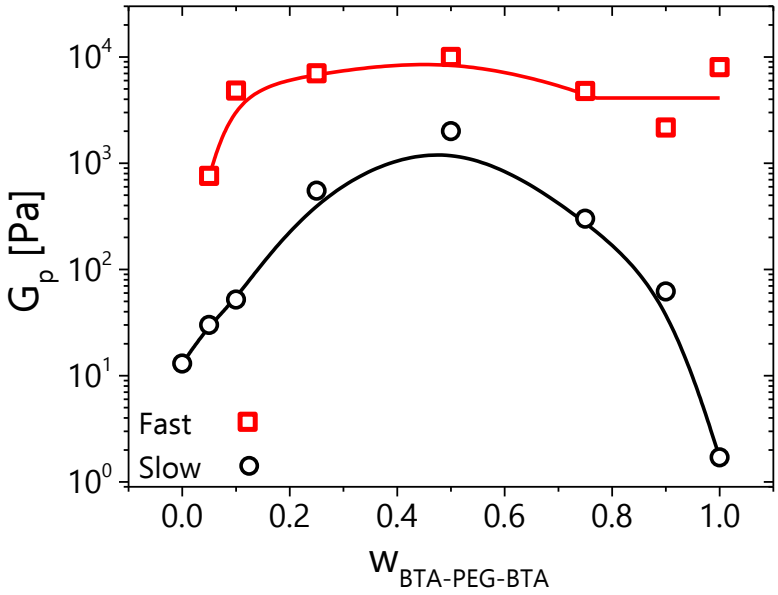

Figure 2.2: Plateau modulus for the high-frequency (fast) and low-frequency (slow) relaxation modes presented in the viscoelastic spectra of the mixtures of Figure 2.1a, plotted against the weight fraction of the telechelic component BTA-PEG-BTA. The values were extracted at the minima of the loss factor tan(δ). Lines are drawn to guide the eye.

To rationalize these findings we first examined whether the supramolecular structures formed at the different mixing ratios can provide insight into the variations in moduli and dynamics. Specifically, a pertinent question is whether the lengths of the supramolecular structures (which will ultimately dictate the relaxation time of the network) as well as the characteristic size of the network (which will ultimately dictate the shear modulus) vary with mixing ratio, and therefore we performed cryo-TEM experiments. Indeed, one can observe a non-monotonic evolution of the characteristic lengths, starting from Figure 2.3a which depicts the network formed by the pure BTA. It is evident that the network comprises very long, persistent fibers as also observed by Leenders et al.[24] The average mesh size of the pure BTA network at a concentration of 582 μM is approximately 50 nm. This value is consistent

with the viscoelastic data, since by applying the theory for networks of semi-flexible chains and subsequent use of the dilution law for the mesh size[35] we obtain a similar value of 53 nm (for a detailed description of this calculation see Figure S18 and relevant discussion). On the other hand, the telechelic hydrogel BTA-PEG-BTA forms a micellar fluid, rather than an entanglement-like polymer network (Figure 2.3d), which yields an elastic response at higher frequencies due to the transient bridges that can be formed by one BTA-PEG-BTA molecule bridging two micelles. At a concentration similar to the one used for rheological measurements (~5wt%), many spherical micelles are observed (5-10 nm in size) along with some elongated objects that are most likely due to bridging between the spherical micelles. This is similar to what has been reported for amphiphilic triblock copolymer solutions[36–38] as well as similar supramolecular systems[25,34]. The contrast in this image originates from the (aggregated) hydrophobic parts of the BTA-PEG-BTA, because the electron density of the hydrated PEG-chain is very similar to the surrounding water. After the preparation of binary networks through the addition of an increasing amount of BTA-PEG-BTA to BTA (Figure 2.3 (b,c) and Figure S19), we observe that the supramolecular fibers become progressively shorter. When 10 mol% of BTA-PEG-BTA is present (Figure 2.3b), it is not possible to distinguish single fibers anymore but instead we observe smaller strands between network junctions. In the 50/50 mixture some short fibers can be observed along with micelles of similar size as in Figure 2.3d. These observations suggest that in the mixtures there is a competition between fiber formation (by BTA) and bridging micelles (by BTA-PEG-BTA), where the BTA units of both components mix. A larger fraction of BTA-PEG-BTA will result in more bridges between micelles but at the same time it will decrease the length of the fibers due to steric effects, i.e., steric hindrance because of the large PEG part of BTA-PEG-BTA that prevents the stacking of many BTA cores on top of one another. The change in the

average size of the assembled structures and the bridging between the fibers are schematically illustrated in Figure 2.4.

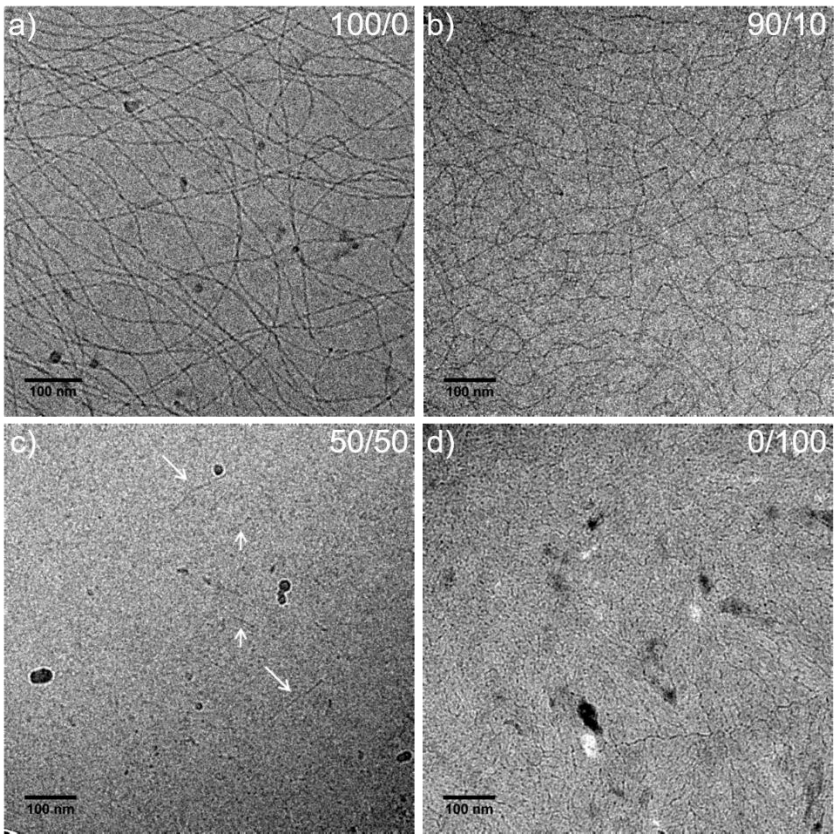

Figure 2.3: Cryo-TEM images from the pure components and different mixtures. In (a) is the network formed from the pure BTA and in (d) is the network formed from the pure BTA-PEG-BTA. In (b) the BTA/BTA-PEG-BTA 90/10 (number fraction of BTA-PEG-BTA: 0.3%) mixture is shown, and in (c) the BTA/BTA-PEG-BTA 50/50 (number fraction of BTA-PEG-BTA: 4.8 %) mixture is shown with white arrows indicating short fibers. In all subfigures the scale bar is 100 nm. The concentration is 582 μM for image (a), 250 μM for image (b), 500 μM for image (c), and 2.2 mM for image (d).

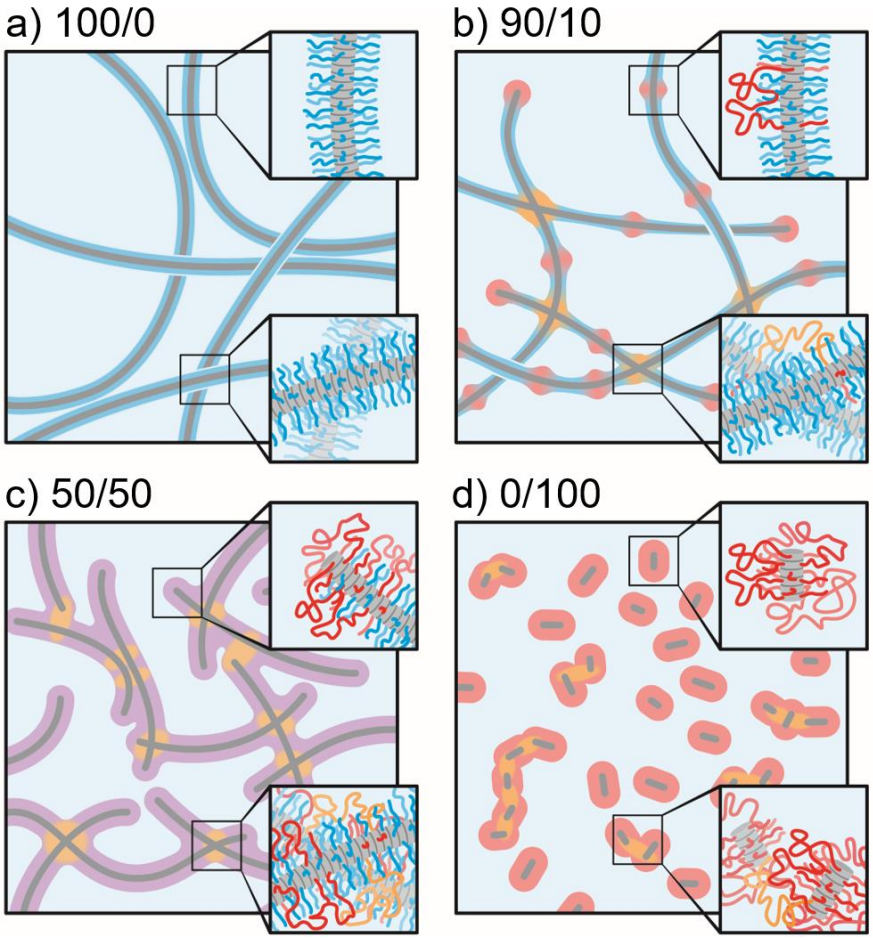

Figure 2.4: Cartoon representations of the supramolecular networks that are formed in the studied hybrid systems, with the hydrophobic part of both molecules coloured in gray, the BTA in cyan, and the BTA-PEG-BTA in red. The PEG-chains of BTA-PEG-BTA that form bridges are coloured orange to be easily distinguishable. Several parts of the networks are enlarged to show individual aggregates (top insets), and interactions between aggregates (bottom insets). In the pure BTA network (a) there is no bridging between the fibers due to the absence of BTA-PEG-BTA and the network is formed only by entanglements of the long fibers. The BTA-PEG-BTA (d) does not form a cohesive network but loosely connected micelles. The mixtures with BTA/BTA-PEG-BTA 90/10 (number fraction of BTA-PEG-BTA: 0.3%) (b) and 50/50 (number fraction of BTA-PEG-BTA: 4.8 %) (c) are characterized by crosslinking between the fibers, which increases when the fraction of BTA-PEG-BTA increases (c), showing PEG bridges as orange lines (bottom insets of b,c). Steric hindrance due to the PEG polymer (detailed in top inset of c) results in shorter fibers with increasing amounts of BTA-PEG-BTA.

We have then investigated the molecular origin of the non-monotonic dependence of the zero-shear viscosity on mixture composition (see Figure S14) that resulted from the mixing of the two compounds, and in particular the interplay between the two different interactions. Recent observations indicated that the telechelic PEG molecules increase the exchange rate of low molecular weight hydrogelators when they are mixed into the supramolecular polymers

formed by the small molecules.[39] The large hydrophilic PEG polymer makes the structures more dynamic, or in other words, decreases the association strength of the small molecules. Consistent with these results, hydrogen/deuterium exchange mass spectrometry (HDX-MS) experiments show that the association between BTAs decreases in the presence of BTA-PEG-BTA (for a detailed description see Figure S20 and Table S1)[40]. Since the association between BTA monomers decreases, they become more dynamic with increasing amounts of BTA-PEG-BTA, hence the average length of the supramolecular polymers should be reduced, as confirmed by the images from cryo-TEM (Figure 2.3). However the value of the viscosity in the mixtures is not determined by the length of the assembly alone, but rather by the complex network resulting from mixing. Actually, the viscosity values of the mixtures rich in BTA (in terms of mass fraction) are much larger than those of pure BTA since the modulus increases by two orders of magnitude, even though the respective relaxation time in most mixtures is shorter as compared to pure BTA (Figure 2.1). On the other hand, the mixtures where BTA-PEG-BTA is in excess, exhibit a larger viscosity value reflecting their much longer relaxation time compared to pure BTA-PEG-BTA.

The experimental system was therefore modelled as a mixture of two different building blocks (beads of diameter d with different association strengths), and an angular potential was applied that dictates the angle formed by three bonded beads depending on the size of the beads using an approach previously developed for colloidal gels[41–43] (for more information, see SI and Figure S21). By changing the association strength, the model comprises two species that, as pure components, self-assemble respectively into a percolated network of semiflexible fibers (I) and into small aggregates between which bonds can break and reform easily (II). Figure 2.5 shows snapshots from the configurations obtained through self-assembly in the molecular dynamics simulations (see SI for more information) for the pure components (Figure 2.5a and d) and for the mixed systems (Figure 2.5b and c) in the

same relative compositions as suggested in Figure 2.4 (here the composition in the numerical simulation samples is expressed in terms of the number fraction of building units that belongs to the strongly associating component (I)). The snapshots show only portion of the simulation box to make distinctive features well visible (see scale bar corresponding to $4d$ in the figure) and demonstrate how the model self-assembled structures, while not including all the complexity of the experimental system, well capture the essential ingredients of the association in the pure components and mixed systems. Furthermore, as discussed in the following, having used non-equilibrium molecular dynamics to compute the viscoelastic spectra of the pure components we could establish also the correspondence between the rheological behavior in simulations and experiments, and therefore used the model to gain insight into the rheological response of the mixed systems. With small amounts of the weaker component (II), we observe additional bridges between the fibers of the main network (Figure 2.5b), formed by the strongly associating units. Once the fraction of the weakly associating unit is increased, the bridging of the fibers is more pronounced and a more tightly connected network seems to develop (Figure 2.5c). The networks of the mixtures shown in Figure 2.5 are reminiscent of double networks investigated in different contexts[44,45], which, however, are usually permanently cross-linked, rubber-like materials with extra reversible interactions such as metal-ligand complexes. Here, instead, all the interactions in our materials are transient which makes the system very dynamic.

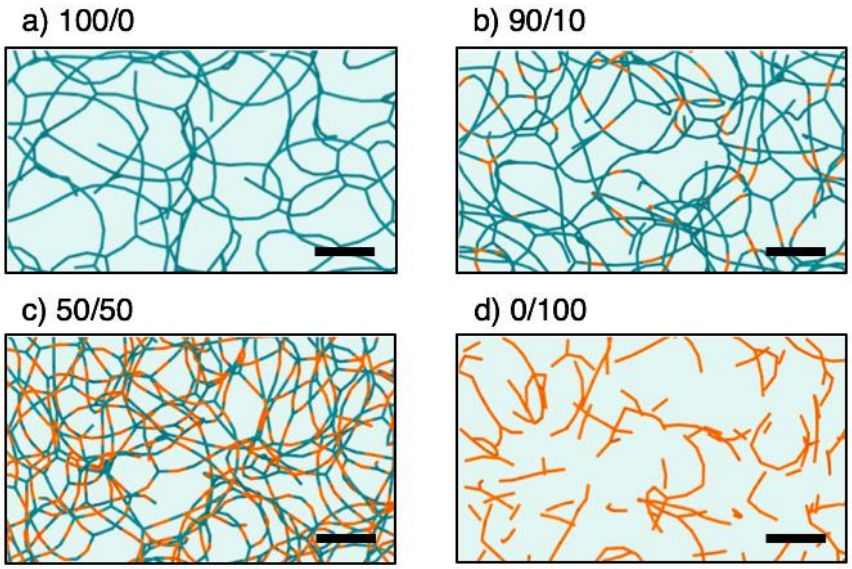

Figure 2.5: Simulation snapshots of structures self-assembled in the molecular dynamics simulations. Grey indicates the strongly associating (entangled) units (pure BTA fibrillar network) while orange indicates the weakly associating units (BTA-PEG-BTA micellar fluid). The entangled network with long fibers formed from the pure model BTA is shown in (a) and the small aggregates obtained from pure model BTA-PEG-BTA in (d). The structure in (b) is obtained with a ratio 90/10, defined by the fraction of pure BTA units, where the micelles of BTA-PEG-BTA form additional connections in the first network and (c) corresponds to a 50/50 mixture with even more connections and effectively shorter fibers. In all subfigures the scale bar is $4d$, with d the diameter of the beads that are used as associating units in the model.

All structures were sheared in silico[42,46] to obtain the viscoelastic spectra of the simulated networks which are shown in Figure 2.6a. To convert the compositions of the mixtures in the model, expressed in terms of the number fraction of the component I associating units, into a weight fraction as used for the experiments, we have to consider that in the real material the self-assembling units of the pure component-II are heavier and have a bigger linear size (≈4 times bigger). Considering the same proportion of two components as in the experiments, we obtain an equivalent weight fraction for each numerical composition, for both components I and II (see also SI). Here and in the following we use the converted weight fraction w_{II}, expressed in terms of component II, consistently with the experimental data of Figure 2.2, to rationalize the non-monotonic dependence of the rheological response on the mixture compositions. The spectrum for the pure component-II is in red and shows

two characteristic relaxation modes, indicated by the red arrows, similar to the pure BTA-PEG-BTA network. The simulations indicate that the high frequency mode corresponds to the relative motion of the nearest neighboring units in each micelle (or aggregate), while the low frequency mode corresponds to the relaxation of the whole aggregate (see SI). In the mixed networks, G' and G'' vary non-monotonically with increasing the weight fraction w_{II}, in analogy to the mixing ratio in the experiments. To map the simulation timescales to the experimental results, we compare the corresponding higher mode relaxation with the experiments and estimate that the highest $\omega\tau_0$ in the simulations should correspond to 10^2 rad/s. By analogy, the range of [10^{-4}-1] $\omega\tau_0$ in the simulations should then correspond to [10^{-2}-10^2] rad/s for ω in the experiments. This allows a fair comparison between the experimental and simulated viscoelastic spectra (Figures 2.1a and 2.6a, respectively).

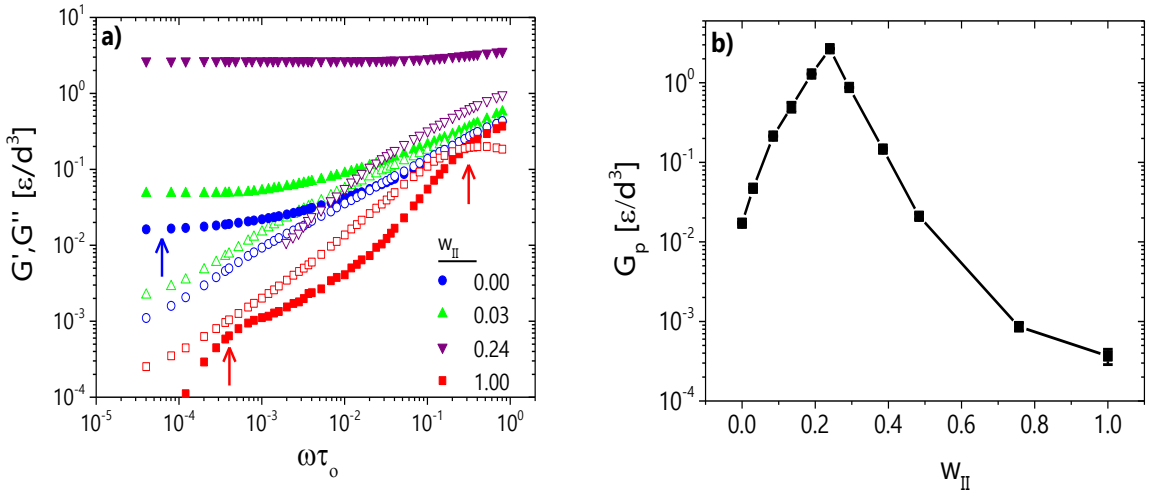

Figure 2.6: (a) The viscoelastic spectra obtained from numerical simulations, for the model mimicking pure BTA and for the model mimicking pure BTA-PEG-BTA, as well as for the mixed networks. Closed symbols indicate the storage modulus (G') and open symbols the loss modulus (G"). Here and in the following plots, error bars are smaller than the symbol size used (see SI). The spectrum for the pure component-I is shown in blue and has a low-frequency plateau in the storage modulus (indicated by a blue arrow), corresponding to the presence of entanglements in the pure BTA network. (b) The low-frequency plateau modulus G_p has a non-monotonic dependence on the mixing ratio w_{II}, as also found in experiments. G_p has a maximum $w_{II,Max} \sim 0.25$. This dependence of G_p on w_{II} can be directly associated with the change in fraction of units forming entanglements and bridges between the fibers in mixed networks, as shown in Figure 2.7(a)).

In Figure 2.6, the moduli are plotted using the reduced units of the simulation model, i.e. ε/d^3, where ε is the interaction strength between units of component-I and d is the diameter of the coarse-grained associating units. To convert the modulus units to real units, we consider that the modulus at crossover frequency of the pure component-II in the simulations is approximately equal to that of the pure BTA-PEG-BTA in the experiment, i.e., we can set $10^{-1}\ \varepsilon/d^3 \approx 10^3$Pa (see Figures 2.1a and 2.6b). This would correspond, for example, to $d \approx 10$nm and $\varepsilon \approx 10kT$ (considering $kT \approx 10^{-20}$J). For the size of coarse-grained units, $d \approx 10$nm seems also a reasonable length-scale since the average mesh size of the pure BTA network in the experiment is about 7nm (see eq. 3 in SI) and the average mesh size of the entangled network of component-I in the simulation is about $2d$ [41]. With this conversion, the values of the moduli obtained in the simulations of the model systems would vary between 1 Pa and 10^4 Pa, which is consistent with the experiments (see Figures 2.1a and 2.2).

From the analysis of the linear viscoelastic spectra obtained by simulations, we extract the dependence of the moduli on the fraction of components. As shown in Figure 2.6b, the plateau modulus from simulations exhibits a non-monotonic behavior with the mixing ratio as well. Indeed, the plateau modulus reaches a maximum at 0.25 weight fraction. While the simple coarse-grained model used in the simulations (see SI) cannot capture the full chemical complexity of the experimental system, the results obtained do capture qualitatively the rheological response of the mixtures, and therefore give the opportunity to investigate its microscopic origin, offering a potentially powerful tool for designing materials described with this kind of interactions. In fact, more information regarding the non-monotonicity can be obtained from the simulations by assessing how the additional bridges formed by the BTA-PEG-BTA in the pure BTA network vary with the mixing ratio. We do this by computing the number of first neighbors of particles (coordination number) in the

simulation box, for each particle, and track how many of them have a coordination number of two (meaning that they are embedded in a fiber) or coordination number of three (i.e. forming entanglements or bridges) as we vary the mixing ratio. In Figure 2.7a, we show the total number of particles with a coordination number three normalized by the total number of particles and the same is done for their presence in each component separately. The fraction of units forming entanglements and bridges between the fibers increases with increasing w_{II} and has a maximum at $w_{II,max} \sim 0.25$, where the maximum in the modulus is observed. When further increasing w_{II}, component-II (pure BTA-PEG-BTA) plays a dominant role in the structure of the mixture and there are less and less fibers available from component-I (pure BTA) to form additional bridges. As a consequence, the modulus of these mixed networks is mainly (or only) due to the entanglements in component-I, which progressively decrease with increasing w_{II} (see Figure 2.7a). Consistently, with increasing w_{II}, the fraction of units forming fibers of component-I continuously decreases (Figure 2.7b) while the respective fraction for component-II that go into small aggregates (i.e., that do not form bridges with component-I) continuously increases. One can see from the plot that the latter increase faster with w_{II} for $w_{II} > w_{II,\,max}$, and therefore the sum of the units that do not participate in entanglements or bridges has a non-monotonic dependence on w_{II}. At large w_{II}, the mixture consists mainly of small linear aggregates of component-II, which reduces the modulus.

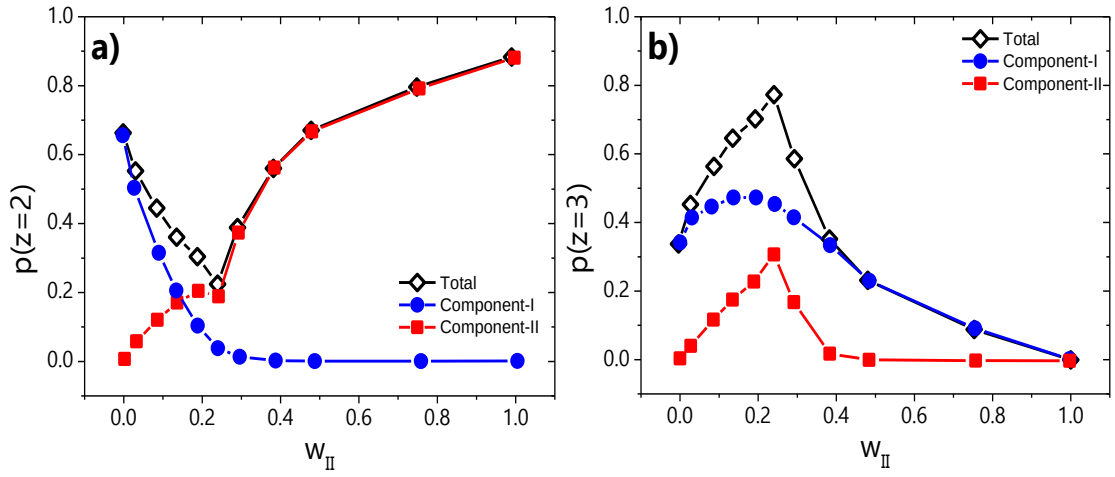

Figure 2.7: Fraction p(z) of units in the two components with a specific coordination number (z) as a function of w_{II}. (a)Fraction of particles forming fibers (z=2). (b) Fraction of particles forming crosslinks (z=3)**.** The units with z = 2 are those that only participates to fibers (component-I) or small linear aggregates (component-II). The units with z = 3 in the component-I correspond to entanglements while units with z = 3 in the component-II correspond to bridges between the fibers of component-I in the mixed network. We use blue circles for the fraction in component-I, red squares for the fraction in component-II, and black diamonds for their sum for a specific z.

These results well elucidate how the competitive association of the BTA-PEG-BTA micelles into the pure BTA fibrillar network depends on the relative composition and therefore controls the resulting non-monotonic dependence of the viscoelastic response on the mixing ratio.

Lastly, we briefly discuss the observation that in the experimental spectra there are two main modes dictating the dynamics (see Figure 2.1a). It is beyond the scope of this study to interpret these in detail, and this will be addressed in the future. Here, we limit the discussion to simple observations and speculate that the complexity in the dynamics of the system originates from the fact that such systems have been shown to have a distribution of monomer exchange times. Put more simply, in such systems there is always an exchange of monomers between supramolecular polymers, however because the self-assembly is not perfect there is local disorder in the structures. There are defects along the fibers, which lead to 'exchange hot-spots' along the fibers[28] that causes a distribution of exchange times. It is reasonable to assume that this is also true for the BTA-PEG-BTA molecule, thus one may think of a situation where there are some bridges that open much faster than the rest, and this could explain why in the mixtures there are two dominant modes. If we use the two predominant models for the dynamics of associating polymers, the supramolecular wormlike model[16] and the sticky reptation model[47], once a bridge is lost the fiber is free to reptate, but it can also break while it reptates, which may or may not lead to more bridges to be released, and so on and so forth. This centipede-like response[48] would lead to a very complex time distribution which is beyond our present capabilities to model.

4. Conclusions

In conclusion, by using state-of-the-art chemistry and a powerful combination of dynamic experiments (rheology) and simulations we have proposed a two-component hydrogel system, comprising two different supramolecular molecules based on the same hydrogen bonding motif, that exhibits a non-monotonic mechanical and structural response by changing the mixing ratio. This study sheds light as to why such two-component supramolecular systems, based on the same motif with different internal structure, forming long topologically entangled fibrils (BTA) and short bridged fibrils (BTA-PEG-BTA), can exhibit a non-monotonic evolution of mechanical properties upon mixing. This bares similarities with wormlike micelles mixed with hydrophobically modified polymers[17] and differs from wormlike micelles mixed with amphiphilic chains[19], however both systems are very different from the present binary hydrogel. With the help of simulations, we have shown that the competitive interactions (making the structure more dynamic and essentially weakening, on average, the association between units) lead to the non-monotonicity in the modulus. In addition, these results illustrate how a counterintuitive increase in the modulus can result from the addition of a weakly interacting supramolecular motif to a more stable entangled network of polymers. By simulating these systems in the simplest possible way as a mixture of two species, one strongly associating into semiflexible entangled fibers and one weakly associating into small micelles we are able to reproduce the non-monotonic evolution of the viscoelastic shear modulus with mixing ratio. The fact that this feature is captured by a simple coarse-grained model suggests that the association strength and the ability to create additional bridges can be the main characteristics to focus on for material design in a variety of different chemical compounds, although more work will be needed in this direction (for example, to examine the role of the internal flexibility of the motif). Hence the approach developed here, combining macroscopic (rheology) and microscopic (cryo-TEM)

experiments with appropriate coarse-grained simulations can elucidate the origin of the reported non-monotonicity in viscoelastic properties and help identify which ingredients are the most important for material design and help further guide the chemical synthesis or the exploration of new compounds. With this in mind, the work discussed here could inspire new ways to carefully tune the properties of two-component gels based only on the binding strength of the two units, e.g., in mixed networks based on peptides, block copolymers or DNA origami rods with telechelic connectors for the design of biomaterials[34], or to understand similar processes in nature, e.g., the crosslinking of macromolecular F-actin chains, composed of G-actin monomers, by actin-binding proteins, such as α-actinin[49,50]. The non-covalent interactions of these proteins promote their hierarchical organization into kinetically trapped gel-like materials in the cytosol. Intriguingly, assemblies of actin filaments have been observed at exceedingly low molar ratios of cross-linker protein, such as 1:90 in α-actinin/G-actin.

References

(1) Lehn, J.-M. Perspectives in Supramolecular Chemistry—From Molecular Recognition towards Molecular Information Processing and Self-Organization. *Angew. Chem. Int. Ed. Engl.* **1990**, *29* (11), 1304–1319. https://doi.org/10.1002/anie.199013041.

(2) Meijer, E. W.; Aida, T. Supramolecular Polymers, We've Come Full Circle. *Isr. J. Chem.* **2019**.

(3) Aida, T.; Meijer, E. W.; Stupp, S. I. Functional Supramolecular Polymers. *Science* **2012**, *335* (6070), 813–817. https://doi.org/10.1126/science.1205962.

(4) Webber, M. J.; Appel, E. A.; Meijer, E. W.; Langer, R. Supramolecular Biomaterials. *Nat. Mater.* **2016**, *15* (1), 13–26. https://doi.org/10.1038/nmat4474.

(5) Du, X.; Zhou, J.; Shi, J.; Xu, B. Supramolecular Hydrogelators and Hydrogels: From Soft Matter to Molecular Biomaterials. *Chem. Rev.* **2015**, *115* (24), 13165–13307. https://doi.org/10.1021/acs.chemrev.5b00299.

(6) Sijbesma, R. P.; Beijer, F. H.; Brunsveld, L.; Folmer, B. J. B.; Hirschberg, J. H. J. K.; Lange, R. F. M.; Lowe, J. K. L.; Meijer, E. W. Reversible Polymers Formed from Self-Complementary Monomers Using Quadruple Hydrogen Bonding. *Science* **1997**, *278* (5343), 1601–1604.

(7) Coleman, M.; Painter, P. Hydrogen Bonded Polymer Blends. *Prog. Polym. Sci.* **1995**, *20* (1), 1–59. https://doi.org/10.1016/0079-6700(94)00038-4.

(8) Yang, Z.; Han, C. D. Rheology of Miscible Polymer Blends with Hydrogen Bonding. *Macromolecules* **2008**, *41* (6), 2104–2118. https://doi.org/10.1021/ma7025385.

(9) Cai, H.; Ait-Kadi, A.; Brisson, J. Dynamic Rheological Analysis of a Miscible Blend Showing Strong Interactions. *Polymer* **2003**, *44* (5), 1481–1489. https://doi.org/10.1016/S0032-3861(03)00019-3.
(10) Miyata, H.; Yamaguchi, M.; Akashi, M. Structure and Viscoelastic Properties of Amorphous Ethylene/1-Hexene Copolymers Obtained with Metallocene Catalyst. *Polymer* **2001**, *42* (13), 5763–5769. https://doi.org/10.1016/S0032-3861(00)00936-8.
(11) Carella, J. M.; Graessley, W. W.; Fetters, L. J. Effects of Chain Microstructure on the Viscoelastic Properties of Linear Polymer Melts: Polybutadienes and Hydrogenated Polybutadienes. *Macromolecules* **1984**, *17* (12), 2775–2786. https://doi.org/10.1021/ma00142a059.
(12) Aamer, K. Rheological Studies of PLLA–PEO–PLLA Triblock Copolymer Hydrogels. *Biomaterials* **2004**, *25* (6), 1087–1093. https://doi.org/10.1016/S0142-9612(03)00632-X.
(13) Breedveld, V.; Nowak, A. P.; Sato, J.; Deming, T. J.; Pine, D. J. Rheology of Block Copolypeptide Solutions: Hydrogels with Tunable Properties. *Macromolecules* **2004**, *37* (10), 3943–3953. https://doi.org/10.1021/ma049885f.
(14) Pham, Q. T.; Russel, W. B.; Thibeault, J. C.; Lau, W. Micellar Solutions of Associative Triblock Copolymers: The Relationship between Structure and Rheology. *Macromolecules* **1999**, *32* (15), 5139–5146. https://doi.org/10.1021/ma990215x.
(15) He, Y.; Lodge, T. P. Thermoreversible Ion Gels with Tunable Melting Temperatures from Triblock and Pentablock Copolymers. *Macromolecules* **2008**, *41* (1), 167–174. https://doi.org/10.1021/ma702014z.
(16) Cates, M. E. Reptation of Living Polymers: Dynamics of Entangled Polymers in the Presence of Reversible Chain-Scission Reactions. *Macromolecules* **1987**, *20* (9), 2289–2296. https://doi.org/10.1021/ma00175a038.
(17) Couillet, I.; Hughes, T.; Maitland, G.; Candau, F. Synergistic Effects in Aqueous Solutions of Mixed Wormlike Micelles and Hydrophobically Modified Polymers. *Macromolecules* **2005**, *38* (12), 5271–5282. https://doi.org/10.1021/ma0501592.
(18) Gouveia, L. M.; Müller, A. J. The Effect of NaCl Addition on the Rheological Behavior of Cetyltrimethylammonium P-Toluenesulfonate (CTAT) Aqueous Solutions and Their Mixtures with Hydrophobically Modified Polyacrylamide Aqueous Solutions. *Rheol. Acta* **2009**, *48* (2), 163–175. https://doi.org/10.1007/s00397-008-0319-7.
(19) Nakaya–Yaegashi, K.; Ramos, L.; Tabuteau, H.; Ligoure, C. Linear Viscoelasticity of Entangled Wormlike Micelles Bridged by Telechelic Polymers: An Experimental Model for a Double Transient Network. *J. Rheol.* **2008**, *52* (2), 359–377. https://doi.org/10.1122/1.2828645.
(20) Besenius, P. Controlling Supramolecular Polymerization through Multicomponent Self-Assembly. *J. Polym. Sci. Part Polym. Chem.* **2017**, *55* (1), 34–78. https://doi.org/10.1002/pola.28385.
(21) Thota, B. N. S.; Lou, X.; Bochicchio, D.; Paffen, T. F. E.; Lafleur, R. P. M.; van Dongen, J. L. J.; Ehrmann, S.; Haag, R.; Pavan, G. M.; Palmans, A. R. A.; Meijer, E. W. Supramolecular Copolymerization as a Strategy to Control the Stability of Self-Assembled Nanofibers. *Angew. Chem. Int. Ed.* **2018**, *57* (23), 6843–6847. https://doi.org/10.1002/anie.201802238.
(22) Appel, R.; Fuchs, J.; Tyrrell, S. M.; Korevaar, P. A.; Stuart, M. C. A.; Voets, I. K.; Schönhoff, M.; Besenius, P. Steric Constraints Induced Frustrated Growth of Supramolecular Nanorods in Water. *Chem. - Eur. J.* **2015**, *21* (52), 19257–19264. https://doi.org/10.1002/chem.201503616.
(23) Kieltyka, R. E.; Pape, A. C. H.; Albertazzi, L.; Nakano, Y.; Bastings, M. M. C.; Voets, I. K.; Dankers, P. Y. W.; Meijer, E. W. Mesoscale Modulation of Supramolecular Ureidopyrimidinone-Based Poly(Ethylene Glycol) Transient Networks in Water. *J. Am. Chem. Soc.* **2013**, *135* (30), 11159–11164. https://doi.org/10.1021/ja403745w.
(24) Leenders, C. M. A.; Mes, T.; Baker, M. B.; Koenigs, Marcel. M. E.; Besenius, P.; Palmans, A. R. A.; Meijer, E. W. From Supramolecular Polymers to Hydrogel Materials. *Mater Horiz* **2014**, *1* (1), 116–120. https://doi.org/10.1039/C3MH00103B.
(25) Noteborn, W. E. M.; Zwagerman, D. N. H.; Talens, V. S.; Maity, C.; van der Mee, L.; Poolman, J. M.; Mytnyk, S.; van Esch, J. H.; Kros, A.; Eelkema, R.; Kieltyka, R. E.

Crosslinker-Induced Effects on the Gelation Pathway of a Low Molecular Weight Hydrogel. *Adv. Mater.* **2017**, *29* (12), 1603769. https://doi.org/10.1002/adma.201603769.
(26) Leenders, C. M. A.; Albertazzi, L.; Mes, T.; Koenigs, M. M. E.; Palmans, A. R. A.; Meijer, E. W. Supramolecular Polymerization in Water Harnessing Both Hydrophobic Effects and Hydrogen Bond Formation. *Chem. Commun.* **2013**, *49* (19), 1963. https://doi.org/10.1039/c3cc38949a.
(27) Bochicchio, D.; Pavan, G. M. Effect of Concentration on the Supramolecular Polymerization Mechanism via Implicit-Solvent Coarse-Grained Simulations of Water-Soluble 1,3,5-Benzenetricarboxamide. *J. Phys. Chem. Lett.* **2017**, *8* (16), 3813–3819. https://doi.org/10.1021/acs.jpclett.7b01649.
(28) Bochicchio, D.; Salvalaglio, M.; Pavan, G. M. Into the Dynamics of a Supramolecular Polymer at Submolecular Resolution. *Nat. Commun.* **2017**, *8* (1). https://doi.org/10.1038/s41467-017-00189-0.
(29) Khatory, A.; Lequeux, F.; Kern, F.; Candau, S. J. Linear and Nonlinear Viscoelasticity of Semidilute Solutions of Wormlike Micelles at High Salt Content. *Langmuir* **1993**, *9* (6), 1456–1464. https://doi.org/10.1021/la00030a005.
(30) Cates, M. E.; Candau, S. J. Statics and Dynamics of Worm-like Surfactant Micelles. *J. Phys. Condens. Matter* **1990**, *2* (33), 6869–6892. https://doi.org/10.1088/0953-8984/2/33/001.
(31) Louhichi, A.; Jacob, A. R.; Bouteiller, L.; Vlassopoulos, D. Humidity Affects the Viscoelastic Properties of Supramolecular Living Polymers. *J. Rheol.* **2017**, *61* (6), 1173–1182. https://doi.org/10.1122/1.4997600.
(32) Provencher, S. W. CONTIN: A General Purpose Constrained Regularization Program for Inverting Noisy Linear Algebraic and Integral Equations. *Comput. Phys. Commun.* **1982**, *27* (3), 229–242. https://doi.org/10.1016/0010-4655(82)90174-6.
(33) Irving, J. B. *Viscosities of Binary Liquid Mixtures: A Survey of Mixture Equations; Report No. 630*; National Engineering Laboratory: East Kilbridge, Glasgow, U.K., 1977.
(34) Cheng, J.; Amin, D.; Latona, J.; Heber-Katz, E.; Messersmith, P. B. Supramolecular Polymer Hydrogels for Drug-Induced Tissue Regeneration. *ACS Nano* **2019**, *13* (5), 5493–5501. https://doi.org/10.1021/acsnano.9b00281.
(35) MacKintosh, F. C.; Käs, J.; Janmey, P. A. Elasticity of Semiflexible Biopolymer Networks. *Phys. Rev. Lett.* **1995**, *75* (24), 4425–4428. https://doi.org/10.1103/PhysRevLett.75.4425.
(36) Annable, T.; Buscall, R.; Ettelaie, R.; Whittlestone, D. The Rheology of Solutions of Associating Polymers: Comparison of Experimental Behavior with Transient Network Theory. *J. Rheol.* **1993**, *37* (4), 695–726. https://doi.org/10.1122/1.550391.
(37) Watanabe, H.; Sato, T.; Osaki, K.; Yao, M.-L.; Yamagishi, A. Rheological and Dielectric Behavior of a Styrene−Isoprene−Styrene Triblock Copolymer in Selective Solvents. 2. Contribution of Loop-Type Middle Blocks to Elasticity and Plasticity. *Macromolecules* **1997**, *30* (19), 5877–5892. https://doi.org/10.1021/ma9617577.
(38) Watanabe, H.; Matsumiya, Y.; Sawada, T.; Iwamoto, T. Rheological and Dielectric Behavior of Dipole-Inverted (SIS) $_p$ -Type Multiblock Copolymers: Estimates of Bridge/Loop Fractions for Respective I Blocks and Effect of Loops on High Extensibility of Bridges. *Macromolecules* **2007**, *40* (19), 6885–6897. https://doi.org/10.1021/ma0712495.
(39) Hendrikse, S. I. S.; Wijnands, S. P. W.; Lafleur, R. P. M.; Pouderoijen, M. J.; Janssen, H. M.; Dankers, P. Y. W.; Meijer, E. W. Controlling and Tuning the Dynamic Nature of Supramolecular Polymers in Aqueous Solutions. *Chem Commun* **2017**, *53* (14), 2279–2282. https://doi.org/10.1039/C6CC10046E.
(40) Lou, X.; Lafleur, R. P. M.; Leenders, C. M. A.; Schoenmakers, S. M. C.; Matsumoto, N. M.; Baker, M. B.; van Dongen, J. L. J.; Palmans, A. R. A.; Meijer, E. W. Dynamic Diversity of Synthetic Supramolecular Polymers in Water as Revealed by Hydrogen/Deuterium Exchange. *Nat. Commun.* **2017**, *8* (1), 15420. https://doi.org/10.1038/ncomms15420.
(41) Colombo, J.; Del Gado, E. Self-Assembly and Cooperative Dynamics of a Model Colloidal Gel Network. *Soft Matter* **2014**, *10* (22), 4003. https://doi.org/10.1039/c4sm00219a.
(42) Colombo, J.; Del Gado, E. Stress Localization, Stiffening, and Yielding in a Model Colloidal Gel. *J. Rheol.* **2014**, *58* (5), 1089–1116. https://doi.org/10.1122/1.4882021.

(43) Bouzid, M.; Gado, E. D. Mechanics of Soft Gels: Linear and Nonlinear Response. In *Handbook of Materials Modeling: Applications: Current and Emerging Materials*; Andreoni, W., Yip, S., Eds.; Springer International Publishing: Cham, 2018; pp 1–29. https://doi.org/10.1007/978-3-319-50257-1_129-1.
(44) Gong, J. P.; Katsuyama, Y.; Kurokawa, T.; Osada, Y. Double-Network Hydrogels with Extremely High Mechanical Strength. *Adv. Mater.* **2003**, *15* (14), 1155–1158. https://doi.org/10.1002/adma.200304907.
(45) Filippidi, E.; Cristiani, T. R.; Eisenbach, C. D.; Waite, J. H.; Israelachvili, J. N.; Ahn, B. K.; Valentine, M. T. Toughening Elastomers Using Mussel-Inspired Iron-Catechol Complexes. *Science* **2017**, *358* (6362), 502–505. https://doi.org/10.1126/science.aao0350.
(46) Bouzid, M.; Keshavarz, B.; Geri, M.; Divoux, T.; Del Gado, E.; McKinley, G. H. Computing the Linear Viscoelastic Properties of Soft Gels Using an Optimally Windowed Chirp Protocol. *J. Rheol.* **2018**, *62* (4), 1037–1050. https://doi.org/10.1122/1.5018715.
(47) Leibler, L.; Rubinstein, M.; Colby, R. H. Dynamics of Reversible Networks. *Macromolecules* **1991**, *24* (16), 4701–4707. https://doi.org/10.1021/ma00016a034.
(48) Baeza, G. P.; Dessi, C.; Costanzo, S.; Zhao, D.; Gong, S.; Alegria, A.; Colby, R. H.; Rubinstein, M.; Vlassopoulos, D.; Kumar, S. K. Network Dynamics in Nanofilled Polymers. *Nat. Commun.* **2016**, *7* (1), 11368. https://doi.org/10.1038/ncomms11368.
(49) Pelletier, O.; Pokidysheva, E.; Hirst, L. S.; Bouxsein, N.; Li, Y.; Safinya, C. R. Structure of Actin Cross-Linked with α -Actinin: A Network of Bundles. *Phys. Rev. Lett.* **2003**, *91* (14), 148102. https://doi.org/10.1103/PhysRevLett.91.148102.
(50) Lieleg, O.; Claessens, M. M. A. E.; Bausch, A. R. Structure and Dynamics of Cross-Linked Actin Networks. *Soft Matter* **2010**, *6* (2), 218–225. https://doi.org/10.1039/B912163N.
(51) Ferry, J. D. *Viscoelastic Properties of Polymers*; Wiley: New York: NY, 1980.
(52) Honerkamp, J.; Weese, J. A Nonlinear Regularization Method for the Calculation of Relaxation Spectra. *Rheol. Acta* **1993**, *32* (1), 65–73. https://doi.org/10.1007/BF00396678.
(53) Del Gado, E.; Kob, W. A Microscopic Model for Colloidal Gels with Directional Effective Interactions: Network Induced Glassy Dynamics. *Soft Matter* **2010**, *6* (7), 1547. https://doi.org/10.1039/b916813c.
(54) Plimpton, S. Fast Parallel Algorithms for Short-Range Molecular Dynamics. *J. Comput. Phys.* **1995**, *117* (1), 1–19. https://doi.org/10.1006/jcph.1995.1039.
(55) Geri, M.; Keshavarz, B.; Divoux, T.; Clasen, C.; Curtis, D. J.; McKinley, G. H. Time-Resolved Mechanical Spectroscopy of Soft Materials via Optimally Windowed Chirps. *Phys. Rev. X* **2018**, *8* (4), 041042. https://doi.org/10.1103/PhysRevX.8.041042.

Chapter 3. Traces of water in oils mediates the viscoelasticity of supramolecular assemblies in oils

I. Introduction

Gels, as defined by Flory four decades ago[1], are formed by the cross-linking of units randomly distributed in space forming a 3D network (e.g. vulcanized rubber). This has been the accepted paradigm for gels[2], however in the last twenty years a new category of molecular gels has drawn attention[3,4]. These gels comprise aqueous (hydrogels) or organic solvents (organogels) immobilized at small concentrations of compounds that self-assemble into high aspect ratio fibers exhibiting polymer-like properties[5]. These compounds are called low molecular weight organic gelators (LMOGs) and usually are small organic molecules[6–8], peptides[9] or surfactants[10–12]. Typically, the cross-linking in the traditional sense, as in the definition of Flory, does not exist and the gel is usually formed through topological interactions reminiscent of entanglements or reversible associations[13–18]. In contrast to permanently cross-linked networks, these molecular gels exhibit elasticity transiently and ultimately relax in a similar fashion to viscoelastic liquids such as polymer melts and high concentration solutions[2]. The stress relaxation dynamics of the material strongly depend on the lifetime of the reversible associations [19–21]. Specifically for the case of entangled living polymers, which are essentially organogels formed purely by the topological constraints of the supramolecular polymers, the characteristic time of reversible scission/recombination that living polymers undergo and how it compares to the reptation time dictates how the stresses will be relaxed[21].

Such supramolecular organogelators have been proposed for several applications in the pharmaceutical industry[22], cosmetics industry[23], art conservation[24] or in biomaterials, nanoelectronics and catalysis[25,26]. Alkanes are widely used as solvents in supramolecular chemistry and recently the effect trace amounts of water present in organic oils[27] was

reported to have a significant effect on the structure and viscoelasticity of the supramolecular polymers[28,29]. Specifically, Van Zee et al.[28] found that hydrogen bonding supramolecular moieties forming long 1D helical assemblies undergo structural changes (helicity changes accompanied by a drop of light scattering intensity) in dodecane by varying temperature due the presence of water in the monomeric state[30] . It was suggested, and confirmed by DFT calculations that water molecules have enthalpic energy in the form of unrealized hydrogen bonds that acts as a thermodynamic driving force to interact with the supramolecular compounds existing in the solution. Earlier, Louhichi et al.[29] had shown that the presence of humidity affects the viscoelasticity of hydrogen bonded living polymers made by 2,4 bis (Ethyl Hexyl Ureido) Toluene (EHUT). It was shown that without drying, the terminal relaxation time is much smaller compared to that under dry conditions while the plateau modulus of the network is weakly affected. The non-linear viscoelasticity was also shown to be sensitive to humidity. Under ambient conditions the solution exhibited shear strain stiffening which however was much weaker compared to the dry case. The results corroborated the hypothesis that water acts as a chain stopper, halting the growth of the EHUT supramolecular polymer and broadening the molecular weight distribution.

Based on the above developments, the need to understand the role water plays on the self-assembly of supramolecular organogelators in alkanes and how it can affect the properties of the resulting gel emerges. Inspired by these two works, we seek the repercussions the structural transitions in the work by Van Zee et al.[28] on the viscoelasticity of self-assemblies formed by the biphenyl tetracarboxamide (**BPTA**) supramolecular compound. We study the system under controlled humidity conditions using a combination of circular dichroism (CD), static light scattering (SLS) and oscillatory rheology. Our findings show that we can achieve similar variation of the linear viscoelasticity of the network by varying temperature or humidity. We find that the terminal relaxation time of the material

depends strongly on the humidity as also shown by Louhichi et al[29] however, the transition from the wet to the dry state is accompanied by a strong variation of the concentration dependence suggesting a fundamental change on the dynamics of the system. On the other hand the modulus of the network is barely affected by humidity. These results indicate universal behavior of this type of supramolecular polymers.

II. Materials and Methods

II.1 Experimental System

The biphenyl tetracarboxamide (**BPTA)** compound (Scheme 1) has been synthesized as previously reported[28].

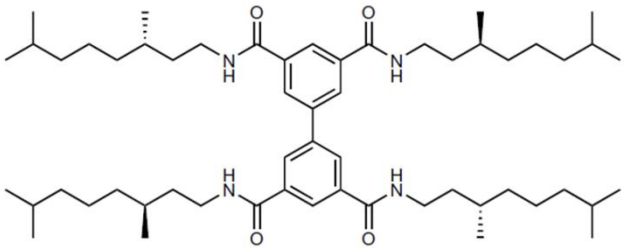

Scheme 3.1 Chemical structure of BPTA.

The solvent used for sample preparation was n-dodecane (>99%) from Alfa Aesar ™.

II.2 Humidity Control

To tailor and control the humidity, a chamber was designed, inspired by Louhichi et al.[29] comprising four stages (Scheme 3.2). Relative humidity (RH) levels were measured with a humidity probe(Testo 645/445;Testo, Germany) while drying of the chamber is achieved through initially saturating the N_2 gas in the chamber (black) and is maintained by P_2O_5 to levels lower than 5% RH for at least 24h (Figure 3.1). The following protocol was used: Sample is loaded before the drying process starts. The time that the trap can sustain RH <5% depends on the humidity of the lab as well as the amount of drying agent. Typically, for 1 g

of drying agent and room RH 40% the humidity in the chamber can be maintained below 5% for 72 hours. For certain humidity levels, a saturated salt solution[31] is used instead of dry P_2O_5 and no N_2 is inserted in the chamber.

Phosphorous pentoxide (P_2O_5 >98%) from Sigma-Aldrich was stored under dry conditions (RH < 10%). The saturated salt solutions were contained sodium chloride (NaCl >99%) and lithium chloride (LiCl >99%) from Sigma-Aldrich. The solvent used for sealing is the same as the one used for sample preparation.

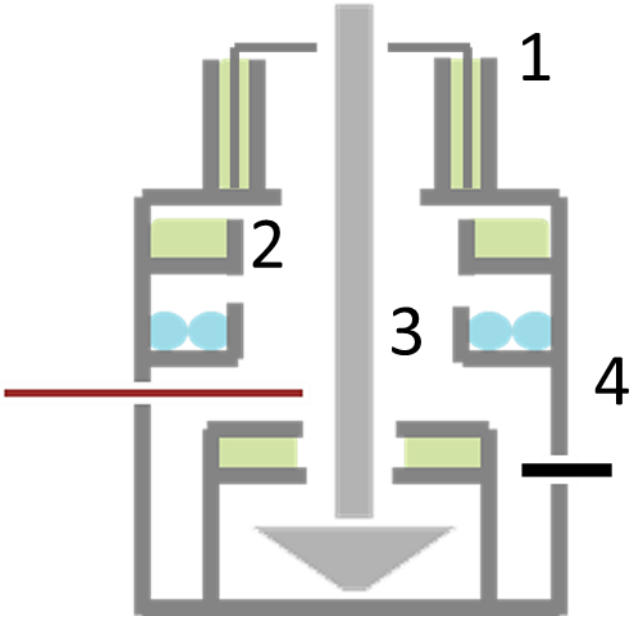

Scheme 3.2 Chamber for humidity control. Chamber is made by stainless steel and consists of four stages. From top to bottom: 1) Sealing ring filled with dodecane (green) and sealing cap 2) Ring filled with cotton drenched with dodecane 3) Ring filled with saturated salt solution or solid salt (cyan) for humidity control 4) Solvent trap used to stop air flow from directly contacting the sample filled with cotton drenched in dodecane. The dodecane in the trap is used to saturate the environment with dodecane vapor to reduce evaporation. Humidity Probe (dark red), N_2 gas nozzle (black).

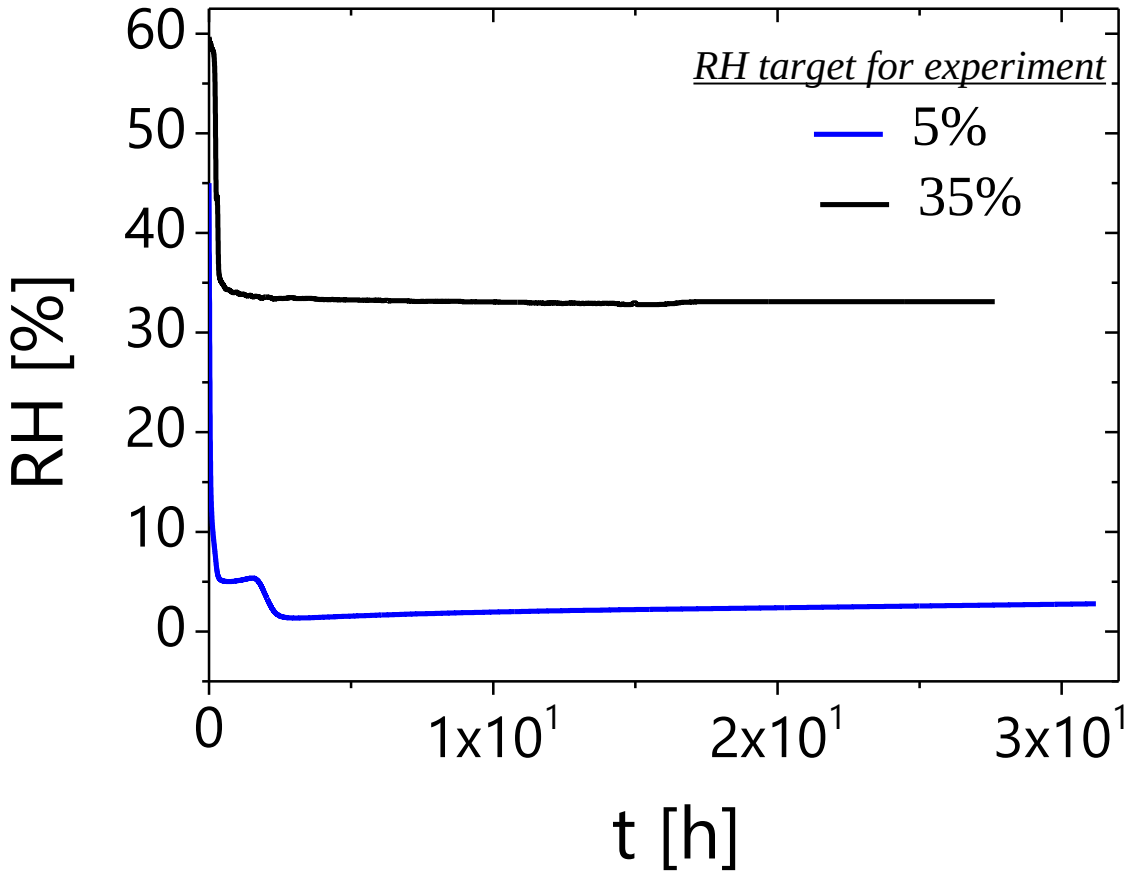

Figure 3.1 Evolution of Relative Humidity (RH) in the drying chamber with time. Black line corresponds to target RH 35% (achieved: 33%) and blue line corresponds to target RH 5% (achieved: 3.5%).

II.3 Oscillatory Rheology

Rheological measurements were performed with an Anton-Paar (Austria) Physica MCR-501 rheometer, operating in the strain-controlled mode, equipped with a Peltier unit for temperature control, which also constitutes the bottom plate, and a top cone geometry. All metallic components were stainless steel. We used four different cones, of diameter (angle), 8 mm (α=1°), 12.5 mm (α=1°), 25 mm (α=2°) and 50 mm (α=2°) in order to increase the torque signal as needed. For the lower concentration samples (less than 5 g/l) a stainless steel Couette geometry (bob diameter=16.5 mm, cup diameter=17.0 mm, bob length=13.0 mm) was used on a strain controlled ARES 100 FRTN1 rheometer (TA USA). Samples were

loaded at the desired temperature and immediately "isolated" with the humidity chamber described previously. After successful loading and equilibration, we performed a rheological rejuvenation test to erase the sample's history due to preparation and loading on the measuring stage. The rejuvenation protocol consists of a dynamic time sweep test at a fixed nonlinear strain, typically 700%, and fixed oscillatory frequency (1 rad/s) for a given time until full liquid-like behavior of the system is reached (typically 300 s). Afterwards, the aging kinetics was followed with consecutive dynamic frequency sweep tests (DFS) in the linear viscoelastic regime and measurements were done after the sample has reached its mechanical steady-state. The linear viscoelastic regime is determined by dynamic strain sweep tests (DSS) and is defined as the regime in which the dynamic moduli are independent of the applied strain amplitude. Creep measurements (step stress), typically used to study materials with solid-like or very slow flow response and were used for the higher concentration samples. When the applied stress is within the linear viscoelastic regime, then the creep response (compliance) can be converted into dynamic moduli through the relaxation/retardation spectra[32]. Here, the creep compliance J(t) was converted to G'(ω) and G''(ω) by means of the NLReg software, based on a generalization of the Tikhonov regularization method[33].

II.4 Static Light Scattering

Measurements were performed at different temperatures in the range of 15 ^{o}C to 35 ^{o}C and at scattering angles (θ) ranging from 15° to 150° using an ALV-5000 (Germany) goniometer setup with a Nd:YAg laser λ_o = 532 nm. The temperature was controlled with a water circulating bath, and time for thermal equilibration (60 minutes) was allowed upon each change in temperature for thermal equilibration. Each observation angle corresponds to a scattering wave-vector $q = \frac{4\pi n_s}{\lambda_o} \sin(\theta/2)$, with n_s being the refractive index of the solvent and θ the scattering angle.

III. Sample Preparation

III.1 Circular Dichroism (CD) and Static Light Scattering (SLS)

The sample was prepared by heating, vortexing, and sonicating for approximately one hour, which was followed by mixing overnight at 20 °C using a sample shaker. It became homogeneous overnight and was then subjected to variable temperature CD and SLS experiments.

III.2 Oscillatory Rheology

The sample was prepared by heating, vortexing, and sonicating every hour for 45 minutes for 3 consecutive days until they became homogeneous to the eye. This was followed by an equilibriation period of 10 days at 20 °C . The specific equilibration period was determined after trials which consisted of following the heating/vortexing/sonicating protocol and subsequent testing of the mechanical properties and aging of the material at well controlled conditions. During the same trials, we noticed that even for equilibrated samples under constant humidity conditions, a change of temperature leading to a state transition as observed with CD spectroscopy leads to a slow evolution of the dynamics and moduli for approximately 12 hours. For example, in figure 3.1 we follow the evolution of the spectra of a 45 g/l BPTA sample which was loaded at the rheometer at temperature 35 ^{o}C with room temperature (and thus, sample temperature before loading) being 20 ^{o}C. This observation helped us differentiate between equilibrated sample and non-equilibrated samples, since the former's properties evolve for a limited amount of time (typically 12 hours) .

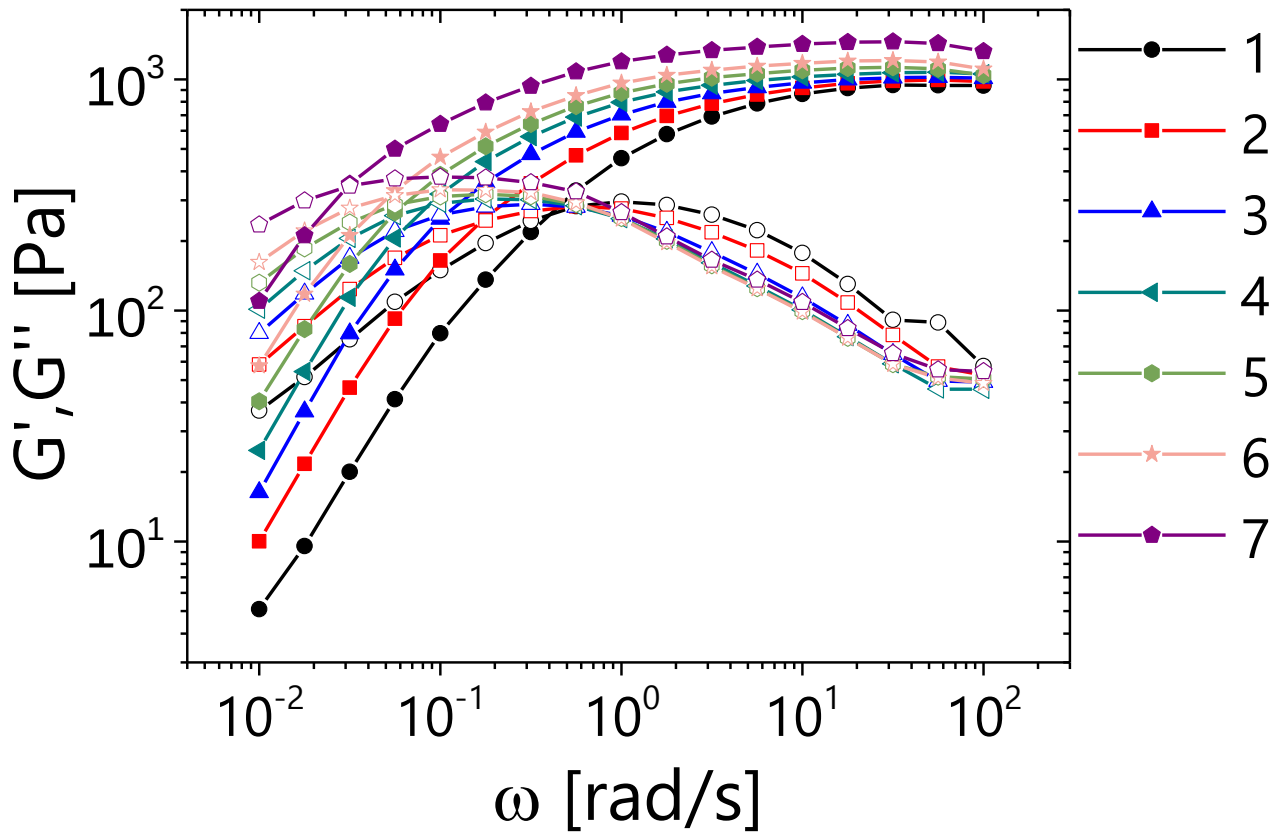

Figure 3.1 Evolution of rheological spectra of a 45 g/l sample upon loading on the rheometer. Room temperature was 20 °C while the temperature on the rheometer plate was 35 °C.

IV. Results and Discussion

IV.1 Structure

The self-assembly of **BPTA** (Figure 3.2A) in dodecane appears to be very similar to that in methylcyclohexane and heptane as previously reported[28] and is followed by CD spectroscopy (Figure 3.2B) in dilute conditions. As the sample is cooled, it exhibits two sharp transitions at 26 and 15 °C. The transition at 26 °C leads to a drop in the CD signal while the one at 15 °C leads to a change of the sign in the signal, meaning tha the helicity has changed.

In this case, the transition at 15 °C leads to a right-handed helix. A heating trace was also recorded immediately after the cooling trace. This curve clearly shows hysteresis between transitions, which is similar to the hysteresis observed in analogous experiments in methylcyclohexane[28]. Furthermore, these transitions in small length scales probed by CD are coupled with transitions in the overall shape of the form factor as measured by SLS in the dilute regime, shown in figure 3.2C, where the excess scaterring ratio, $R_{vv,}$ is plotted as a function of wave-vector q. The data exhibit a change in the scaling from q^{-2} at 15 ^{o}C to q^{-1} at 25 ^{o}C or higher. Moreover, the levelling-off of the intensity at lower q values at 15 ^{o}C denotes that the overall size of the supramolecular assembly is captured, however, that does not hold for higher temperatures suggesting that the contour length of the assembly as well as the persistence length is severly affected by the transitions. The form factor at 15 ^{o}C has been fitted with the Kholodenko form factor[34] for semi-flexible polymers to obtain the contour length (L) and persistence length (l_p) of the supramolecular polymer (L=2000 nm , l_p=80 nm).

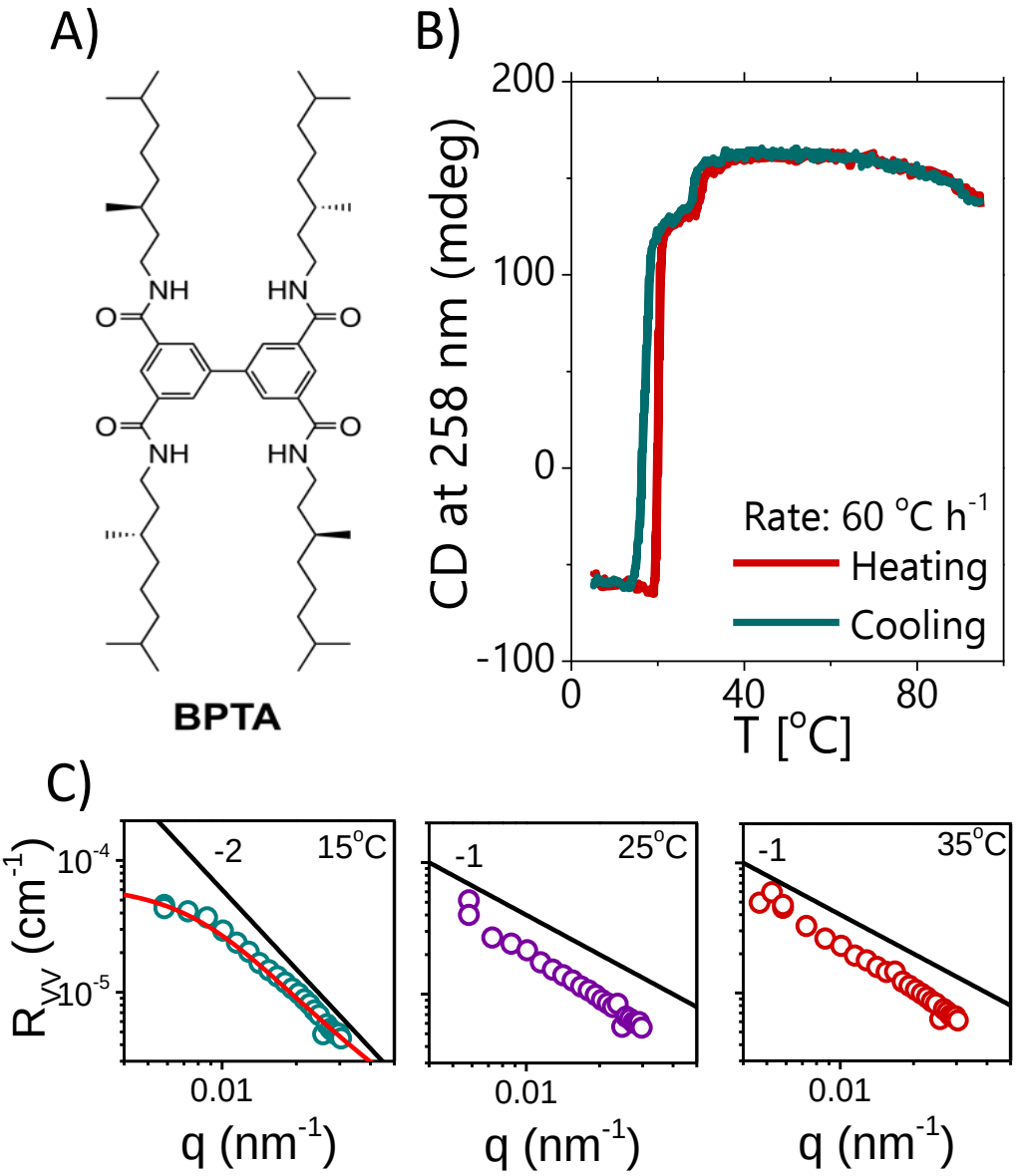

Figure 3.1. Self-assembly of **BPTA** in dodecane at 100 μM concentration. A) Chemical structure of **BPTA**. B) Self-assembly of **BPTA** (100 μM in as-received dodecane) followed by CD at 258 nm. C) Excess scattering ratio as a function of wave-vector for three temperatures. In the case of 15°C the curve was fitted with the Kholodenko form factor [34] for semi-flexible polymers yielding the total length of the assembly and the persistence length.

We term the structures before each transition with **A**, **B** and **C,** with **A** being the structure at high temperatures, **B** the intermediate structure accompanied by the small drop in

CD signal and **C** the structure exhibiting negative CD signal. Thus, the transition at 26 ^{o}C is the transition **A→B** and the transition at 15 ^{o}C is the transition **B→C**. As proposed by Van Zee et al.[28] based on calorimetric measurements coupled with density functional theory calculations, these transitions are due to the incorporation of water molecules into the self-assembled structure, and are schematically shown in figure 3.3. At **C,** the structure is completely saturated with water with two water molecules binding on one BPTA molecule. The structure at state **A** is completely dry, with no water molecules binding with BPTA, while state **B** seems to be an intermediate state where there are some water molecules binding with BPTA with the ratio being 1:2 (1 water molecule per 2 BPTA molecules).

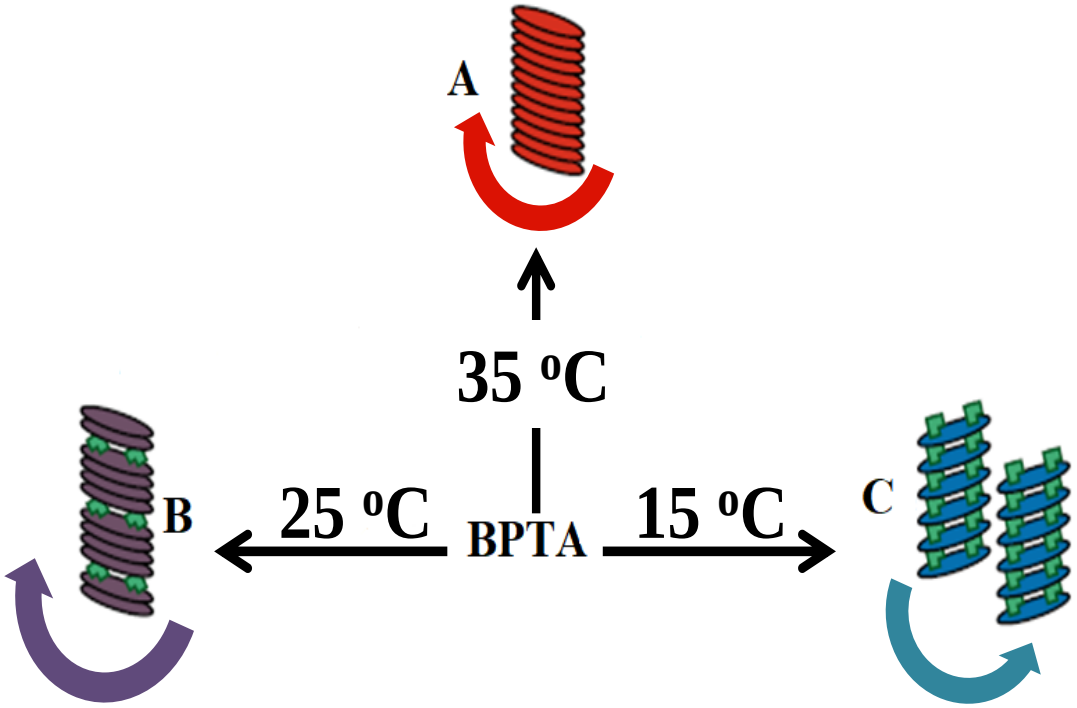

Figure 3.3. Schematic representation of the three structures observed with CD spectroscopy and light scattering

IV.2 Linear Viscoelasticity

Figure 3.4 depicts the rheological spectra for several concentrations of **BPTA** at ambient humidity (60%). The main characteristic is that at 25 ^{o}C the system seems to be

entangled, exhibiting a clear plateau modulus at all concentrations in contrast to the system at 15 ^{o}C and 35 ^{o}C which at the lowest concentrations seem to barely form entanglements. Combined with the information from SLS, one can assume that at 15 ^{o}C the chains are not long enough to form entanglements at lower concentrations. Regarding the system at 35 ^{o}C, it is unclear whether the supramolecular polymer is longer or shorter or more rigid compared to 25^{o}C. There are three scenarios at this point: (i) the system at 35^{o}C is indeed made up by shorter polymers than at 25 ^{o}C (ii) the polymer is longer but more persistent, thus hindering the formation of entanglements (iii) the polymer at 35^{o}C is equally or less rigid and longer than the one at 25 ^{o}C but has quite different dynamics which can be the result of different breaking/reformation time and/or molecular weight distribution. The last scenario would suggest that the entanglement plateau would be visible at higher frequencies for the 35 ^{o}C and that in figure 4 at the lowest concentration we only observe a small part of the plateau modulus. The second and third scenarios could be greatly influenced by polydispersity because in the case of large polydispresities (which are expected here) the system will be a mixture of shorter polymers with their conformation similar to rigid-rods and longer semi-flexible chains, able to entangle. The former are acting as an effective solvent diluting the tube affecting the value of the modulus as well as the relaxation time. Judging from the spectra at larger concentrations, it would seem that the third scenario is more credible since in the well-entangled regime the system at 25 ^{o}C relaxes faster than the one at 35 ^{o}C suggesting that the length of the assembly is longer in the case of 35 ^{o}C and also the plateau modulus of the system at 35 ^{o}C is larger, implying that the system is more flexible. This in turn means that the scaling behavior of the terminal relaxation time at these two temperatures should be different. Similarly, the modulus seems to scale differently for the two temperatures with the moduli initially being equal and at higher concentrations the modulus of the system at 35 ^{o}C

being larger. The differences at this regime are small, and seem to increase with increasing concentration. At the same time, the modulus at 15 ^{o}C is always lower compared to the rest.

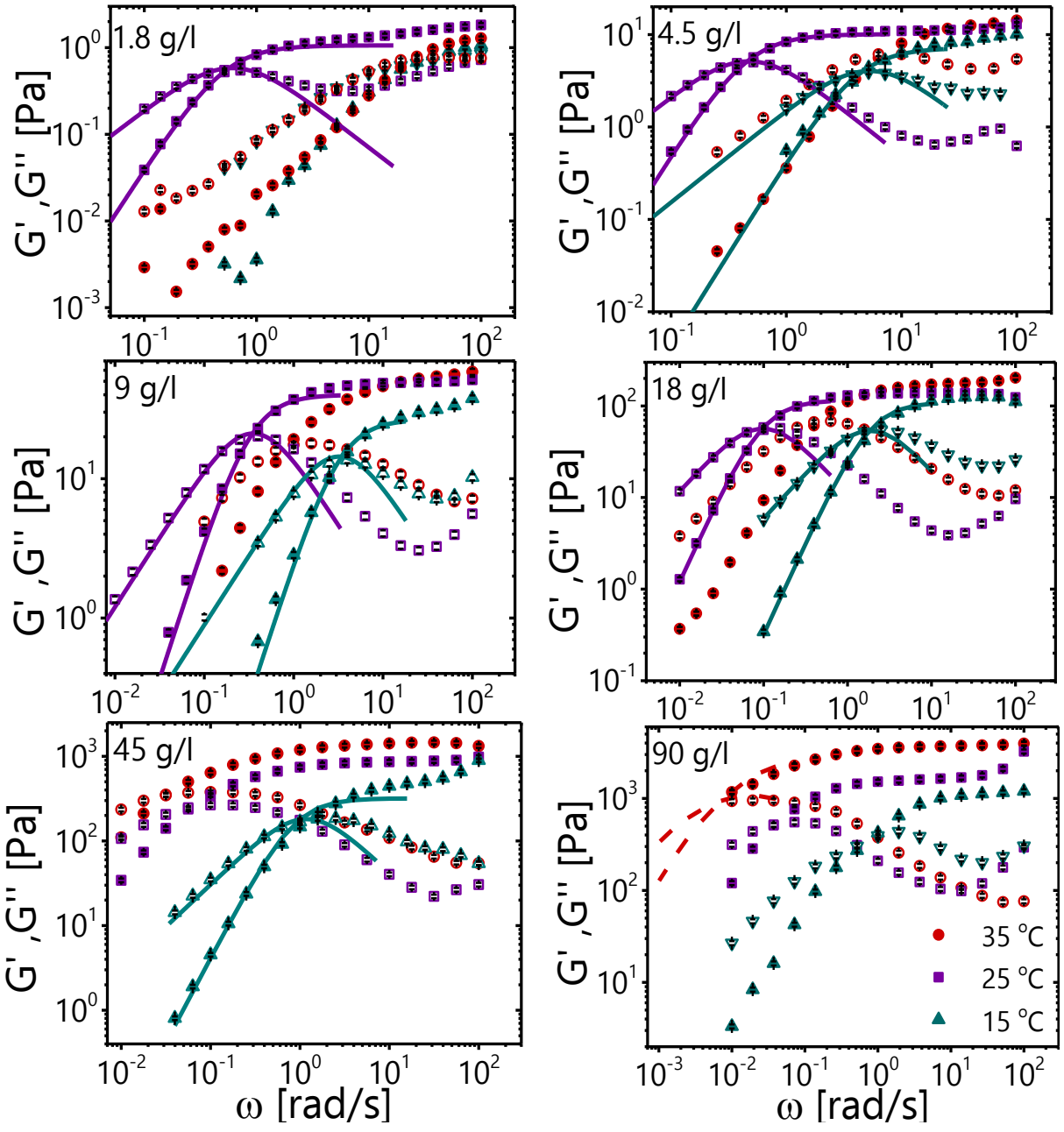

Figure 3.4 Storage (G') and Loss (G'') moduli as a function of angular frequency. Each plot corresponds to one concentration of **BPTA** in dodecane, written on the top left corner. Closed symbols correspond to the storage moduli while open symbols to the loss moduli. The color coding is the same for all graphs and is shown on the bottom right corner of the last graph. Red circles correspond to 35 ^{o}C, purple squares to 25 ^{o}C and cyan triangles

to 15 ^{o}C. The lines in all graphs show the fits of the terminal relaxation with one Maxwell mode, where that was done.. The dashed lines shown in the graph corresponding to 90 g/l show the converted creep compliance. Error bars (smaller than symbols) are shown in black and are typically between 3%-8% of the specific value. Error bars are acquired from at least 3 independent measurements of each sample under same experimental conditions.

Moreover, one can clearly see that the terminal relaxation of the system at 35 ^{o}C is much broader compared to the other two temperatures where it is described by a single Maxwell mode similar to living polymers in the fast breaking limit[21]. However, at large concentrations even the lower temperatures seem to deviate from the simple Maxwellian behavior, suggesting either that the breaking time is somehow dependent on concentration or that the interactions in the system start to become more complex at larger concentrations. Indeed, the best fits with a single Maxwell mode of the terminal relaxation regime are shown as lines in figure 3.5. It is clear, that in the case of 35 ^{o}C the terminal relaxation cannot be described by a single Maxwell mode. However, for the two other temperatures, the data at concentrations up to 45 g/l are well-described by a single Maxwell mode as predicted for well-entangled living polymers by Cates[21]. The deviation from the living polymer behavior could be attributed to the fact that since this is essentially a ternary system, if water molecules are not sufficient to saturate the structure a mixture of polymers saturated with water and those with less water in them which can lead to a much more complex terminal relaxation than a single Maxwell mode, and this might be the case for the larger concentrations, however, this still does not explain the deviation from the living polymer behavior at 35 ^{o}C.

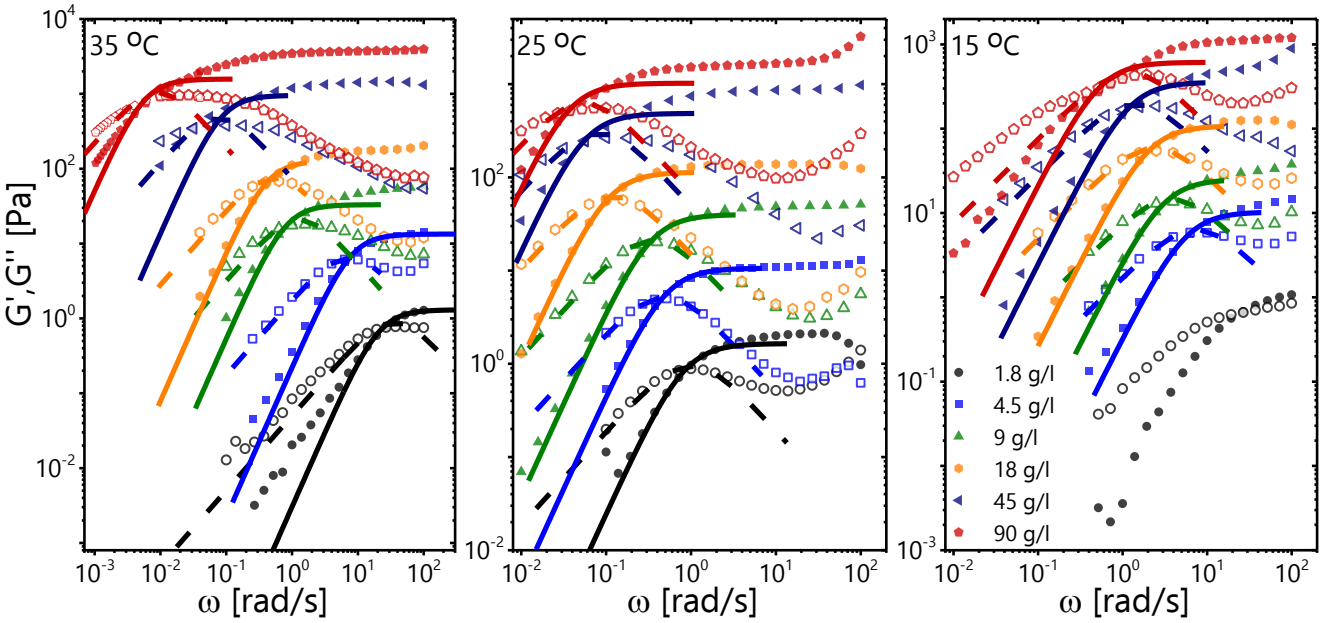

Figure 3.5 Viscoelastic spectra for different concentrations for the three different temperatures studied. The color coding is the same for all plots and is shown at the plot corresponding to 15 ^{o}C. The lines show the best fit of the data with a single Maxwell mode. Dashed lines correspond to the loss modulus and solid lines to the storage modulus.

We can obtain further insight into this from the scaling of the plateau modulus and the terminal relaxation time with concentration. In figure 3.6A the logarithm of the plateau modulus, extracted from the minimum of G'', is shown as a function of concentration for all temperatures and another living polymer based on the EHUT supramolecular moiety[29]. **BPTA** follows the scaling predicted by Cates[21], with the green line having slope of 2 and the predicted value being 2.25. On the other hand, when it comes to terminal the relaxation time (Figure 3.6B), the scaling observed experimentally for similar supramolecular polymers such as EHUT is $\tau_d \sim c^{0.77}$, is followed at both 15 ^{o}C and 25 ^{o}C, but not at 35 ^{o}C. In the latter we obsere $\tau_d \sim c^{2.2}$ which is close to the scaling for linear polymers in good solvency conditions[2]. This is strong indication that when the system is at 35 ^{o}C it is not in the fast breaking limit of Cates, hence it is reasonable that it deviates from the expected single Maxwell mode

behavior. Such behavior has been reported previously for wormlike micelles with large breaking times[10,35] comparable or larger than the reptation time.

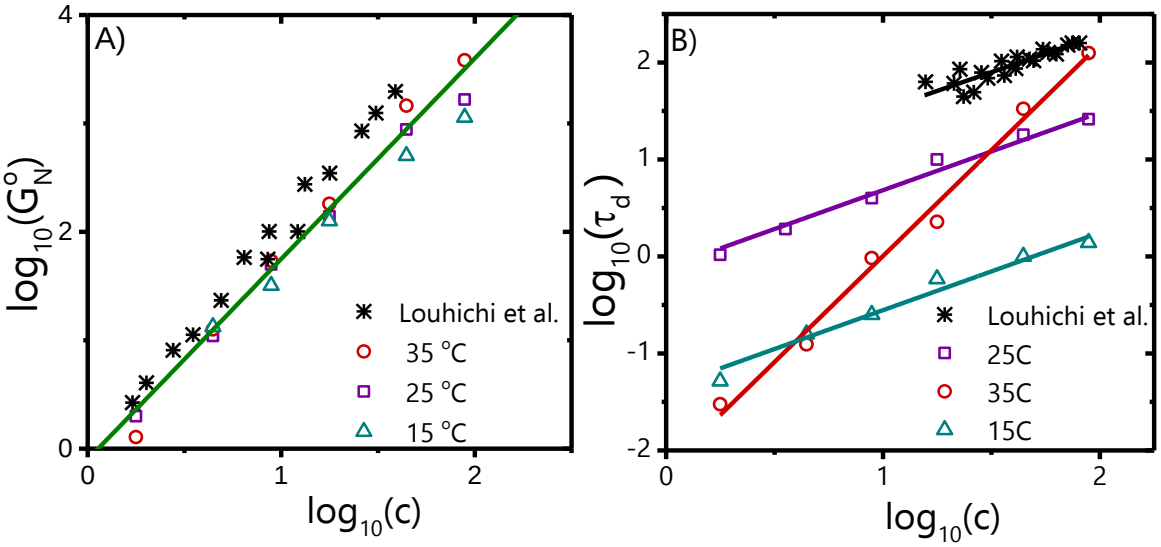

Figure 3.6 A) Scaling of the logarithm of the plateau modulus with the logarithm of concentration. The green line has slope of 2.0. B) Scaling of the logarithm of the terminal relaxation time as extracted from the cross-over of the moduli with the logarithm of concentration. The lines correspond to best fits of the data with a linear regression algorithm. The red line has slope 2.2, while the black, cyan and purple have slopes 0.8.

IV.3 Humidity Effect

The viscoelastic spectra of BPTA seem counterintuitive. For example, what would be expected is for the breaking rate to become larger with increasing temperature or concentration according to the theory of Cates[35]. To ascertain that the transitions observed are actually due to the presence of water in the system, we examined the viscoelastic response at 15 ^{o}C and 35 ^{o}C under dry conditions (RH <5%). In figure 3.8A, the viscoelastic spectra of a 90 g/l sample at 15 ^{o}C and 35 ^{o}C are compared with the viscoelastic spectra of the same sample under ambient conditions. It is clear that the culprit for the transitions on the viscoelasticity and dynamics of the system with temperature is the presence of water and its interactions with **BPTA**. The only difference in the spectra is that the system seems to relax slower at 15 ^{o}C than at 35 ^{o}C, as expected. The driving force should be the same as what has

been previously reported by Van Zee et al. [28]. Water in oil has large enthalpic energy due to the fact that it is in monomeric state, having unfulfilled hydrogen bonds. Moreover, it has been shown that the transition temperatures are affected by humidity[28]. To that end, we have tried to exploit humidity as a means to willingly change the viscoelasticity of these materials. In figure 3.8B, we keep the temperature constant at 25 ^{o}C but vary the relative humidity progressively from dry conditions (RH=5%) to humid (RH=100%). The spectra change progressively with humidity and there seems to exist an intermediate state between states **B** and **C** discussed in the previous sections. It is not clear from this study whether there is really a different state between **B** and **C** meaning that the water packs in different ratios in the supramolecular polymer or if this is the result of a mixture of **B** supramolecular polymers and **C** supramolecular polymers since the relaxation is quite broad in general. Note that the viscoelastic spectra at RH=5% ,60% and 100% are almost the same as the ones measured at 35 ^{o}C, 25 ^{o}C and 15 ^{o}C under ambient humidity conditons, respectively. The emerging picture is that due to the sensitivity of the transitions to humidity, the system can be driven to the fully wet state or the fully dry just by varying the humidity with the repercussions that this has on the viscoelasticity of the system.

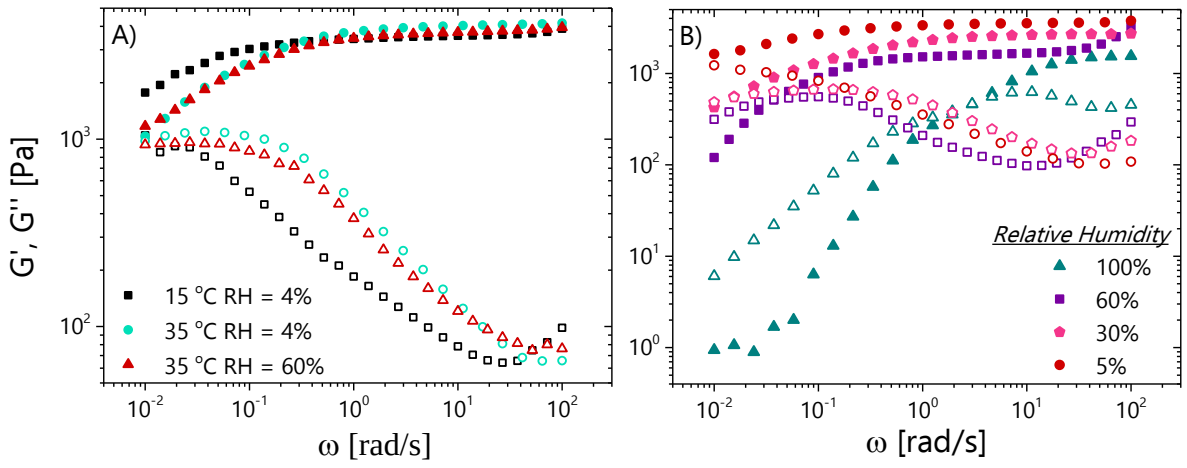

Figure 3.8 A) Viscoelastic Spectra for 15 ^{o}C under dry conditions (black squares), 35 ^{o}C under dry conditions (cyan circles) and 35 ^{o}C under ambient conditions (red triangles) of a 90 g/l organogel B) Spectra for a 90 g/l

organogel under constant temperature (T=25 ^{o}C) and different relative humidities. Relative humidity 100% corresponds to the cyan triangles, 60% to the purple squares, 30% to the pink petnagons and 5% to the red circles.

V. Conclusions

We have investigated the properties of a supramolecular moiety that in organic solvents self-assembles into long 1D helical living polymers. It undergoes three state transitions affecting the structure of the supramolecular polymer due to the potential enthalpic energy of trace amounts of water molecules in organic oils. The question we have considered in this work is if and how these structural transitions on local length scales probed in a previous work[22] affect the bulk properties of a transient network formed from this supramolecular compound. Hereto, we studied the system by varying the concentration, temperature and humidity. Our findings indicate that the structural transitions due to water interacting with the supramolecular polymers have strong and important consequences on the viscoelasticity and dynamics of the system. The particular BPTA system can be thought of as a living polymer similarly to previous studies on supramolecular polymers. However, here we find that the transition associated with water entirely leaving the supramolecular polymer is associated with a transition of the system from the fast breaking limit (where the polymer breaks and recombine several times while reptating) to the slow breaking limit (where the rate of breakage/reformation is comparable or smaller than the inverse of the reptation time), changing completely the relaxation of the system. Combining this with the information from light scattering showing that as water leaves the supramolecular polymer, the contour length increases it leads us to the conclusion that the fact that water molecules interfere with the

assembly leads to smaller binding energies by effectively “diluting” the interactions and ultimately determines the breaking time of the assembly as well as contour length. This work demonstrates that trace amounts of water in dodecane can be used to tailor the viscoelasticity of supramolecular assemblies through co-assembly. In the future, this approach can be considered for supramolecular gelators based on compounds that can co-assemble either randomly[36] or in a more controlled way similar to the recently reported supramolecular block copolymers[37].

References

(1) Flory, P. J. Introductory Lecture. *Faraday Discuss. Chem. Soc.* **1974**, *57*, 7. https://doi.org/10.1039/dc9745700007.

(2) Rubinstein, M.; Colby, R. H. *Polymer Physics*; Oxford University Press: Oxford, 2003.

(3) *Molecular Gels: Materials with Self-Assembled Fibrillar Networks*; Weiss, R. G., Terech, P., Eds.; Springer: Dordrecht, 2006.

(4) *Supramolecular Science: Where It Is and Where It Is Going*; Ungaro, R., Dalcanale, E., Eds.; Springer Netherlands: Dordrecht, 1999. https://doi.org/10.1007/978-94-011-4554-1.

(5) Raghavan, S. R.; Douglas, J. F. The Conundrum of Gel Formation by Molecular Nanofibers, Wormlike Micelles, and Filamentous Proteins: Gelation without Cross-Links? *Soft Matter* **2012**, *8* (33), 8539. https://doi.org/10.1039/c2sm25107h.

(6) Bouteiller, L. Assembly via Hydrogen Bonds of Low Molar Mass Compounds into Supramolecular Polymers. In *Hydrogen Bonded Polymers*; Binder, W., Ed.; Springer Berlin Heidelberg: Berlin, Heidelberg, 2007; Vol. 207, pp 79–112. https://doi.org/10.1007/12_2006_110.

(7) Feldman, K. E.; Kade, M. J.; Meijer, E. W.; Hawker, C. J.; Kramer, E. J. Model Transient Networks from Strongly Hydrogen-Bonded Polymers. *Macromolecules* **2009**, *42* (22), 9072–9081. https://doi.org/10.1021/ma901668w.

(8) Hanabusa, K.; Koto, C.; Kimura, M.; Shirai, H.; Kakehi, A. Remarkable Viscoelasticity of Organic Solvents Containing Triakyl-1,3,5-Benzenetricarboxamides and Their Intermolecular Hydrogen Bonding. *Chem. Lett.* **1997**, *26* (5), 429–430.

(9) Hamley, I. W. Peptide Fibrillization. *Angew. Chem. Int. Ed.* **2007**, *46* (43), 8128–8147. https://doi.org/10.1002/anie.200700861.

(10) Rehage, H.; Hoffmann, H. Rheological Properties of Viscoelastic Surfactant Systems. *J. Phys. Chem.* **1988**, *92* (16), 4712–4719. https://doi.org/10.1021/j100327a031.

(11) Khatory, A.; Lequeux, F.; Kern, F.; Candau, S. J. Linear and Nonlinear Viscoelasticity of Semidilute Solutions of Wormlike Micelles at High Salt Content. *Langmuir* **1993**, *9* (6), 1456–1464. https://doi.org/10.1021/la00030a005.

(12) Inoue, T.; Inoue, Y.; Watanabe, H. Nonlinear Rheology of CTAB/NaSal Aqueous Solutions: Finite Extensibility of a Network of Wormlike Micelles. *Langmuir* **2005**, *21* (4), 1201–1208. https://doi.org/10.1021/la048292v.

(13) Chen, Q.; Tudryn, G. J.; Colby, R. H. Ionomer Dynamics and the Sticky Rouse Model. *J. Rheol.* **2013**, *57* (5), 1441–1462. https://doi.org/10.1122/1.4818868.

(14) Zhuge, F.; Hawke, L. G. D.; Fustin, C.-A.; Gohy, J.-F.; van Ruymbeke, E. Decoding the Linear Viscoelastic Properties of Model Telechelic Metallo-Supramolecular Polymers. *J. Rheol.* **2017**, *61* (6), 1245–1262. https://doi.org/10.1122/1.4997593.

(15) Filippidi, E.; Cristiani, T. R.; Eisenbach, C. D.; Waite, J. H.; Israelachvili, J. N.; Ahn, B. K.; Valentine, M. T. Toughening Elastomers Using Mussel-Inspired Iron-Catechol Complexes. *Science* **2017**, *358* (6362), 502–505. https://doi.org/10.1126/science.aao0350.

(16) Annable, T.; Buscall, R.; Ettelaie, R.; Whittlestone, D. The Rheology of Solutions of Associating Polymers: Comparison of Experimental Behavior with Transient Network Theory. *J. Rheol.* **1993**, *37* (4), 695–726. https://doi.org/10.1122/1.550391.

(17) Knoben, W.; Besseling, N. A. M.; Bouteiller, L.; Cohen Stuart, M. A. Dynamics of Reversible Supramolecular Polymers: Independent Determination of the Dependence of Linear Viscoelasticity on Concentration and Chain Length by Using Chain

Stoppers. *Phys. Chem. Chem. Phys.* **2005**, *7* (11), 2390. https://doi.org/10.1039/b503463a.
(18) Berret, J.-F. Transient Rheology of Wormlike Micelles. *Langmuir* **1997**, *13* (8), 2227–2234. https://doi.org/10.1021/la961078p.
(19) Leibler, L.; Rubinstein, M.; Colby, R. H. Dynamics of Reversible Networks. *Macromolecules* **1991**, *24* (16), 4701–4707. https://doi.org/10.1021/ma00016a034.
(20) Rubinstein, M.; Semenov, A. N. Thermoreversible Gelation in Solutions of Associating Polymers. 2. Linear Dynamics. **1998**, *31* (4), 12.
(21) Cates, M. E. Reptation of Living Polymers: Dynamics of Entangled Polymers in the Presence of Reversible Chain-Scission Reactions. *Macromolecules* **1987**, *20* (9), 2289–2296. https://doi.org/10.1021/ma00175a038.
(22) Anand, B.; Pisal, S. S.; Paradkar, A. R.; Mahadik, K. R. Applications of Organogels in Pharmaceuticals. 8.
(23) Martinez, R. M.; Rosado, C.; Velasco, M. V. R.; Lannes, S. C. S.; Baby, A. R. Main Features and Applications of Organogels in Cosmetics. *Int. J. Cosmet. Sci.* **2019**, *41* (2), 109–117. https://doi.org/10.1111/ics.12519.
(24) Carretti, E.; Dei, L.; Macherelli, A.; Weiss, R. G. Rheoreversible Polymeric Organogels: The Art of Science for Art Conservation. *Langmuir* **2004**, *20* (20), 8414–8418. https://doi.org/10.1021/la0495175.
(25) Aida, T.; Meijer, E. W.; Stupp, S. I. Functional Supramolecular Polymers. *Science* **2012**, *335* (6070), 813–817. https://doi.org/10.1126/science.1205962.
(26) Meijer, E. W.; Aida, T. Supramolecular Polymers, We've Come Full Circle. *Isr. J. Chem.* **2019**.
(27) Riddick, J. A.; Bunger, W. B.; Sakano, T. K. *Organic Solvents: Physical Properties and Methods of Purification.*; John Wiley & Sons: New York, 1986.
(28) Van Zee, N. J.; Adelizzi, B.; Mabesoone, M. F. J.; Meng, X.; Aloi, A.; Zha, R. H.; Lutz, M.; Filot, I. A. W.; Palmans, A. R. A.; Meijer, E. W. Potential Enthalpic Energy of Water in Oils Exploited to Control Supramolecular Structure. *Nature* **2018**, *558* (7708), 100–103. https://doi.org/10.1038/s41586-018-0169-0.
(29) Louhichi, A.; Jacob, A. R.; Bouteiller, L.; Vlassopoulos, D. Humidity Affects the Viscoelastic Properties of Supramolecular Living Polymers. *J. Rheol.* **2017**, *61* (6), 1173–1182. https://doi.org/10.1122/1.4997600.
(30) Christian, S. D.; Taha, A. A.; Gash, B. W. Molecular Complexes of Water in Organic Solvents and in the Vapour Phase. *Q. Rev. Chem. Soc.* **1970**, *24* (1), 20. https://doi.org/10.1039/qr9702400020.
(31) Stokes, R. H.; Robinson, R. A. Standard Solutions for Humidity Control at 25° C. *Ind. Eng. Chem.* **1949**, *41* (9), 2013–2013. https://doi.org/10.1021/ie50477a041.
(32) Ferry, J. D. *Viscoelastic Properties of Polymers*; Wiley: New York: NY, 1980.
(33) Honerkamp, J.; Weese, J. A Nonlinear Regularization Method for the Calculation of Relaxation Spectra. *Rheol. Acta* **1993**, *32* (1), 65–73. https://doi.org/10.1007/BF00396678.
(34) Kholodenko, A. L. Analytical Calculation of the Scattering Function for Polymers of Arbitrary Flexibility Using the Dirac Propagator. *Macromolecules* **1993**, *26* (16), 4179–4183. https://doi.org/10.1021/ma00068a017.
(35) Cates, M. E.; Candau, S. J. Statics and Dynamics of Worm-like Surfactant Micelles. *J. Phys. Condens. Matter* **1990**, *2* (33), 6869–6892. https://doi.org/10.1088/0953-8984/2/33/001.
(36) Vantomme, G.; ter Huurne, G. M.; Kulkarni, C.; ten Eikelder, H. M. M.; Markvoort, A. J.; Palmans, A. R. A.; Meijer, E. W. Tuning the Length of Cooperative

Supramolecular Polymers under Thermodynamic Control. *J. Am. Chem. Soc.* **2019**, *141* (45), 18278–18285. https://doi.org/10.1021/jacs.9b09443.
(37) Adelizzi, B.; Aloi, A.; Markvoort, A. J.; Ten Eikelder, H. M. M.; Voets, I. K.; Palmans, A. R. A.; Meijer, E. W. Supramolecular Block Copolymers under Thermodynamic Control. *J. Am. Chem. Soc.* **2018**, *140* (23), 7168–7175. https://doi.org/10.1021/jacs.8b02706.

Chapter 4. Conclusions and Perspectives

The emerging picture from this work is that competitive associations affect the rheological properties of gels made from supramolecular polymers. These interactions can be manifested by introducing a second supramolecular moiety as reported in chapter 2 and previous works[1–5] or triggered by the environment, such as humidity, as discussed in chapter 3 and some earlier works[6,7]. In both cases, the driving force altering the rheological properties is the change of unimer dynamics due to change of the association energy.

More specifically, in the case of the hydrogel mixture of Chapter 2, a combination of oscillatory rheology, cryo-TEM and molecular dynamics simulations reveal a non-monotonic dependence of the structural and rheological properties on the mixing ratio. The fact that the experimental results can be reproduced qualitatively by a coarse-grained model (without chemical details, simply by considering two units with different interaction potentials) used in the MD simulations, suggests that the coupling of different association energies between the two units is crucial for the non-monotonicity. It further suggests that the association strength and the ability to create additional bridges are the main features to account for in material design with a variety of different chemical compounds, although more work will be needed in this direction such as studying the role of the internal flexibility of the motif as well as the size of the bridging component. In a recent work with systems similar to those reported here, Noteborn et al.[4] have reported that the non-monotonicity appears when the linker is rigid but not when it is flexible. This is of course related to the range of concentration investigated, since one can think of a regime where the rigid linker will be able to still bridge neighboring “worms” while the flexible one will create less bridges.

Chapter 3 discusses the properties of a physical network formed by a moiety that self-assembles into 1D helical columnar aggregates in organic solvents. The structural characteristics of the self-assembly vary with temperature because of the presence of trace

amounts of water in the solvent[7]. Water can interact with the supramolecular moiety and influence the structural and dynamic properties of the assembly. Light scattering in the dilute regime indicated that water "plasticizes" the self-assembly, leading to a reduction of the binding energy compared to the dry state, which translates into a smaller average contour length as well as a faster breaking/reformation time. The latter is evident from the analysis of the dynamic rheological spectra, which reveals a clear difference in the concentration dependence of the relaxation time at three different temperatures, representing distinct regimes (dry, humid, transitional). By tailoring and controlling the level of humidity the dynamics vary from that of a living polymer with small relaxation time to a complex viscoelastic solution exhibiting complex relaxation. These results show how humidity in oils could potentially be utilized to change the viscoelasticity of organogels made by supramolecular compounds through co-assembly of water molecules with the supramolecular organogelators. Moreover, it elucidates the role of competitive interactions at molecular level in imparting substantial changes in the bulk mechanical properties of these materials. The latter finding connects to those of the hydrogel mixtures studied in Chapter 2.

The above findings motivate further investigations and some specific perspectives are presented here. Expectedly, the varying interactions discussed are not only reflected on the linear viscoelastic properties, but also on the nonlinear response. For example, in the case of organogels, unusual shear-strain hardening phenomena are obsrerved, as shown in Figure 4.1.

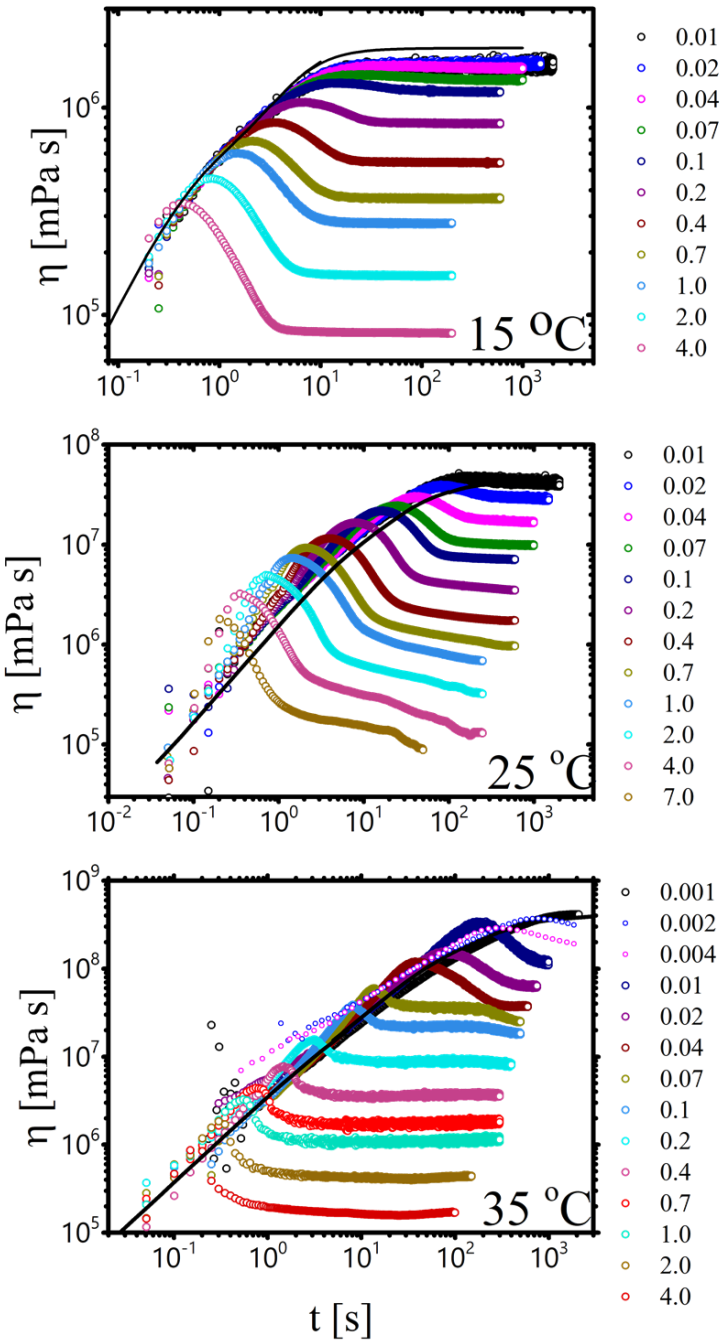

Figure 4.1. Transient start-up viscosity at different shear rates (values in legends reported in s^{-1}) at three different temperatures (reported on the bottom right corner). At 15 °C the supramolecular assembly is completely saturated with water, at 25 °C only a quarter of the monomers are bound with water molecules while at 35 °C the supramolecular assembly is completely dry. Black lines represent the linear viscoelastic envelope obtained from oscillatory measurements and subsequently converted through the Cox-Merz and Gleissle rules[8].

Strain hardening has been observed in the past for several biopolymer networks[9–11] as well as wormlike micelles[12–14] and supramolecular polymers[6]. It has been suggested that the semi-flexible nature of these materials leads to their strain hardening behavior under shear[15]. However, recent studies with wormlike micellar systems having similar bending rigidities, suggest that that the origin of shear-strain hardening is not the semi-flexible nature of the system but its ability to create transient bridges that lead to shear-induced bundling of micelles and consequently an increased ability to sustain strain. [13] A detailed investigation of the well-studied CTAB/NaSal surfactant in water by means of step-strain measurements indicates that the appearance or not of transient shear-strain hardening depends on the concentration. [12]

Preliminary shear-strain hardening results

Similarly to recent work from Larson's group[12], here we use step strain measurements to study the hardening behavior of BPTA in dodecane at 90 g/l. Figure 4.2 indicates softening for applied strains larger than 0.2 at 15^{o}C. On the other hand, at 25 ^{o}C, for intermediate strains $0.2<\gamma<1$ the system seems to harden with the relaxation modulus exceeding that of the linear viscoelastic regime (LVE, red line in Figure 4.2). However, at times longer than 0.3 s the relaxation modulus for all strains in the nonlinear regime is lower than the LVE. Furthermore, for $\gamma>1$ the material is only exhibiting shear-strain softening. At 35 ^{o}C the behavior is qualitatively similar, with transient shear-strain hardening giving rise to shear-strain softening at long times and large strains. The main difference is that the hardening seems to be more persistent in time (maintained for times up to 10 s after applying the step strain). To a first approach, the explanation of Ref. [12] seems relevant here, i.e., there some bundling may occur under shear by bridges created from small supramolecular polymers, which is not the case in equilibrium or that the entanglements formed here may not be purely

topological but could be partly "sticky". This behavior resembles that of collagen networks which have been shown to shear-strain harden transiently[16].

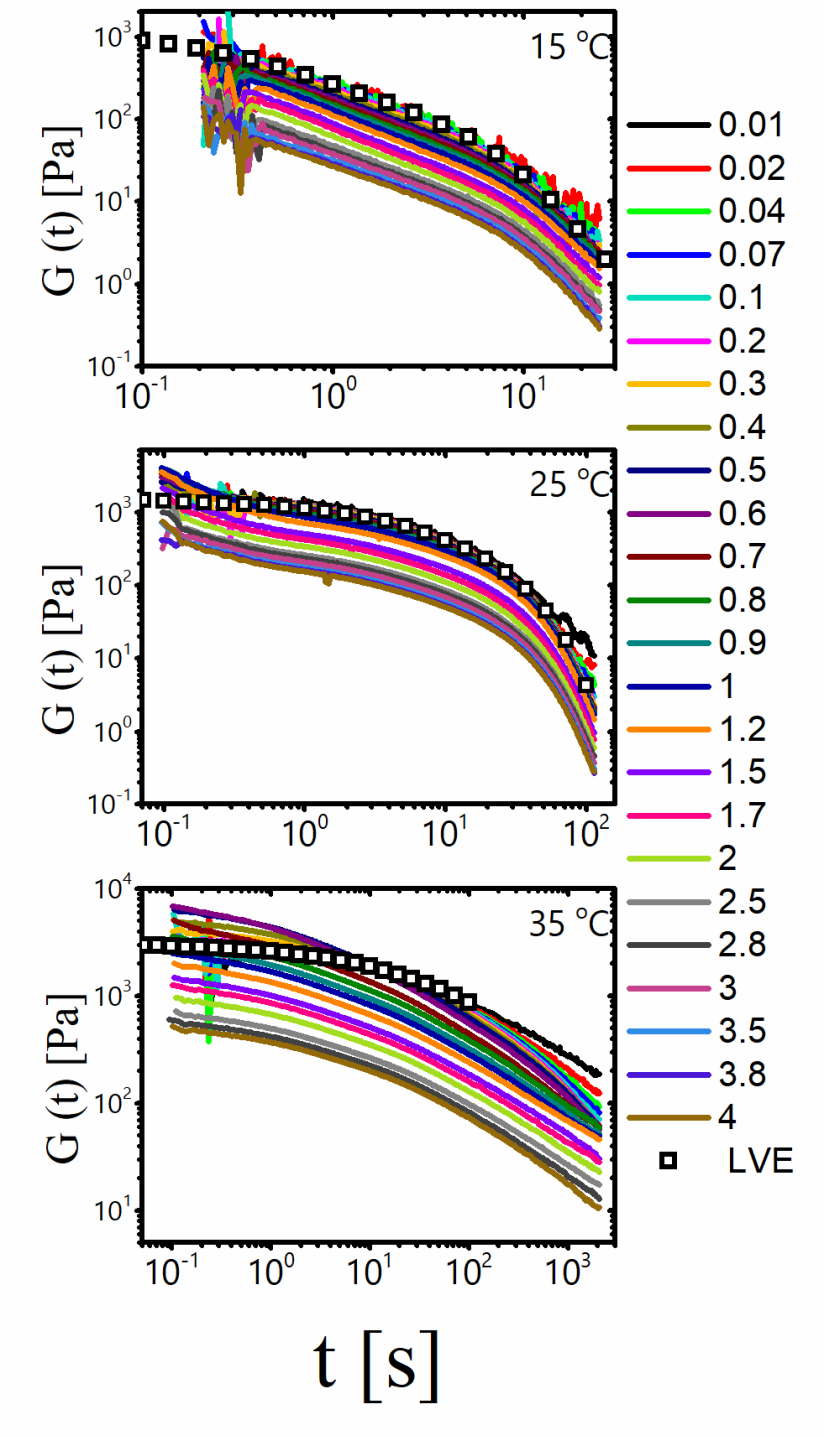

Figure 4.2. Stress relaxation after step strain experiments for several strains in the range 0.01 to 4 at three temperatures studied. The red line is the conversion of the linear viscoelastic spectrum to the stress relaxation modulus using the Schwarzl algorithm[17].

To elaborate on the "sticky" interactions, in collagen networks they are a combination of electrostatic and van der Waals interactions that are weak enough to break under strong flows allowing the collagen bundles to slide past each other[16]. Such an effect could explain the behavior of the present BPTA system where "sticky" entanglements cannot be ruled out. On the other hand, the spontaneous breaking/reformation could also lead to transient hardening. One could thus speculate that the hardening could originate from the semi-flexible nature of the supramolecular polymer, which stretches and shear-strain hardens[14,15], but will relax once breaking events occur. This scenario provide a hint about the breaking time of the system and indeed, the hardening behavior is more persistent in time for the system at 35 ^{o}C where, according to linear rheology, we expect the system to have the largest breaking time.

Figure 4.3 depicts the time- and strain-dependent relaxation modulus normalized by its LVE value at a specific time after the start of the test. For simple linear polymers, where time-strain separability applies (beyond retraction) shifting the moduli data at different strain with respect to the LVE line yields a master curve from which the damping function is extracted [18,19]. This appears to be the case for the system at 15 ^{o}C. Trying to model the damping function at this temperature may provide useful information about the system. Furthermore, qualitative information about the persistence length of the system at the two higher temperatures can be acquired from the strain at which the system starts to harden[15] (eq. 1).

$$\gamma_c = \frac{1}{6}\frac{l_c}{l_p} \tag{1}$$

Here, l_c is the length of the segment between two topological constraints and l_p is the persistence length.

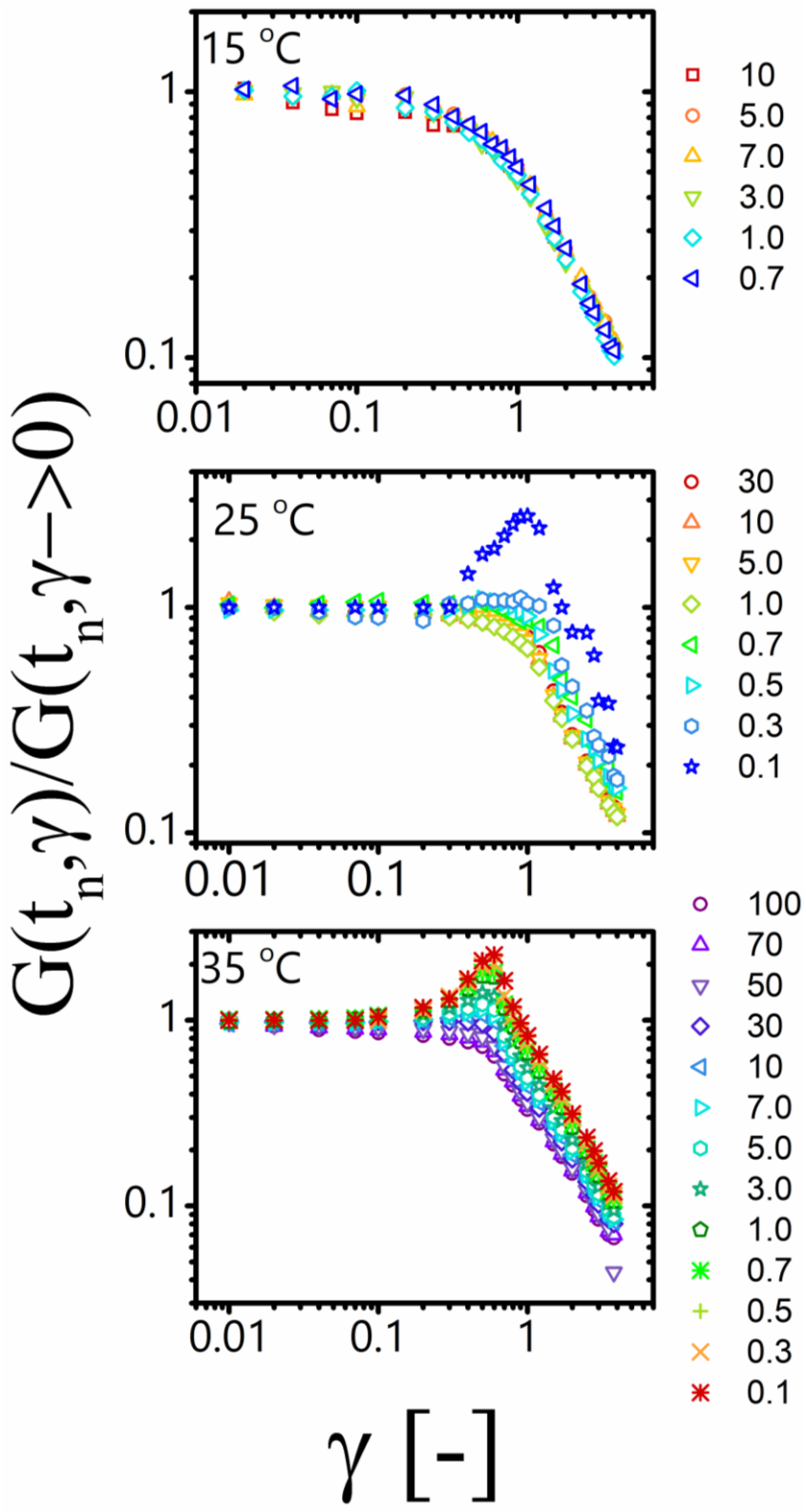

Figure 4.3. Relaxation Modulus $G(t_n,\gamma)$ normalized by the LVE modulus, $G(t_n,\gamma\rightarrow0)$ at a certain time (t_n) after the start of the test as a function of the applied strain. t_n is reported in seconds in the legend.

We know from linear rheology that l_c should be larger at 25 ^{o}C compared to 35 ^{o}C (the plateau modulus at 35 ^{o}C is larger by approximately a factor of 2). Since the plateau modulus $G_o^N \sim l_c^{-3}$ [14] it follows that l_c at 25 ^{o}C will be larger by a factor of 1.3. It is clear in Figure 4.3 that the critical strain for hardening (determined by the point where a line with slope 0 meets a line crossing through the hardening part of the curve) at 25^{o}C is approximately 0.3 strain units while at 35 ^{o}C is approximately 0.1 strain units, suggesting that whereas the persistence length of the BPTA self-assembly does not change significantly from 35 ^{o}C to 25 ^{o}C, it is nevertheless larger at 35 ^{o}C.

This BPTA organogel that can exhibit shear-strain softening or hardening by small temperature variation could act as a model system for a systematic investigation of shear-strain hardening also in associating systems and serve as a platform for developing design guidelines for responsive materials with desired properties. One pertinent question is how to develop a synthetic system with analogous behavior to biological systems such as networks made from collagen[16] and later on transfer that knowledge into an aqueous system which can be used in the field of biomaterials and tissue engineering. This type of approach seems to become increasingly important since recent studies have shown that the behavior of the extracellular matrix (ECM), which exhibits strong shear-strain hardening is key for understanding some of the signaling pathways involved in cell motility[20] and differentiation[21] and mediating long-range mechanical signaling between cells[22].

Preliminary results at steady shear

A possible argument against the existence of "sticky" entanglements is the fact that, as shown in Figure 4.4, the steady state viscosity (open symbols) is in all cases equal or lower (at larger rates) than the complex viscosity (filled symbols). In associating polymers where "sticky" interactions exist (are are typically strong), the opposite has been observed, at larger rates the steady state viscosity exceeds the complex viscosity[23,24]. Furthermore, at larger shear

rates there is a change in the slope of the steady state viscosity from -0.9 to -1.0 implying that the flow is becoming unstable. An additional observation is that the empirical Cox-Merz rule expectedly does not apply here.

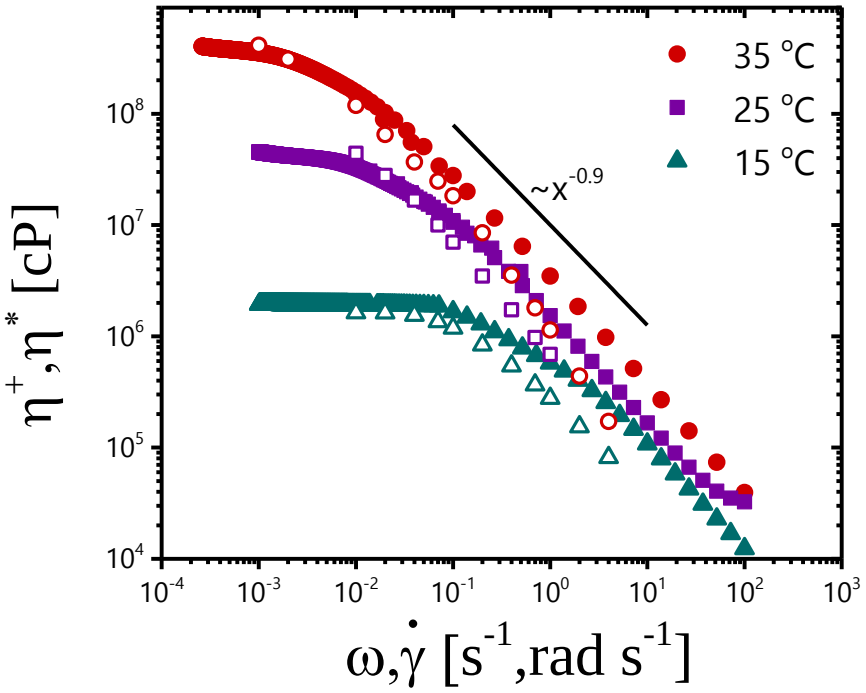

Figure 4.4. Comparison of the steady state viscosities (open symbols) with complex viscosities (filled symbols) as obtained from transient and oscillatory measurements in the linear regime, respectively.

Unambiguous evidence of instabilities is provided in Figure 4.5a where the steady state stress normalized by the plateau modulus is plotted as a function of the terminal Weissenberg number ($Wi_d = \tau_d \dot{\gamma}$). In all three temperatures there is a stress plateau at intermediate shear rates which is typically observed for living polymers and is attributed to the existence of bands of different shear rates formed in the material[25–29]. Interestingly, at 35 ^{o}C the stress drops after the stress plateau, reflecting flow instability. Here, the possible occurrence of edge fracture and/or slip should be examined. In addition, a deeper investigation of this behavior renders velocity profile measurements necessary, likely by

means of particle tracking Velocimetry, necessary. Such an approach may elucidate the transient behavior of the velocity profile, especially at the onset of shearing. In general, optical techniques coupled with rheology (e.g. flow birefringence) could help us understand much better the structural evolution of the system under flow. Specifically, the fact that the strain at which the stress overshoot appears at 15 ^{o}C appears at strains below 2.3 (the characteristic strain associated with orientation of tube segments under flow according to Doi-Edwards model for entangled polymers[30]) is interesting because overall at that temperature the system behaves as a simple linear polymer if one just looks at the transient viscosity curves (Figure 4.1). However, it is important to remember that even at that temperature where the system seems to have a flexible like conformation according to the static light scattering data presented in Chapter 3 the persistence length is still quite high (~100 nm) so the reduced peak strain (compared to the expected for linear polymers) might be due to the semi-flexible nature of the assembly at smaller length scales. The behavior of the system for the two higher temperatures is expected, since due to shear-strain hardening and/or finite extensibility the peak stress/viscosity appears at progressively smaller strains. To our knowledge, decrease of the peak strain with increasing shear rate has not been reported before, however it can be extracted from the start-up shear data reported by Inoue et al.[14]. It is interesting that here, in contrast to the work by Inoue et al. [14], the peak strain is always below 2.3. This could be due to the already extended conformation of these supramolecular polymers (due to their large persistent lengths), so they presumably cannot withstand more strain under flow, something that is backed-up by the leveling-off of the peak strain at higher rates. Moreover, at 35 ^{o}C the constant value of the peak strain is the same as the value of strain where the maximum hardening is observed during step-strain tests (dashed line in Figure 4.5b), supporting the scenario that the hardening is due to the semi-flexible nature of the assembly and its transient character is due to the fact the system can still break and reform

spontaneously, and not because of “sticky” entanglements that can break under nonlinear flow.

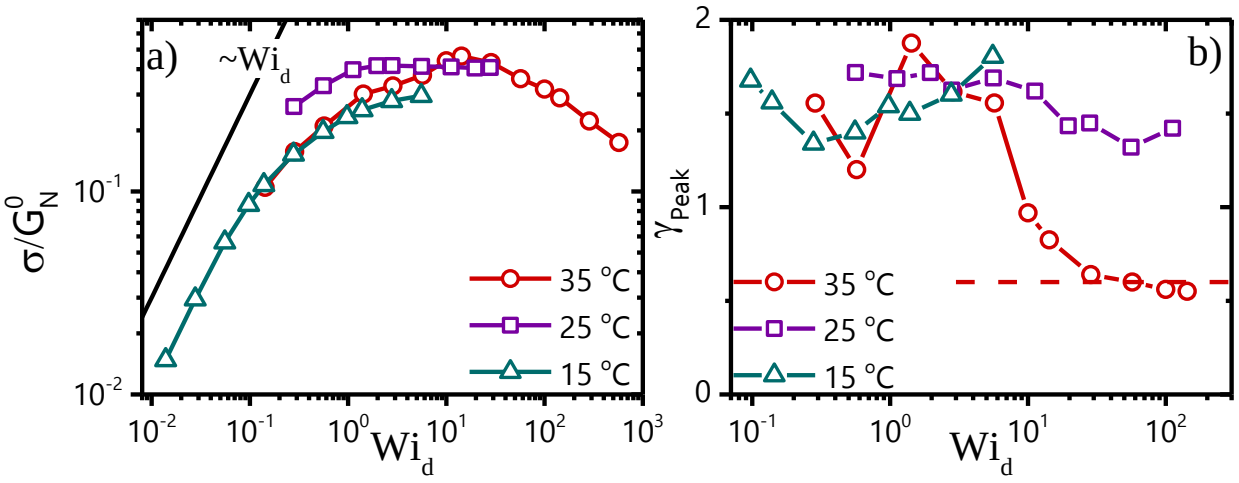

Figure 4.5 a) Steady state stress normalized with the plateau modulus as a function of the terminal Weissenberg number for all three temperatures b) Peak strain as a function of terminal Weissenberg number.

In summary, the supramolecular BPTA assembly presented in Chapter 3 exhibits interesting and unusual behavior under nonlinear shear flows, marked by shear thinning at lower temperatures and shear-strain hardening at short time scales and shear-strain softening at long time scales. Shear-strain hardening is proposed to reflect the semi-flexible nature of the system and its transient behavior might be related to the breaking/reformation process. Further investigations will help elucidating these points and providing a link to properties of networks consisting of biomacromolecules[9–11] (e.g., extracellular matrix) [20–22]. This offer insights into the design of novel supramolecular systems for use in biomaterials where such similarities with biological systems are profound[31]. A material with such versatile behavior, exhibiting such a broad spectrum of rheological phenomena by small changes in temperature, can serve as a model system for several rheological studies, for example, its response in

uniaxial extension. To this end, some fragmental evidence of strong extension hardening is promising.

References

(1) Cheng, J.; Amin, D.; Latona, J.; Heber-Katz, E.; Messersmith, P. B. Supramolecular Polymer Hydrogels for Drug-Induced Tissue Regeneration. *ACS Nano* **2019**, *13* (5), 5493–5501. https://doi.org/10.1021/acsnano.9b00281.

(2) Gouveia, L. M.; Müller, A. J. The Effect of NaCl Addition on the Rheological Behavior of Cetyltrimethylammonium P-Toluenesulfonate (CTAT) Aqueous Solutions and Their Mixtures with Hydrophobically Modified Polyacrylamide Aqueous Solutions. *Rheol. Acta* **2009**, *48* (2), 163–175. https://doi.org/10.1007/s00397-008-0319-7.

(3) Nakaya–Yaegashi, K.; Ramos, L.; Tabuteau, H.; Ligoure, C. Linear Viscoelasticity of Entangled Wormlike Micelles Bridged by Telechelic Polymers: An Experimental Model for a Double Transient Network. *J. Rheol.* **2008**, *52* (2), 359–377. https://doi.org/10.1122/1.2828645.

(4) Noteborn, W. E. M.; Zwagerman, D. N. H.; Talens, V. S.; Maity, C.; van der Mee, L.; Poolman, J. M.; Mytnyk, S.; van Esch, J. H.; Kros, A.; Eelkema, R.; Kieltyka, R. E. Crosslinker-Induced Effects on the Gelation Pathway of a Low Molecular Weight Hydrogel. *Adv. Mater.* **2017**, *29* (12), 1603769. https://doi.org/10.1002/adma.201603769.

(5) Kieltyka, R. E.; Pape, A. C. H.; Albertazzi, L.; Nakano, Y.; Bastings, M. M. C.; Voets, I. K.; Dankers, P. Y. W.; Meijer, E. W. Mesoscale Modulation of Supramolecular Ureidopyrimidinone-Based Poly(Ethylene Glycol) Transient Networks in Water. *J. Am. Chem. Soc.* **2013**, *135* (30), 11159–11164. https://doi.org/10.1021/ja403745w.

(6) Louhichi, A.; Jacob, A. R.; Bouteiller, L.; Vlassopoulos, D. Humidity Affects the Viscoelastic Properties of Supramolecular Living Polymers. *J. Rheol.* **2017**, *61* (6), 1173–1182. https://doi.org/10.1122/1.4997600.

(7) Van Zee, N. J.; Adelizzi, B.; Mabesoone, M. F. J.; Meng, X.; Aloi, A.; Zha, R. H.; Lutz, M.; Filot, I. A. W.; Palmans, A. R. A.; Meijer, E. W. Potential Enthalpic Energy of Water in Oils Exploited to Control Supramolecular Structure. *Nature* **2018**, *558* (7708), 100–103. https://doi.org/10.1038/s41586-018-0169-0.

(8) Bird, R. B.; Armstrong, R. C.; Hassager, O. *Dynamics of Polymeric Liquids*; Wiley: New York, 1987.

(9) Kang, H.; Wen, Q.; Janmey, P. A.; Tang, J. X.; Conti, E.; MacKintosh, F. C. Nonlinear Elasticity of Stiff Filament Networks: Strain Stiffening, Negative Normal Stress, and Filament Alignment in Fibrin Gels †. *J. Phys. Chem. B* **2009**, *113* (12), 3799–3805. https://doi.org/10.1021/jp807749f.

(10) Storm, C.; Pastore, J. J.; MacKintosh, F. C.; Lubensky, T. C.; Janmey, P. A. Nonlinear Elasticity in Biological Gels. *Nature* **2005**, *435* (7039), 191–194. https://doi.org/10.1038/nature03521.

(11) MacKintosh, F. C.; Käs, J.; Janmey, P. A. Elasticity of Semiflexible Biopolymer Networks. *Phys. Rev. Lett.* **1995**, *75* (24), 4425–4428. https://doi.org/10.1103/PhysRevLett.75.4425.

(12) Adams, A. A.; Solomon, M. J.; Larson, R. G.; Xia, X. Concentration, Salt and Temperature Dependence of Strain Hardening of Step Shear in CTAB/NaSal Surfactant Solutions. *J. Rheol.* **2017**, *61* (5), 967–977. https://doi.org/10.1122/1.4996008.

(13) Tung, S.-H.; Raghavan, S. R. Strain-Stiffening Response in Transient Networks Formed by Reverse Wormlike Micelles. *Langmuir* **2008**, *24* (16), 8405–8408. https://doi.org/10.1021/la704045t.
(14) Inoue, T.; Inoue, Y.; Watanabe, H. Nonlinear Rheology of CTAB/NaSal Aqueous Solutions: Finite Extensibility of a Network of Wormlike Micelles. *Langmuir* **2005**, *21* (4), 1201–1208. https://doi.org/10.1021/la048292v.
(15) Broedersz, C. P.; MacKintosh, F. C. Modeling Semiflexible Polymer Networks. *Rev. Mod. Phys.* **2014**, *86* (3), 995–1036. https://doi.org/10.1103/RevModPhys.86.995.
(16) Nam, S.; Hu, K. H.; Butte, M. J.; Chaudhuri, O. Strain-Enhanced Stress Relaxation Impacts Nonlinear Elasticity in Collagen Gels. *Proc. Natl. Acad. Sci.* **2016**, *113* (20), 5492–5497. https://doi.org/10.1073/pnas.1523906113.
(17) Schwarzl, F. R. Numerical Calculation of Stress Relaxation Modulus from Dynamic Data for Linear Viscoelastic Materials. *Rheol. Acta* **1975**, *14* (7), 581–590. https://doi.org/10.1007/BF01520809.
(18) Ferry, J. D. *Viscoelastic Properties of Polymers*; Wiley: New York: NY, 1980.
(19) Rolón-Garrido, V. H.; Wagner, M. H. The Damping Function in Rheology. *Rheol. Acta* **2009**, *48* (3), 245–284. https://doi.org/10.1007/s00397-008-0308-x.
(20) Petrie, R. J.; Gavara, N.; Chadwick, R. S.; Yamada, K. M. Nonpolarized Signaling Reveals Two Distinct Modes of 3D Cell Migration. *J. Cell Biol.* **2012**, *197* (3), 439–455. https://doi.org/10.1083/jcb.201201124.
(21) Das, R. K.; Gocheva, V.; Hammink, R.; Zouani, O. F.; Rowan, A. E. Stress-Stiffening-Mediated Stem-Cell Commitment Switch in Soft Responsive Hydrogels. *Nat. Mater.* **2016**, *15* (3), 318–325. https://doi.org/10.1038/nmat4483.
(22) Wen, Q.; Janmey, P. A. Effects of Non-Linearity on Cell–ECM Interactions. *Exp. Cell Res.* **2013**, *319* (16), 2481–2489. https://doi.org/10.1016/j.yexcr.2013.05.017.
(23) Annable, T.; Buscall, R.; Ettelaie, R.; Whittlestone, D. The Rheology of Solutions of Associating Polymers: Comparison of Experimental Behavior with Transient Network Theory. *J. Rheol.* **1993**, *37* (4), 695–726. https://doi.org/10.1122/1.550391.
(24) Pellens, L.; Gamez Corrales, R.; Mewis, J. General Nonlinear Rheological Behavior of Associative Polymers. *J. Rheol.* **2004**, *48* (2), 379–393. https://doi.org/10.1122/1.1645517.
(25) Cates, M. E.; Fielding, S. M. Rheology of Giant Micelles. *Adv. Phys.* **2006**, *55* (7–8), 799–879. https://doi.org/10.1080/00018730601082029.
(26) Olmsted, P. D. Dynamics and Flow-Induced Phase Separation in Polymeric Fluids. *Curr. Opin. Colloid Interface Sci.* **1999**, *4* (2), 95–100. https://doi.org/10.1016/S1359-0294(99)00016-3.
(27) Olmsted, P. D. Perspectives on Shear Banding in Complex Fluids. *Rheol. Acta* **2008**, *47* (3), 283–300. https://doi.org/10.1007/s00397-008-0260-9.
(28) Spenley, N. A.; Cates, M. E.; McLeish, T. C. B. Nonlinear Rheology of Wormlike Micelles. *Phys. Rev. Lett.* **1993**, *71* (6), 939–942. https://doi.org/10.1103/PhysRevLett.71.939.
(29) Germann, N.; Cook, L. P.; Beris, A. N. A Differential Velocities-Based Study of Diffusion Effects in Shear Banding Micellar Solutions. *J. Non-Newton. Fluid Mech.* **2016**, *232*, 43–54. https://doi.org/10.1016/j.jnnfm.2016.03.011.
(30) Doi, M.; Edwards, S. F. *The Theory of Polymer Dynamics*; Clarendon Press: Oxford, 1986.
(31) Webber, M. J.; Appel, E. A.; Meijer, E. W.; Langer, R. Supramolecular Biomaterials. *Nat. Mater.* **2016**, *15* (1), 13–26. https://doi.org/10.1038/nmat4474.

Appendix A: Cates Model for living polymers

In 1987 Cates proposed an extended version of the tube model[1] incorporating micellar reactions that can occur during stress relaxation leading to a predictive constitutive model for the viscoelasticity of solutions of wormlike micelles[2]. As described in section 3, it has been shown experimentally that this model can describe the viscoelasticity of supramolecular polymers. In the fast breaking limit where the breaking time, τ_b, is much smaller than the reptation time τ_{rep} the reptation-reaction prediction is recovered. Considering linear micelles, the possible reaction schemes are (i) the scission/recombination scheme, where a micelle can break at some point along its backbone and recombine with itself or with a neighboring micelle; (ii) the end interchange scheme where a micelle "bites" and carries away part of it; and (iii) the bond interchange scheme where two micelles will fuse together , forming a transient structure similar to a 4-arm star polymer and then split again into two differently connected components. These reaction shemes are schematically illustrated in Figure A1.A. These schemes can, of course, co-exist thus one of the assumptions in the model is that the scheme with the fastest rate will dominate.

The stress relaxation function, $\mu(t)$, describing the survival probability of a tube segment without a chain broken is the same as for the classic tube model[1]. However, by incorporating the scission/reformation scheme in the fast-breaking limit, the original chain ends do not survive long enough (since $\tau_b << \tau_{rep}$) for reptation to occur (through the same original tube). Instead, the relaxation is controlled by the fact that a tube segment can find itself very close to a chain end due to the random breaking process. The distance a chain end can move by curvilinear diffusion during its lifetime (which is essentially τ_b) is $l \sim (D_C(L)\tau_b)^{1/2}$,where D_C is the diffusion coefficient, L is the average length of the living polymers. This leads to a relation $l/L=(\tau_b/\tau_{rep})^{0.5}$. The new chain end created by the

breaking reaction needs time $\tau=\tau_b L/l$ for a new end to appear within distance l to recombine and finally relax (see schematic in Figure A1.B). Thus, the stress relaxation time will be:

$$\tau = (\tau_b \tau_{rep})^{1/2} \quad (1)$$

This holds also for the end interchange scheme, for which the new chain end is created by the reactive micelle end "biting" into the backbone of another micelle and destroying itself by its own reaction with a central part of another chain (Figure A1.C). In the fast reaction limit, the length of a living polymer "seen" by the tube segment as well as the position of the tube segment along the backbone of the living polymer are randomized by the rapid reaction rate, and this leads to a rapid averaging and consequently nearly identical relaxation rates for all tube segments, yielding the well-known mono-exponential relaxation of living polymers.

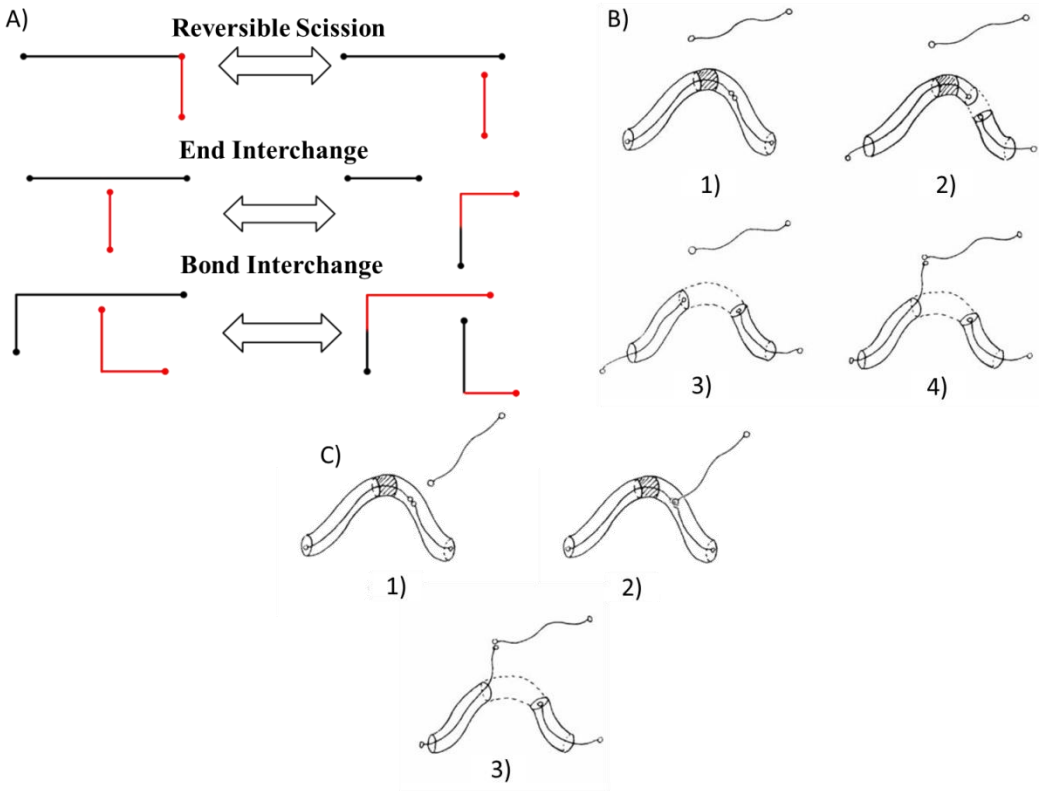

Figure A1. A) Schematic representations of the three different reaction schemes. B) Snasphsots of the relaxation process based on the scission/reformation reaction scheme with 1) being the first snapshot and 4) the

last. C) Snapshsots of the relaxation process based on the end interchange reaction scheme with 1) being the first snapshot and 3) the last. Figures are taken from [2,3]

Furthermore, when the ratio $\zeta=\tau_b/\tau_{rep}$ falls below 1/Z with Z being the number of tube segments, the dominant chain end motion is not the curvilinear diffusion but the so-called breathing modes or contour length fluctuations, well-known for linear polymers. This will change the relaxation time in (1) to:

$$\tau = {\tau_b}^{\frac{3}{4}}{\tau_{rep}}^{\frac{1}{4}}Z^{\frac{1}{4}}$$

On the other hand, the bond interchange reaction is not as effective relaxing stress , since it does not create or destroy chain ends, however it still does promote the relaxation due to the fact that it can bring a distant chain end close to a given tube segment, speeding-up relaxation compared to an unbreakable chain. Furthermore, there is a second effect, the so called tube evaporation where two chains can pass through one another. The bond interchange, without the tube evaporation effect, requires the creation of a chain end within a distance *l*. This will lead to a relaxation time which is not the geometric mean of the breaking and reptation times but becomes:

$$\tau = {\tau_b}^{1/3}{\tau_{rep}}^{2/3}$$

In the case of slow reaction limit where the breaking time is comparable to the reptation time, the relaxation behavior deviates from Maxwellian and becomes a stretched exponential relaxation.

The reptation-reaction model has been extended to the nonlinear regime[4,5]. Assuming that the system is highly entangled and $Z^{-1}<\zeta<1$, the linear viscoelasticity is described by a Maxwell mode and the reaction rates are unperturbed by the shear flow. As for linear polymers, after a rapid deformation is applied and the tube segments orient under flow, a fast retraction process occurs where the chain ends move towards the center of the tube, essentially evacuating their neighboring tube segments. However, in the fast breaking limit the retraction affects all tube segments equally since

each tube has lost memory of its length and position along the chemical backbone of the living polymer due to the rapid scission/reformation process. The stress is $\sigma = \frac{15}{4} G_o[\boldsymbol{W} - \frac{1}{3}\boldsymbol{I}]$, where **W** is the second moment of the orientational distribution function for tube segments in flow and **I** the unit vector. **W** depends on the birth ($B=1/\tau$) and death rates of tube segments ($D=v+1/\tau$, with v the drift velocity of chain ends towards the center of the tube due to retraction). The birth and death rates assume this simple form because in the averaging process described above there is no dependence on the position of the tube segments along the chemical backbone of the living polymer. The reduced stress (σ/G_o) is plotted in Figure A2 as function of the reduced shear rate (scaled by the terminal relaxation time). The theory predicts a maximum of the stress at σ^* at a shear rate $\dot{\gamma}_1$, due to the fact that as a tube segment is subjected to increasing shear deformation its stress tends to a constant value (orientation saturates), while the death rate increases indefinitely (due to increased retraction) so the tube segments are renewed faster, causing the stress to fall. This indicates an unstable flow[6], which is characterized by the existence of different fluid layers, normal to the velocity gradient direction. Rheologically the material exhibits the same stress at different deformation rates, one with rate $\dot{\gamma}_1$ and another with rate $\dot{\gamma}_2$ which are both on a stable increasing part of the curve . The volume fraction of each of the two bands follows the lever rule to match the macroscopically imposed shear rate[3,5–10]. Note that the original Doi-Edwards (DE) model predicted an instability[1] as well, but the experimental confirmation of such an effect remains a subtle point[11–13]. The DE model has been rectified by incorporating Convective Constraint Release (CCR)[14–17] , which is a mechanism that partial loss of entanglements due to flow. CCR corrects for the chain over-orientation of chain predicted in the original DE model that leads to a drop in the steady state stress. Furthermore, it has been observed that moderate polydispersity can "soften" the instability. In essence, this type of flow instability is a direct prediction of constitutive models for both linear and living polymers, but it has been confirmed experimentally only for living polymers in the fast breaking limit. In comparing the two systems one may remark that for living polymers the fact that the mechanism of stress relaxation is local leads to a stress overshoot even at significantly high shear rates, whereas for linear polymers it disappears due to constraint release[18].

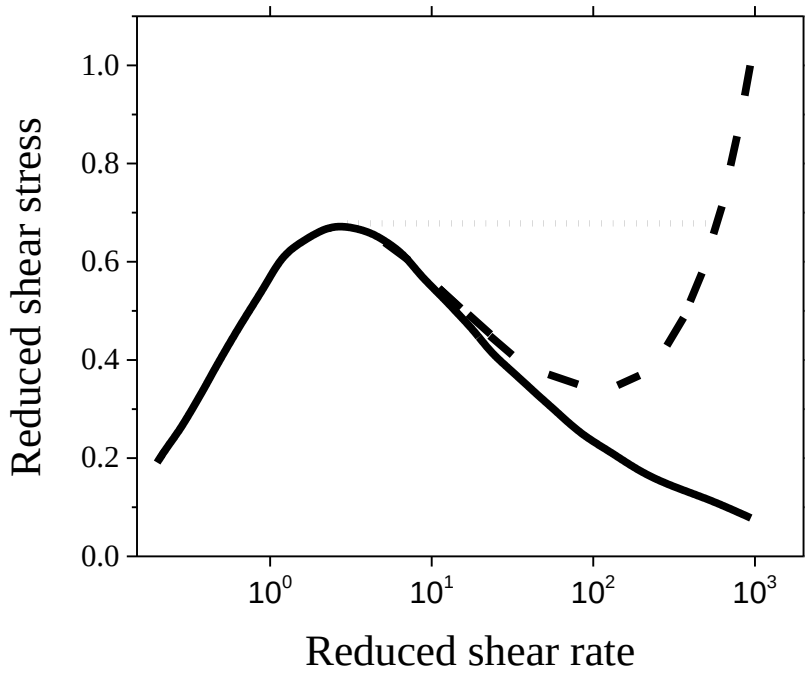

Figure A2. Reduced shear stress as a function of the reduced shear rate $\dot{\gamma}\tau$. Long-dashed line: upturn of the stress at high shear rates. Short-dashed line: The (measured) shear stress in the unstable branch region. Reproduced from [5].

References

(1) Doi, M.; Edwards, S. F. *The Theory of Polymer Dynamics*; Clarendon Press: Oxford, 1986.

(2) Cates, M. E. Reptation of Living Polymers: Dynamics of Entangled Polymers in the Presence of Reversible Chain-Scission Reactions. *Macromolecules* **1987**, *20* (9), 2289–2296. https://doi.org/10.1021/ma00175a038.

(3) Cates, M. E.; Fielding, S. M. Rheology of Giant Micelles. *Adv. Phys.* **2006**, *55* (7–8), 799–879. https://doi.org/10.1080/00018730601082029.

(4) Cates, M. E. Nonlinear Viscoelasticity of Wormlike Micelles (and Other Reversibly Breakable Polymers). *J. Phys. Chem.* **1990**, *94* (1), 371–375. https://doi.org/10.1021/j100364a063.

(5) Spenley, N. A.; Cates, M. E.; McLeish, T. C. B. Nonlinear Rheology of Wormlike Micelles. *Phys. Rev. Lett.* **1993**, *71* (6), 939–942. https://doi.org/10.1103/PhysRevLett.71.939.

(6) Olmsted, P. D. Dynamics and Flow-Induced Phase Separation in Polymeric Fluids. *Curr. Opin. Colloid Interface Sci.* **1999**, *4*, 95.

(7) Dhont, J. K. G.; Briels, W. J. Gradient and Vorticity Banding. *Rheol. Acta* **2008**, *47* (3), 257–281. https://doi.org/10.1007/s00397-007-0245-0.

(8) Olmsted, P. D. Perspectives on Shear Banding in Complex Fluids. *Rheol. Acta* **2008**, *47* (3), 283–300. https://doi.org/10.1007/s00397-008-0260-9.

(9) Adams, J. M.; Fielding, S. M.; Olmsted, P. D. Transient Shear Banding in Entangled Polymers: A Study Using the Rolie-Poly Model. *J. Rheol.* **2011**, *55* (5), 1007–1032. https://doi.org/10.1122/1.3610169.

(10) Lerouge, S.; Olmsted, P. D. Non-Local Effects in Shear Banding of Polymeric Flows. *Front. Phys.* **2020**, *7*, 246. https://doi.org/10.3389/fphy.2019.00246.

(11) Snijkers, F.; Pasquino, R.; Olmsted, P. D.; Vlassopoulos, D. Perspectives on the Viscoelasticity and Flow Behavior of Entangled Linear and Branched Polymers. *J. Phys. Condens. Matter* **2015**, *27* (47), 473002. https://doi.org/10.1088/0953-8984/27/47/473002.

(12) Wang, S.-Q.; Ravindranath, S.; Boukany, P. E. Homogeneous Shear, Wall Slip, and Shear Banding of Entangled Polymeric Liquids in Simple-Shear Rheometry: A Roadmap of Nonlinear Rheology. *Macromolecules* **2011**, *44* (2), 183–190. https://doi.org/10.1021/ma101223q.

(13) Li, Y.; Hu, M.; McKenna, G. B.; Dimitriou, C. J.; McKinley, G. H.; Mick, R. M.; Venerus, D. C.; Archer, L. A. Flow Field Visualization of Entangled Polybutadiene Solutions under Nonlinear Viscoelastic Flow Conditions. *J. Rheol.* **2013**, *57* (5), 1411–1428. https://doi.org/10.1122/1.4816735.

(14) Marrucci, G. Dynamics of Entanglements: A Nonlinear Model Consistent with the Cox-Merz Rule. *J. Non-Newton. Fluid Mech.* **1996**, *62* (2–3), 279–289.

(15) Graessley, W. W. Molecular Entanglement Theory of Flow Behavior in Amorphous Polymers. *J. Chem. Phys.* **1965**, *43*, 2696.

(16) Baig, C.; Mavrantzas, V. G.; Kröger, M. Flow Effects on Melt Structure and Entanglement Network of Linear Polymers: Results from a Nonequilibrium Molecular Dynamics Simulation Study of a Polyethylene Melt in Steady Shear. *Macromolecules* **2010**, *43* (16), 6886–6902. https://doi.org/10.1021/ma100826u.

(17) Ianniruberto, G.; Marrucci, G. Convective Constraint Release (CCR) Revisited. *J. Rheol.* **2014**, *58* (1), 89–102. https://doi.org/10.1122/1.4843957.

(18) Milner, S. T.; McLeish, T. C. B.; Likhtman, A. E. Microscopic Theory of Convective Constraint Release. *J. Rheol.* **2001**, *45* (2), 539–563. https://doi.org/10.1122/1.1349122.

Appendix B Supporting Information for Chapter 2

I. Molecular structure of the BTA-based motifs and synthetic details

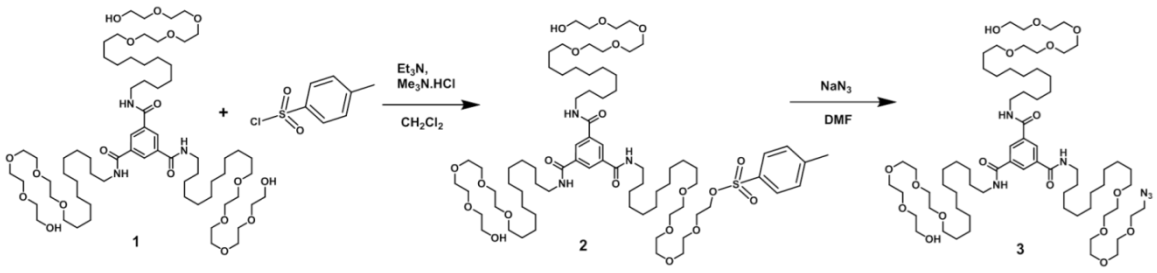

Figure S1: Synthetic scheme for the synthesis of **3**.

1-(3,5-bis((1-hydroxy-3,6,9,12-tetraoxatetracosan-24-yl)carbamoyl)phenyl)-1-oxo-15,18,21,24-tetraoxa-2-azahexacosan-26-yl 4-methylbenzenesulfonate **(2)**. N^1,N^3,N^5-tris(1-hydroxy-3,6,9,12-tetraoxatetracosan-24-yl)benzene-1,3,5-tricarboxamide **1** (3.0 g, 2.33 mmol, BTA), of which the synthesis has been previously reported[1], and trimethyl amine hydrochloride (0.111 g, 1.16 mmol) were dissolved in dichloromethane (30 mL). After adding triethyl amine (0.7 mL, 6,98 mmol) the mixture was cooled to 0 °C and p-Toluenesulfonyl chloride (0.4 g, 2.09 mmol) dissolved in dichloromethane (30 mL) was added dropwise. The mixture was stirred overnight at room temperature and then washed twice with 1M aqueous hydrochloric acid (50 mL). After back extraction of the aqueous phase the combined organic layers were washed with brine and dried over sodium sulfate. Evaporation of the solvent yielded 3.4 g of a waxy solid. The crude product is a mixture of non-, mono-, di- and tri-tosylated product that was used in the next step without further purification.

^{1}H-NMR (400 MHz, $CDCl_3$) δ 8.37 (s, 3H, Ar), 7.79 (d, 2H, CH=C<u>H</u>C(S)C<u>H</u>=CH), 7.34 (d, 2H, CH=C<u>H</u>C(CH_3)C<u>H</u>=CH), 6.76 (m, 3H, C=ON<u>H</u>CH_2), 4,14 (t, 2H, C<u>H_2</u>-O-S), 3.74-3.56 (m, 46H, O-(C<u>H_2</u>)$_2$-O), 3.43 (m, 12H, CH_2C<u>H_2</u>NHC=O, CH_2CH_2C<u>H_2</u>O), 2.72 (q, 2H, CH_2-O<u>H</u>), 2.45 (s, 2.6H, Ar-C<u>H_3</u>), 1.61 (m, 6H, CH_2C<u>H_2</u>CH_2O), 1.55 (m, 6H, CH_2C<u>H_2</u>CH_2NHC=O), 1.37-1.20 (m, 48H, aliphatic).

N1-(1-azido-3,6,9,12-tetraoxatetracosan-24-yl)-N3,N5-bis(1-hydroxy-3,6,9,12-tetraoxatetracosan-24-yl)benzene-1,3,5-tricarboxamide **(3)**. 1-(3,5-bis((1-hydroxy-3,6,9,12-tetraoxatetracosan-24-yl)carbamoyl)phenyl)-1-oxo-15,18,21,24-tetraoxa-2-azahexacosan-26-yl 4-methylbenzenesulfonate **2** (3.02 g, 2.09 mmol) and sodium azide (0.15 g, 2,3 mmol) were dissolved in dry N,N-dimethylformamide (45 mL). The reaction was stirred overnight at 50 °C. Evaporation of the solvent yielded 3,5 g of the crude product. The material was purified by column chromatography (eluent chloroform/methanol 95/5–90/10 v/v) yielding 1.03 g (37%) of the desired mono-azide product as a waxy solid.

^{1}H NMR (400 MHz, $CDCl_3$) δ 8.37 (s, 3H, Ar), 6.62 (m, 3H, C=ON<u>H</u>CH_2), 3.71 (m, 4H, CH_2C<u>H_2</u>-OH), 3.65 (m, 32H, O-(C<u>H_2</u>)$_2$-O), 3.59 (m, 10H, O-(C<u>H_2</u>)$_2$-O), 3.45 (m, 12H, CH_2C<u>H_2</u>NHC=O, CH_2CH_2C<u>H_2</u>O), 3.38 (t, 2H, OCH_2C<u>H_2</u>N_3), 2.64 (t, 2H, CH_2-O<u>H</u>), 1.61 (m, 6H, CH_2C<u>H_2</u>CH_2O), 1.55 (m, 6H, CH_2C<u>H_2</u>CH_2NHC=O), 1.41-1.21 (m, 48H, aliphatic). ^{13}C NMR (100 MHz, $CDCl_3$) δ 165.8, 135.4, 128.2, 72.7, 71.7, 70.8, 70.8, 70.7, 70.5, 70.2, 61.9, 50.8, 40.5, 29.8, 29.7, 29.7, 29.7, 29.6, 29.6, 29.5, 29.4, 29.4, 27.10, 27.07, 26.22, 26.19. FT-IR (ATR) ν (cm-1): 3300, 2918, 2851, 2097, 1643, 1535, 1468, 1443, 1348, 1290, 1110, 937, 881, 837, 721, 706, 694. MALDI-TOF-MS: calculated MW = 1313.8 g/mol, observed *m/z* = 1313.5 $[M+H]^+$, 1336.0 $[M+Na]^+$. LC-MS *m/z* = 1314.2 $[M+H]^+$. GPC (DMF, 10mM LiBr) Mn = 915 g/mol, Mw = 965 g/mol.

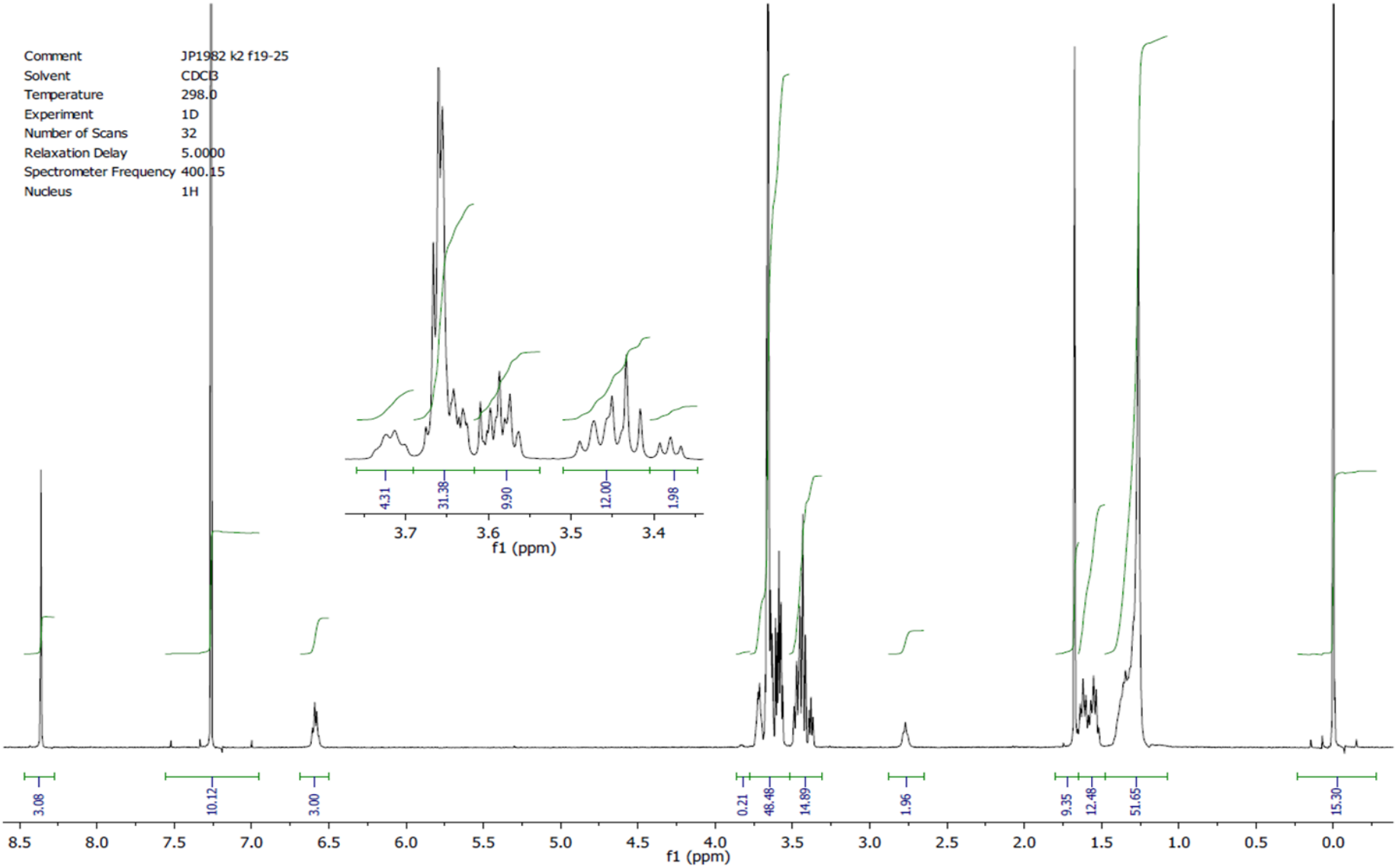

Figure S2: ^{1}H-NMR of **3** in $CDCl_3$.

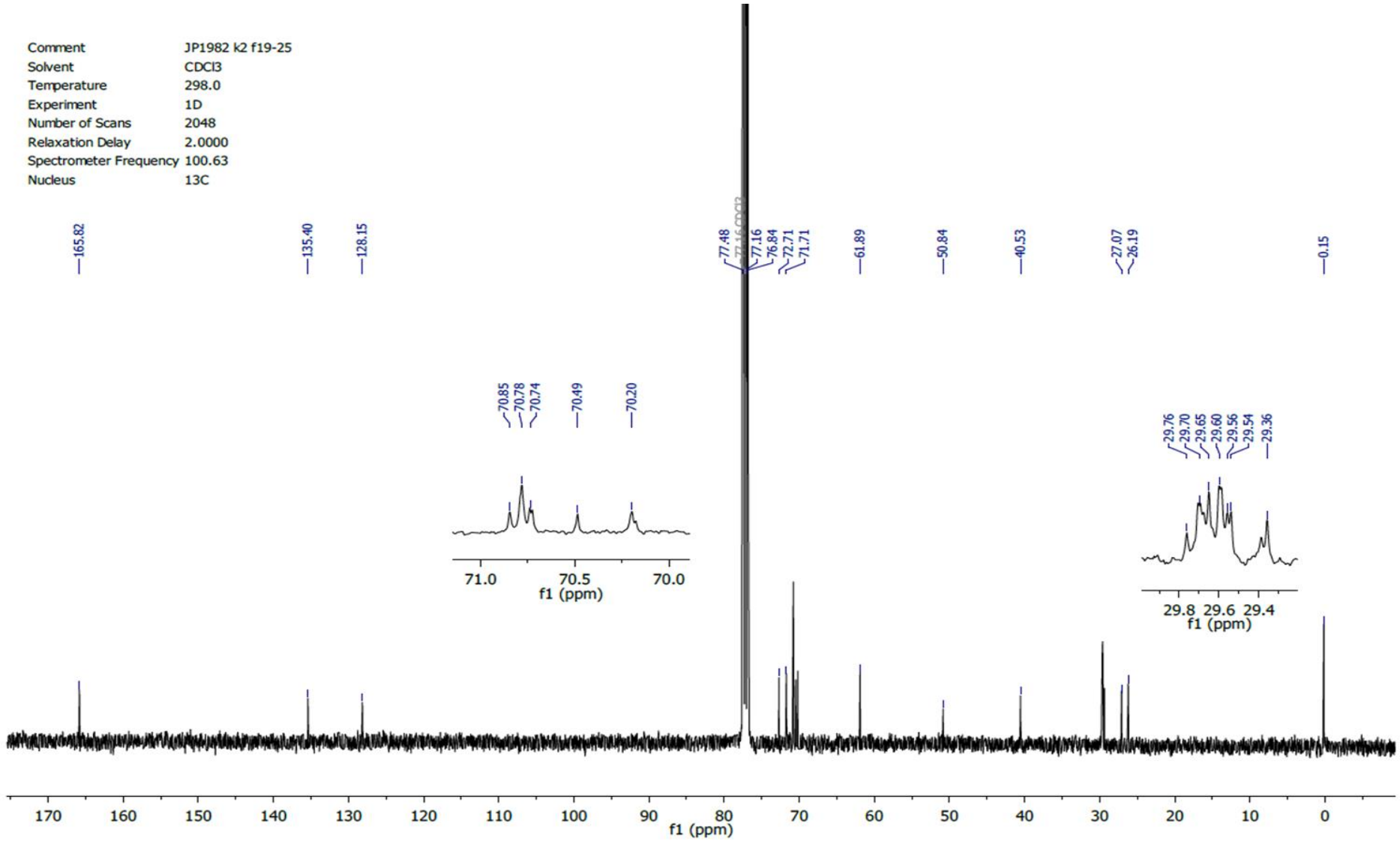

Figure S3: ^{13}C-NMR of **3** in $CDCl_3$.

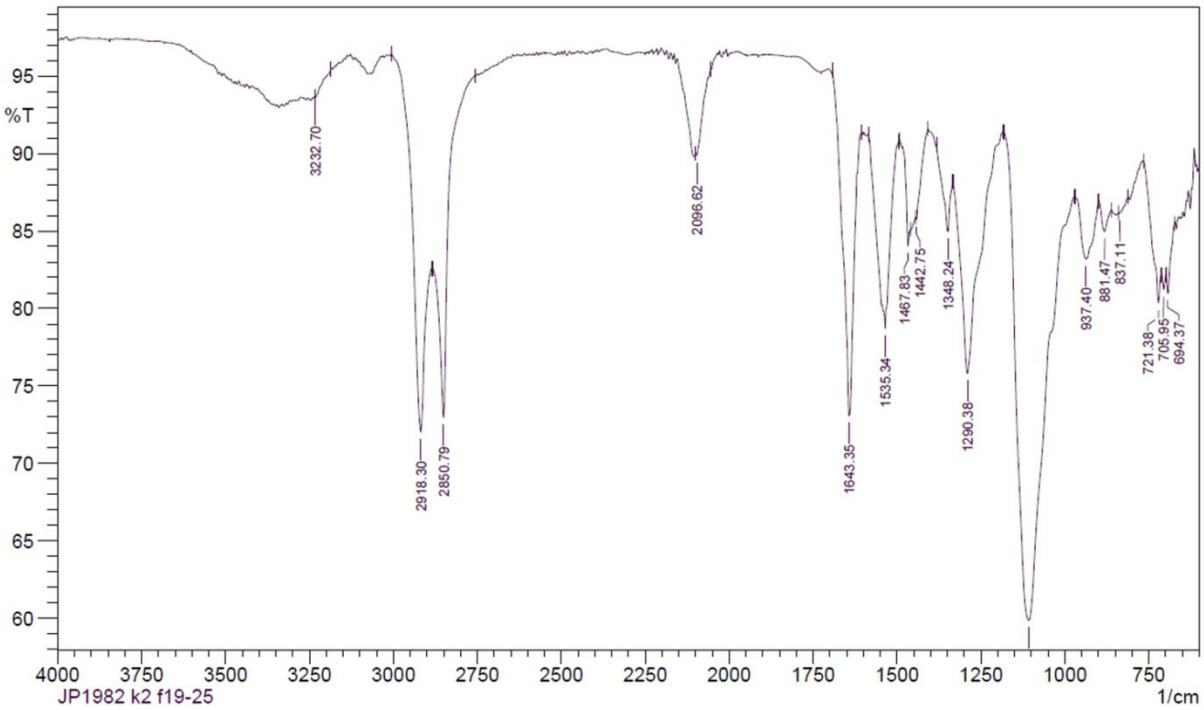

Figure S4: IR spectrum of **3**.

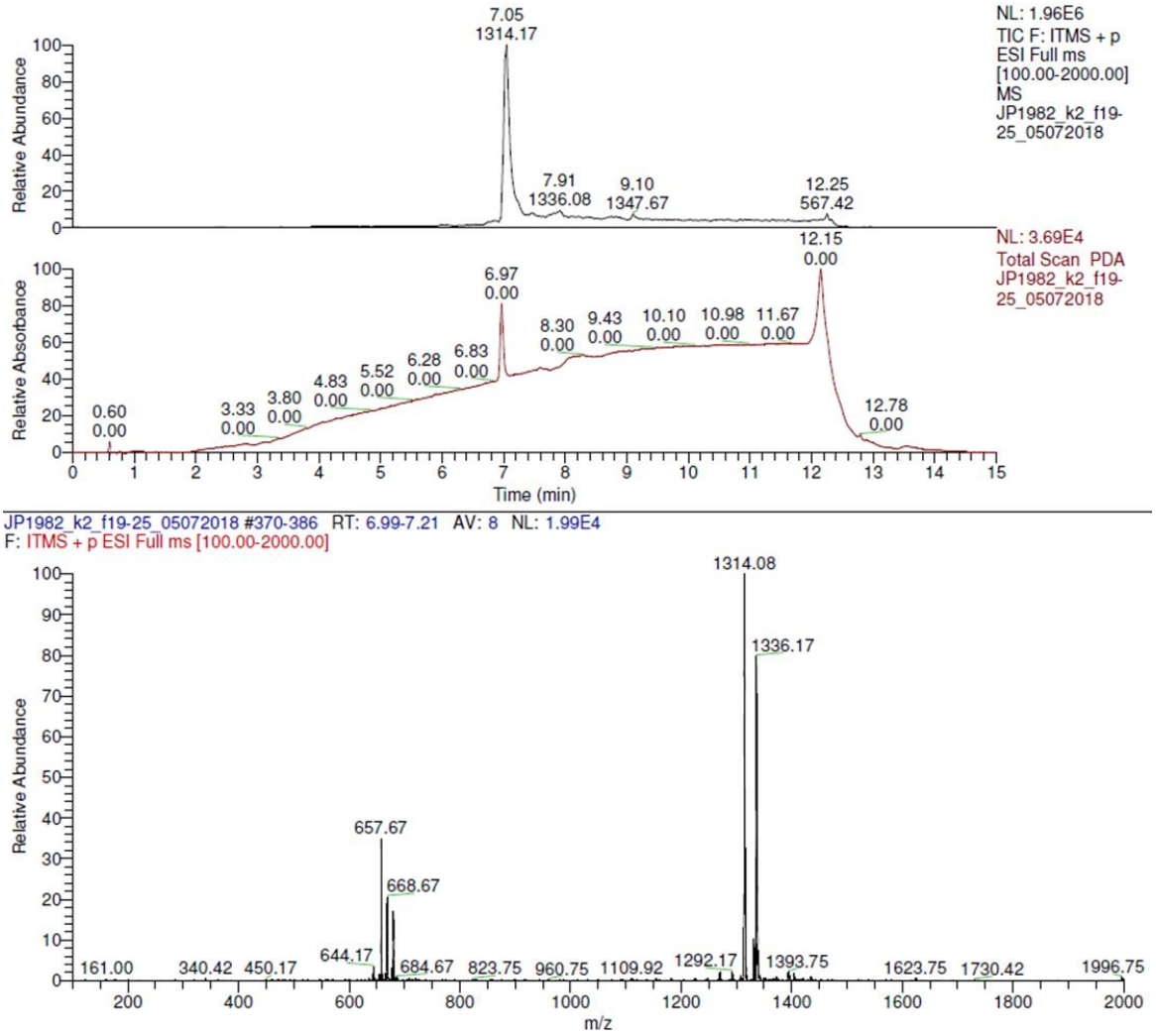

Figure S5: LC-MS of **3**.

Figure S6: Synthetic scheme for the synthesis of dialkyne functionalized PEG (molecule **4**).

Polyethylene glycol dialkyne (Mn = 20 kg/mol) **(4)**. Polyethylene glycol (Mn = 20 kg/mol) (20 g, 1 mmol) was dried at 120 °C under reduced pressure in the presence of Phosphorus pentoxide for 2 hours. Then, under argon atmosphere at 70 °C it was dissolved in dry tetrahydrofuran (100 mL). After cooling towards 40 °C sodium hydride (0.32 g, 60%, 8 mmol) was added giving a slightly hazy orange solution which was stirred for 45 minutes. Tetrabutylammonium iodide (18 mg, 0.05 mmol) and propargyl bromide (1.34 mL, 80%, 12 mmol) were added and the darkening mixture was stirred overnight at 40 °C. The mixture was concentrated *in vacuo*, dissolved in chloroform (100 mL) and filtered over celite. To the filtrate was slowly added diethyl ether (600 mL) resulting in a white precipitate which was collected by filtration and washing with diethyl ether. Drying of the residue yielded 19.5 g (98%) white powder.

^{1}H NMR (400 MHz, $CDCl_3$) δ 4.21 (s, 4H, $OC\underline{H}_2C{\equiv}CH$), 3.65 (s, 1650H, $O\text{-}(C\underline{H}_2)_2\text{-}O$), 2.45 (s, 2H,$OCH_2C{\equiv}C\underline{H}$). GPC (DMF, 10mM LiBr) Mn = 19.7 kg/mol, Mw = 20.5 kg/mol.

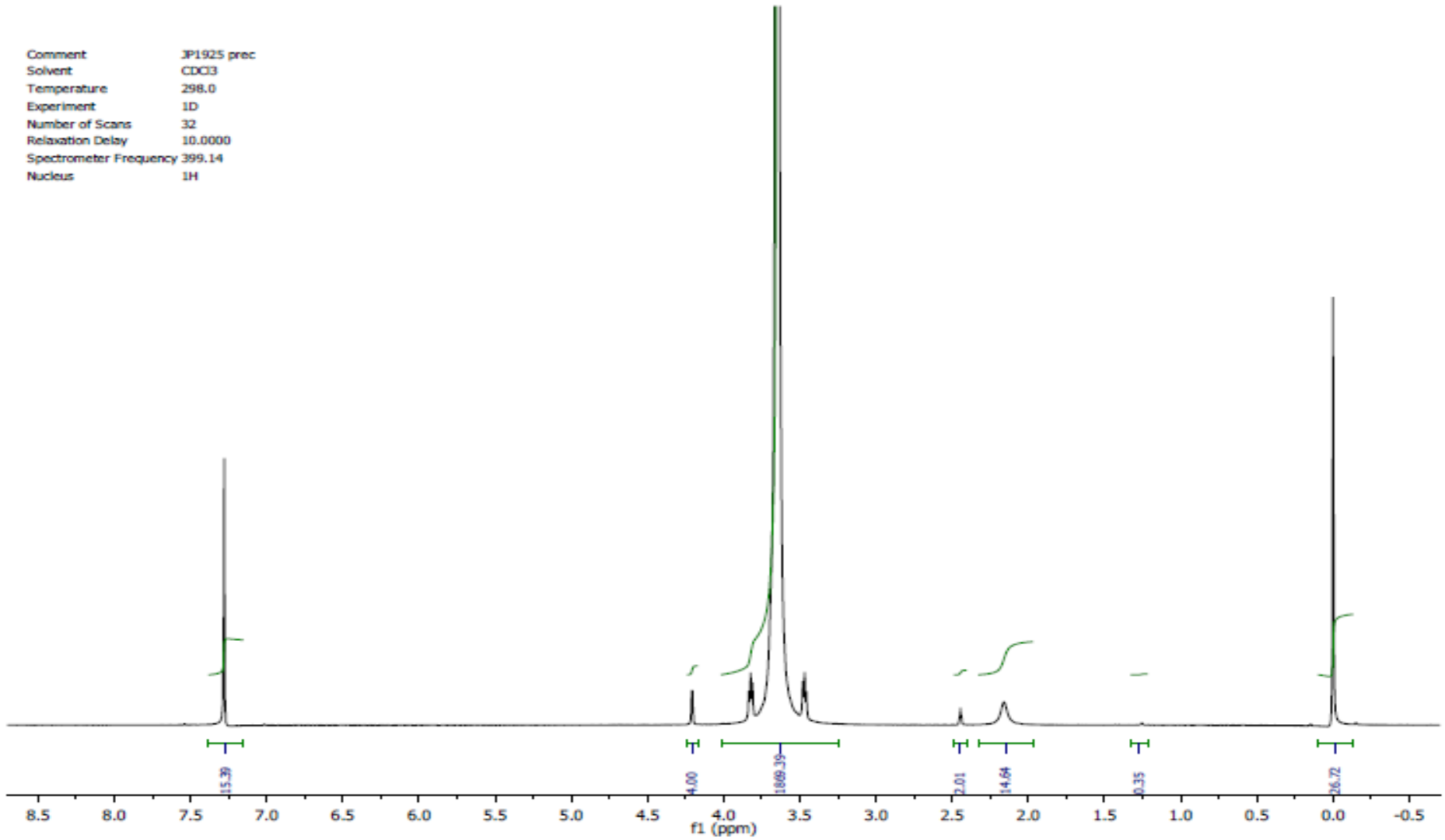

Figure S7: ^{1}H-NMR spectrum of **4**.

N1,N1'-(polyethylene glycol) bis (1H-1,2,3-triazole-4,1-diyl)) bis (3,6,9,12-tetraoxatetracosane -1,24-diyl)) bis (N3,N5-bis (1-hydroxy-3,6,9,12-tetraoxatetracosan-24-yl) benzene-1,3,5-tricarboxamide) **(5, BTA-PEG-BTA)**. Polyethylene glycol dialkyn (Mn = 20 kg/mol) **4** (6.9 g, 0.35 mmol), copper sulfate (0.086 g, 0.76 mmol) and sodium ascorbate (0.10 g, 0.52 mmol) were dissolved in water (20 mL) and ethanol (20 mL). N1-(1-azido-3,6,9,12-tetraoxatetracosan-24-yl)-N3,N5-bis(1-hydroxy-3,6,9,12-tetraoxatetracosan-24-yl)benzene-1,3,5-tricarboxamide **3** (1 g, 0.76 mmol), dissolved in ethanol (30 mL) and water (10 mL) was added. After stirring for 4 hours the solvent was evaporated *in vacuo* and the residue dissolved in chloroform (450 mL). This milky solution was washed twice with aqueous 0.1 M disodium ethylenediaminetetra-acetate (EDTA-Na_2) (225 mL). The first aqueous washing phase turned blue, the second which was back extracted stayed colorless.

The combined organic phases were washed with brine and dried over sodium sulfate. After concentration *in vacuo* the residue was dissolved in chloroform/ethanol (5/1 v/v) and filtrated over celite. To the filtrate was slowly added diethyl ether (600 mL) resulting in a white precipitate which was collected by filtration and washing with diethyl ether. Drying of the residue yielded 6.7 g (86%) of a white powder.

^{1}H NMR (400 MHz, $CDCl_3$) δ 8.40 (s, 6H, Ar), 7.73 (s, 2H, N-C<u>H</u>=C), 6.82 (m, 6H, C=ON<u>H</u>CH_2), 4.66 (s, 4H, O-C<u>H</u>$_2$C(N)=CH) , 4.53 (t, 4H, OC<u>H</u>$_2$$CH_2$N), 3.86 (t, 4H, OCH_2C<u>H</u>$_2$N), 3.81 (t, sat), 3.64 (m, 2156H, O-(C<u>H</u>$_2$)$_2$-O), 3.44 (m, 42H, sat, CH_2C<u>H</u>$_2$NHC=O, CH_2CH_2C<u>H</u>$_2$O, OCH_2C<u>H</u>$_2$N), 2.70 (t, 4H, CH_2-O<u>H</u>), 1.59 (m, 24H, CH_2C<u>H</u>$_2CH_2$O, CH_2C<u>H</u>$_2CH_2$NHC=O), 1.26 (m, 96H, aliphatic). ^{13}C NMR (100 MHz, $CDCl_3$) δ 165.9, 135.4, 128.3, 123.9, 72.6, 71.7, 70.7, 70.5, 70.2, 69.7, 69.6, 64.7, 61.9, 50.3, 40.5, 29.7, 29.6, 29.5, 29.4, 27.1, 26.2. FT-IR (ATR) ν (cm-1): 2884, 1659, 1466, 1360, 1342, 1279, 1240, 1146, 1101, 1061, 961, 947, 841. GPC (DMF, 10mM LiBr) Mn = 22.3 kg/mol, Mw = 23.1 kg/mol.

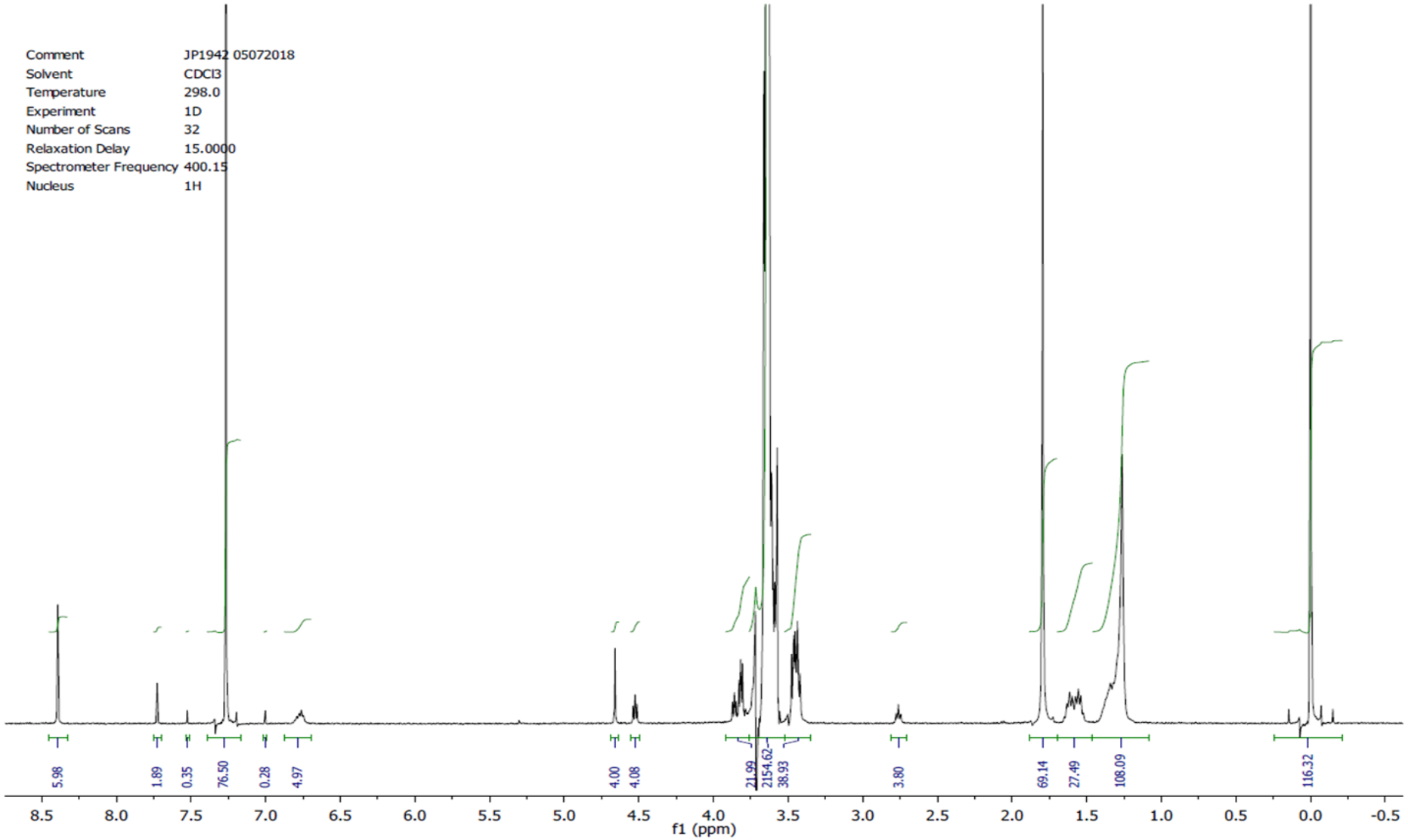

Figure S8: ^{1}H-NMR of BTA-PEG-BTA in $CDCl_3$.

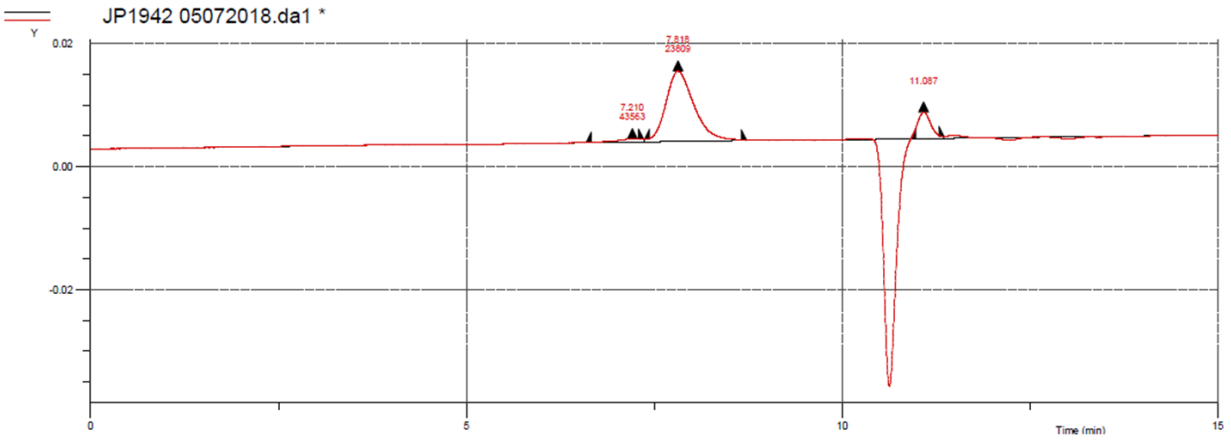

Point to point noise (V): 2.2867E-05 (0.04%); RMS Noise (V): 1.4945E-05 (0.03%)

Peak	Top (min)	Plates	Height (V)	Area (V.min)	Area fract. %	Mp	Mw	Mn	D	Norm.are
1	7.210		0.00054281	0.00021688	3.56%	43563	50171	47997	1.045	4.3(
2	7.818	2224	0.011428	0.0049759	81.7%	23809	23071	22290	1.035	100.0(
3	11.087	17897	0.0043222	0.00089694	14.7%					18.0:
3 of 3 peaks				0.0060897	100.0%					

Figure S9: GPC of BTA-PEG-BTA.

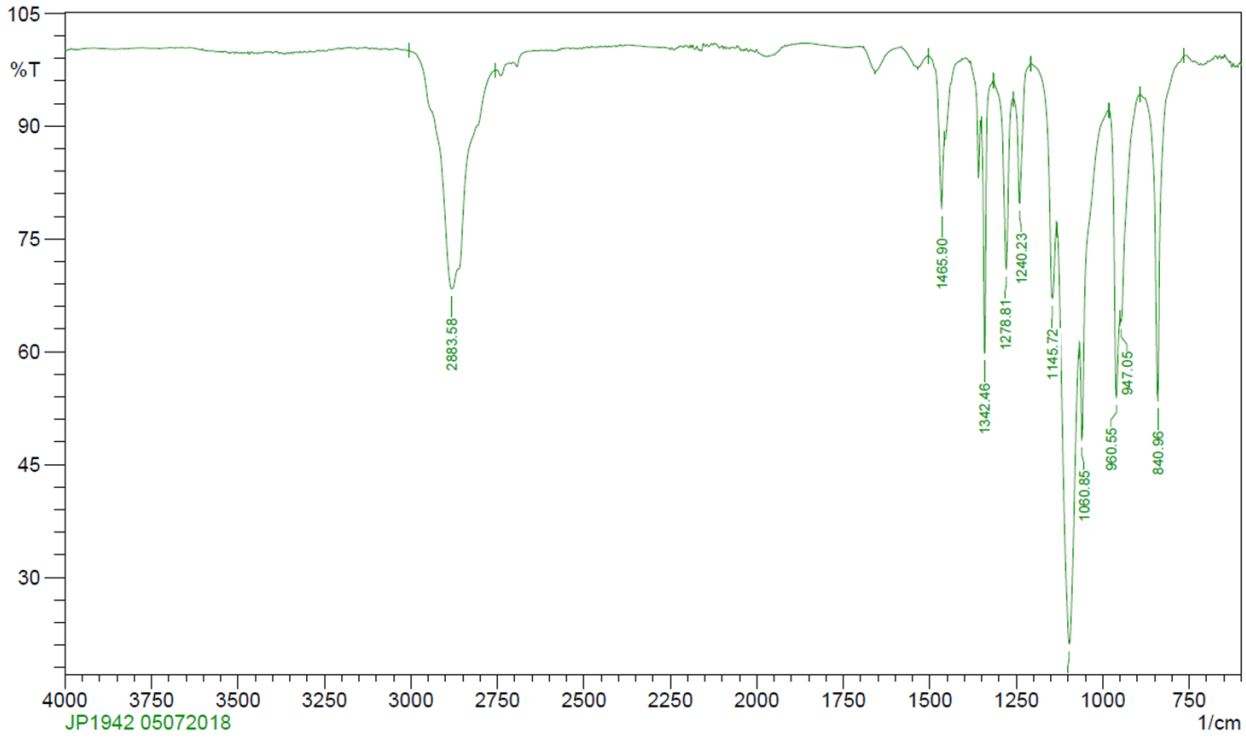

Figure S10: IR spectrum of BTA-PEG-BTA.

II. Linear Viscoelastic data of single components and binary hydrogels

The concentration of all hydrogels is 5wt% in all experiments.

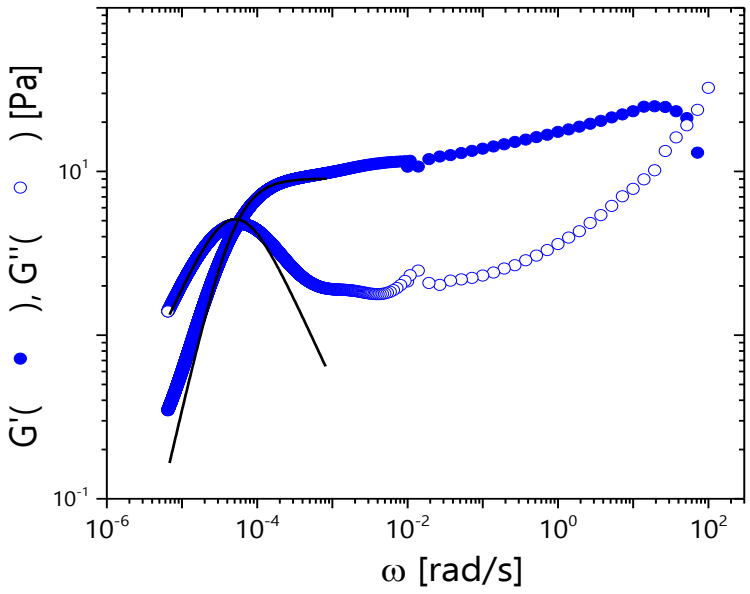

Figure S11: Maxwell-model fit (black lines) of the terminal relaxation process of the linear viscoelastic spectrum of the pure BTA component at 20 °C. The storage modulus (G') is represented by filled circles while the loss modulus (G") is represented with open circles. The fit yielded a plateau modulus G_p = 9 Pa and a crossover frequency $\omega_c = 5 \times 10^{-5}$ s^{-1}.

The Maxwell model[2] is represented by a purely viscous dashpot, characterized by the viscosity η, and a purely elastic spring, characterized by a spring constant $\boldsymbol{G_o}$, connected in series. This model is used to describe simple viscoelastic liquids, where the spring constant gives the modulus of the material and a characteristic relaxation time can be extracted from the viscosity, $\boldsymbol{\lambda = \eta / G_o}$:

$$\boldsymbol{G'(\omega) = G_o \frac{(\lambda\omega)^2}{1+(\lambda\omega)^2}, G''(\omega) = G_o \frac{\lambda\omega}{1+(\lambda\omega)^2}}.$$

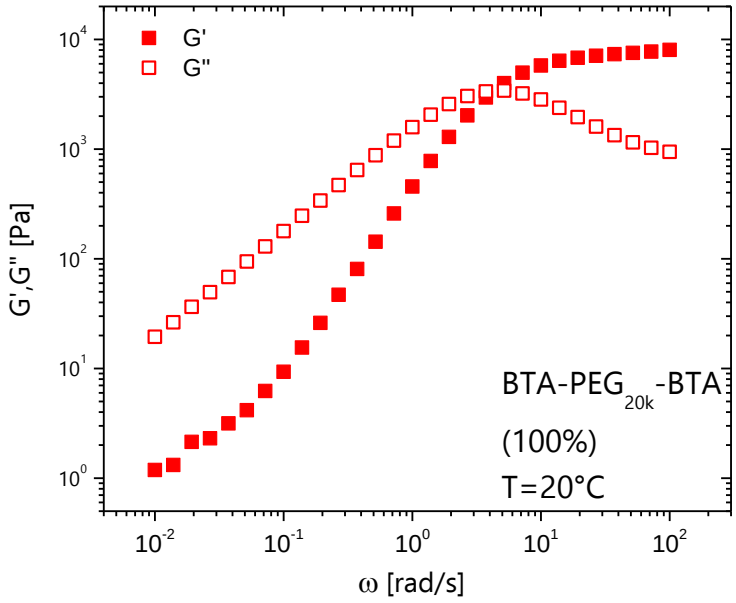

Figure S12: BTA-PEG-BTA linear viscoelastic spectrum measured at 20 °C.

In order to check whether the viscoelastic response of the BTA-PEG-BTA hydrogel (5% w/w) is due to the topological entanglements of the PEG chains or not, we estimated the molecular weight that a PEG chain should have to yield the specific viscoelastic response. The molecular weight of a pure PEG chain needed to yield such a plateau modulus and reptation time, if the gel was only made out of PEG chains is calculated using the equation 1[3]

$$\boldsymbol{\eta - \eta_s \approx G_p \tau_{rep} \approx \eta_s \frac{N^3}{N_e} \varphi^{-3/(3\nu-1)}, \nu = 0.5} \quad (1)$$

Where G_p is the plateau modulus, τ_{rep} is the characteristic time a chain needs to get free from the topological constraints (entanglements), N is the degree of polymerization of the chain, N_e=45 is the degree of polymerization of one entanglement strand in the melt, $\varphi = 0.045$ is the volume fraction (which is the fraction of PEG in the hydrogel of BTA-PEG-BTA), and ν is the Flory exponent, which in the case of good solvency conditions is equal to 0.588[3]. This yields N=25244, so the same G_p can be obtained by a PEG chain with molecular

weight $M_w = NM_{mon} = 1.1 \times 10^6\ g/mol$, with M_{mon} being the molecular weight of an ethylene glycol monomer.

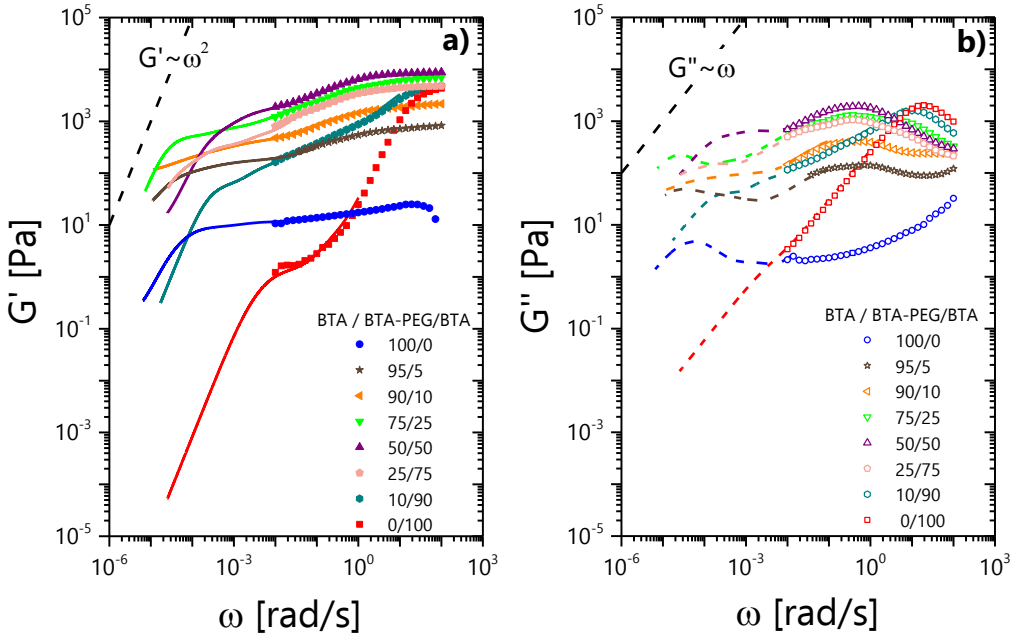

Figure S13: a) Storage Modulus as a function of angular frequency for the pure components and all the mixtures measured. b) Loss Modulus as a function of angular frequency for the pure components and all the mixtures measured. Black dashed lines represent the terminal slopes for G' (a) and G'' (b).

Determination of the zero-shear viscosity and its dependence on composition

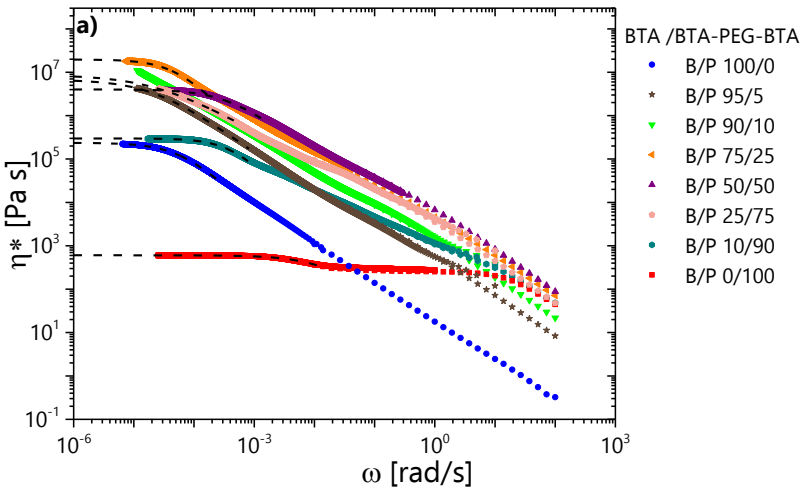

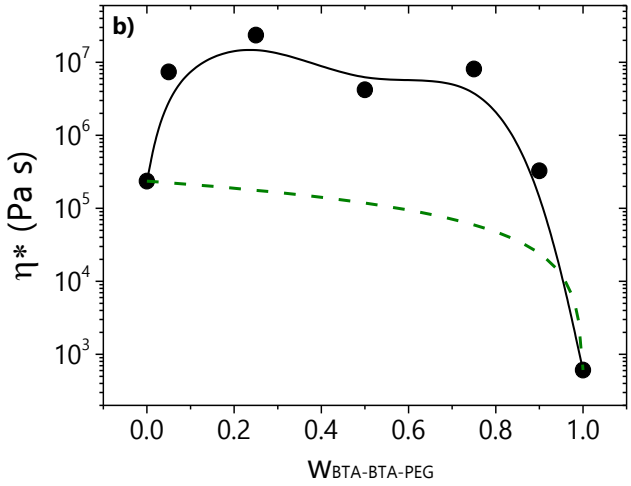

Figure S14: a) Complex viscosity as a function of the angular frequency. Black dashed lines represent the best fit with the Cross model[5] to obtain the zero-shear viscosity. The viscosity of the 90/10 mixture cannot be extracted since the sample does not reach terminal relaxation in the accessible range of frequencies. b) Variation of zero-shear viscosity as function of the weight fraction of the telechelic component BTA-PEG-BTA. The green line represents the linear mixing rule[6].

The Cross model[5] describes the dependence of non-Newtonian fluids, whose viscosity depends on shear rate.

$$\eta = \eta_\infty + \frac{\eta_o - \eta_\infty}{[1+(C\dot{\gamma})^\nu]}$$

where η_∞ is the value of the viscosity at very high shear rate, η_o is the zero-shear viscosity, C is a coefficient related to the relaxation time of the material, γ is the shear rate and ν is the thinning exponent. Typically η_∞ is set to zero, since most experiments never reach the regime of constant viscosity at high shear rates.

In the case of oscillatory shear, the complex viscosity as a function of angular frequency can still be fitted with the same model.

III. Dynamic light scattering characterization in dilute solution

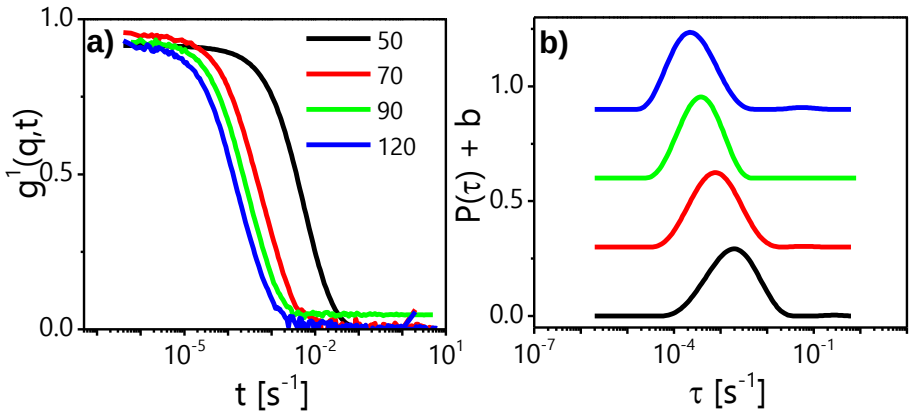

Figure S15: Dynamic Light Scattering measurements of BTA-PEG-BTA in dilute conditions (c=0.3 wt %). a) Field correlation functions at different angles. b) Laplace transform of the correlation functions to obtain the distribution of characteristic relaxation times.

From the Laplace transform of the correlation functions we obtain the characteristic relaxation time for each angle. The inverse of the relaxation time (Γ) is proportional to the squared wave-vector (q) if the motion is diffusive. The proportionality constant is the diffusion coefficient (D). Thus, $\Gamma=Dq^2$. From the diffusion coefficient we can obtain the hydrodynamic radius (R_h) using the Stokes-Einstein-Sutherland (SES) relation: $R_h = {kT}/{6\pi\eta D}$, where k is Boltzmann's constant, T is the temperature, η is the solvent viscosity[4]. We note that the SES relation does not provide accurate sizes for non-spherical particles, however the sole purpose of the analysis here is to demonstrate aggregation of the BTA-PEG-BTA component in dilute solution.

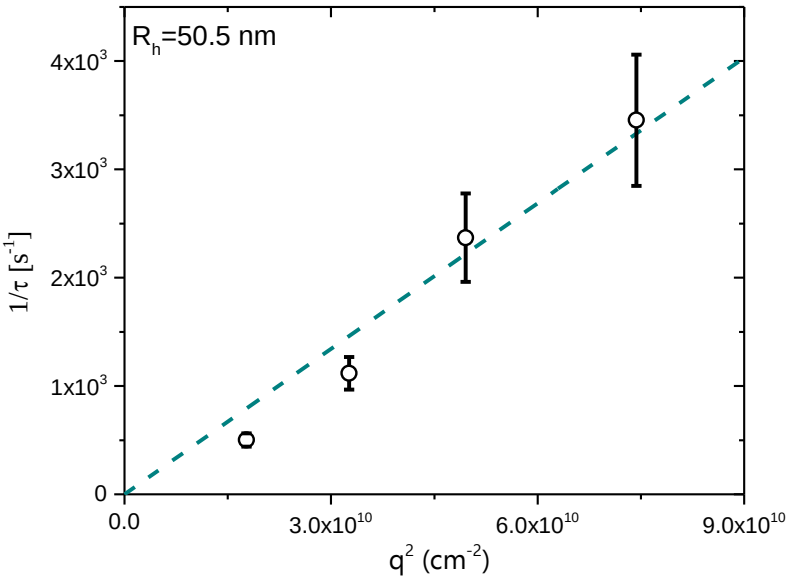

Figure S16: Inverse relaxation time as a function of the squared wave-vector. The cyan line is the least squares linear fit, with the slope yielding the diffusion coefficient and the intercept zero. The error bars are obtained from five separate measurements

IV. Response to Large Amplitude Oscillatory Shear Strain

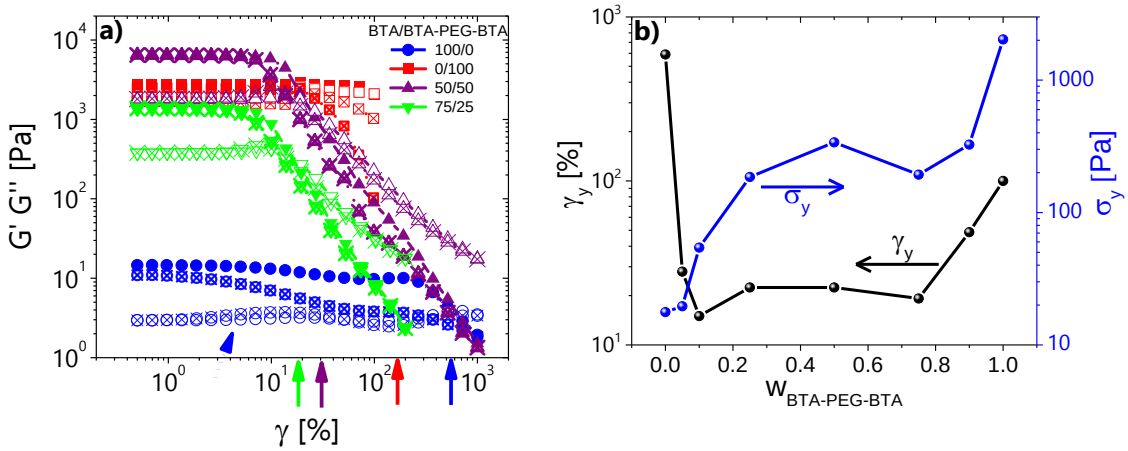

Figure S17: a) Variation of the storage and loss moduli with the applied strain amplitude for the same systems (color coding is the same). The symbols with x represent the scan from large strain amplitudes to low strain amplitudes while the solid lines vice versa. The reversible response indicates that there is no thixotropy. Arrows show the yield strain for each sample. The dotted arrow indicates the first yielding process observed in the pure BTA network. The oscillatory frequency for the mixtures and the pure BTA is 1 rad/s, while for the BTA-PEG-BTA is 10 rad/s. b) The yield stress (blue) and the yield strain (black) as a function of the weight fraction of BTA-PEG-BTA. The two pure components exhibit yield strain values which are typically encountered in (highly deformable) polymeric materials whereas the mixtures in the range of BTA fractions from 0.2 to 0.9

exhibit much lower yield strains, closer to those observed in colloidal gels and pastes[7,8]. The yield stress exhibits a smoother dependence on fraction, with continuing decrease, except for the 0.5 fraction which is associated with the maximum value of G_p (Figure 2). The range of yield strains is huge, from about 2kPa for BTA-PEG-BTA to about 20 Pa for BTA. These observations corroborate the notion of complex interplay of interactions dictating their properties.

V. Estimation of mesh size from the linear viscoelastic data

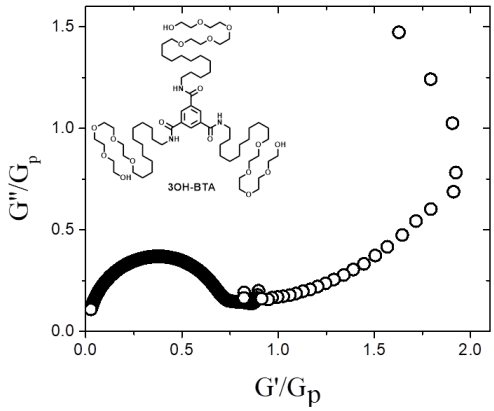

Figure S18: Cole-Cole plot of the pure BTA hydrogel network (5wt%).

From the theory of stress relaxation in living wormlike polymers proposed by Cates[9] it is known that the minimum of the so-called Cole-Cole plot of G'' versus G' is proportional to the inverse number of entanglements. We use the Cole-Cole plot to calculate the average entanglement length needed for the calculation of the mesh size in the theory of networks of semiflexible chains of MacKintosh[10], who proposed that the plateau modulus of such a network depends on the bending modulus κ of the chain (proportional to the persistence

length of the chain which has been reported to be in the order of 100 nm[11]) , the mesh size ξ, the entanglement length L_e and the thermal energy, as shown in equations (2) and (3):

$$\frac{L_e}{L} = \left(\frac{G''}{G_p}\right)_{\boldsymbol{minimum}} \rightarrow \frac{L_e}{L} = 0.136 \rightarrow L_e = 612\ nm \qquad (1)$$

In equation (2), L is the total length of a fiber which we expect from atomic force microscopy to be in the order of 5 μm[12].

$$\mathbf{G_p = \frac{\kappa^2}{kT}\xi^{-2}L_e^{-3}\ , \xi = 6.8\ nm} \qquad (2)$$

By applying a dilution law we get [10]: $\xi \sim c^{-1/2} \rightarrow \xi\ (582\ \mu M) = 52.6\ nm$.

VI. Cryo-TEM: Additional images and experimental methodology

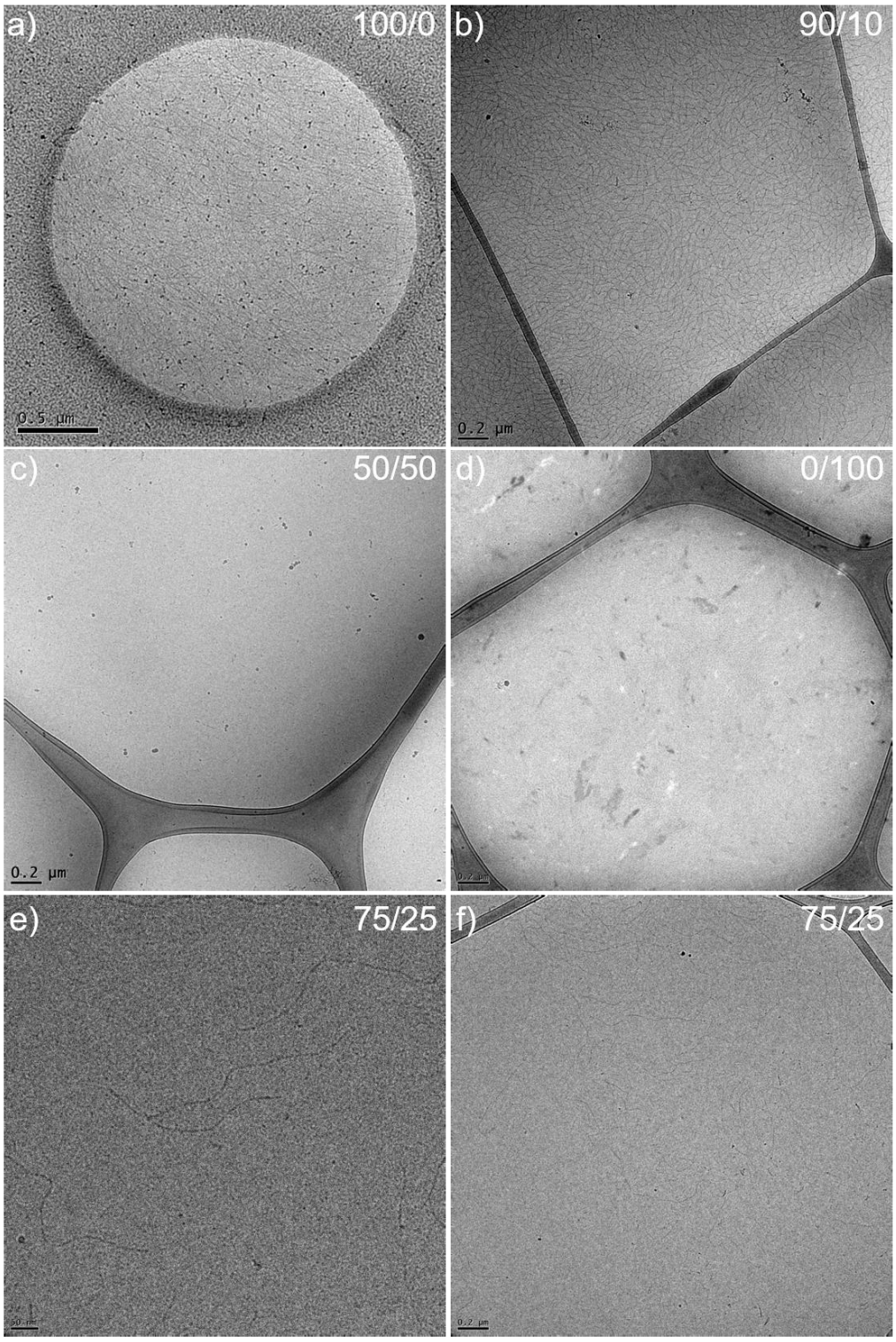

Figure S19: Cryo-TEM images of the mixtures, showing the lower magnification images corresponding to Figure 3 of the main text in a) – d). The BTA / BTA-PEG-BTA 75/25 mixture at 250 µM in e) shows the presence of fibers that are shorter as compared to the 90/10 mixture, but longer as compared to the 50/50 mixture. Image f) is the corresponding lower magnification image.

Cryogenic transmission electron microscopy

Samples were prepared at a concentration of 582 µM (BTA), 250 µM (90/10 molar ratio), 500 µM (50/50) and 2210 µM (BTA-PEG-BTA). The pure samples were prepared by adding MQ-water to the solids in a glass vial equipped with a magnetic stir bar. The vials were heated at 80°C for 15 minutes while vigorously stirring, with short intervals of vortexing. Mixtures were prepared by the addition of BTA polymers in water (that were prepared one day in advance according to the aforementioned protocol), to the solid BTA-PEG-BTA. Vials containing the mixtures were also heated at 80°C for 15 minutes while vigorously stirring, with short intervals of vortexing. All samples were left to equilibrate at room temperature overnight. The next day, vitrified films were prepared using a computer controlled vitrification robot (FEI Vitrobot^{TM} Mark III, FEI Company) at 22°C, and at a relative humidity of 100%. In the preparation chamber of the 'Vitrobot', 3 µl sample was applied on a Lacey film (LC200-CU, Electron Microscopy Sciences). In the case of the pure BTA sample, the 3 µl sample was applied on a Quantifoil grid (R 2/2, Quantifoil Micro Tools GmbH). Both types of grids were surface plasma treated just prior to use, with a Cressington 208 carbon coater operating at 5 mA for 40 s. Excess sample was removed by blotting using filter paper for 3 s at –3 mm, and the thin film thus formed was plunged (acceleration about 3 g) into liquid ethane just above its freezing point. Blotting was observed to be inefficient for the pure BTA-PEG-BTA because of the high viscosity of the sample that was due to the high concentration. Therefore only ~10-20% of the grid was suitable for imaging. Vitrified films were transferred into the vacuum of a CryoTITAN equipped with a field emission gun that was operated at 300 kV, a post-column Gatan energy filter, and a 2048 x 2048 Gatan CCD camera. In the case of the pure BTA sample, vitrified films were transferred into the vacuum of a Tecnai Sphera microscope with a Gatan 626 cryoholder. This microscope is equipped with an LaB_6 filament that was operated at 200 kV, and a bottom mounted 1024x1024 Gatan charged-coupled device (CCD) camera. Micrographs were taken at low dose conditions,

starting at a magnification of 6500 with a defocus setting of 40 µm. Subsequently images were acquired at a magnification of 24000 (TITAN) / 25000 (Sphera) and at a defocus of 10 and 15 µm. The contrast in the images of Figure 3 (b,c,d) in the manuscript was enhanced using Fiji software[13]. To this end, the images were first filtered using a median with a radius of three pixels. Subsequently, the contrast was enhanced using the settings 'saturated pixels 0.4%' and 'normalize'. The scale bars of Figure 3 were set to match with one another using the same software. As a reference, a straight line of known distance was drawn in raw microscopy files (originating from Digital micrograph software). Using 'set scale' in the 'analyze' menu of Fiji the length of the line in pixels was defined as the known distance, and the box 'global' was ticked to apply the calibration to all images opened in the Fiji session. Scale bars were subsequently added to the (contrast enhanced) images by opening 'scale bar' in the 'analyze/tools' menu of Fiji.

VII. Hydrogen/deuterium exchange mass spectrometry (HDX-MS)

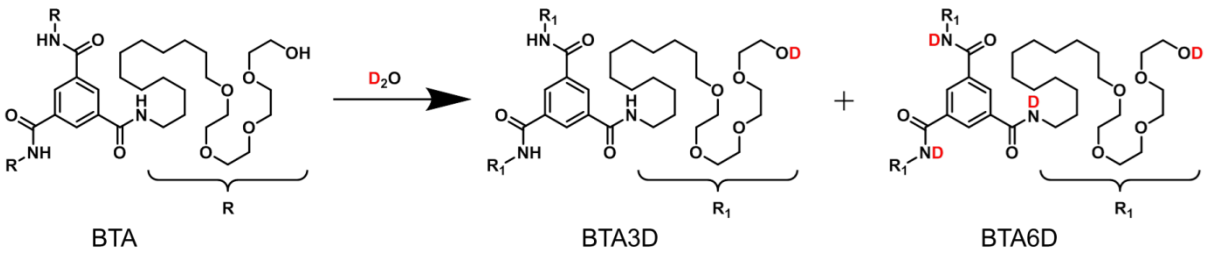

Figure S20: Hydrogen/deuterium exchange (HDX) of the BTA after dilution into D_2O.

The BTA molecule contains six exchangeable hydrogen atoms that can be substituted by deuterium, resulting in two BTA species that have an increased molecular weight. Upon dilution into excess D_2O the OH groups at the periphery of the molecule will immediately exchange to OD, resulting in BTA3D. When the hydrophobic core of a BTA3D molecule

comes into contact with D_2O, e.g. through their dissociation from a supramolecular polymer, the NH groups in the core become deuterated. Hence after the initial dilution step BTA3D molecules will convert into BTA6D depending on the association strength between the molecules. The amount of BTA3D and BTA6D is quantified using electrospray ionization mass spectrometry (ESI-MS). In the presence of 25 or 50 mol% of BTA-PEG-BTA, the percentage of BTA3D was observed to decrease more rapidly as compared to a sample with pure BTA (see Table S1). These results indicate that BTA-PEG-BTA weakens the association strength between the BTA molecules. BTA-PEG-BTA molecules will also increase in their molecular weight upon dilution into D_2O due to the presence of ten exchangeable hydrogen atoms. However, due to the polydispersity of the supramolecular polymer this relatively small shift of 10 g/mol cannot be detected in the mass spectra.

The samples were prepared at a concentration of 500 µM in H_2O and diluted 100 times into D_2O and then subjected to ESI-MS. For the 50/50 mixture, all BTAs were fully deuterated (BTA6D) already at the first measurement that was performed three minutes after the dilution step. For the instrument settings and the calculation of BTA3D% we refer the reader to recent work[14].

Table S1: BTA3D% as a function of time for three different mixtures.

HDX time	BTA / BTA-PEG-BTA 100/0 a)	BTA / BTA-PEG-BTA 0/100 b)	BTA / BTA-PEG-BTA 50/50 c)
3 min	71.8	20.1	0
6 min	62.8	17.2	-
10 min	57.6	16.5	-
20 min	52.3	16.0	-
30 min	51.0	14.9	-
1 hour	49.3	13.6	-
5 hours	43.9	12.2	-
24 hours	36.1	10.9	-

a) The values in this column have been previously reported (ref [14]) and are an average of three measurements with standard deviations below 3%.

b) These measurements were not repeated because some of the BTA-PEG-BTA was observed to become trapped in the apparatus.

VIII. Details of the MD simulations

Each component is made of self-assembling units (particles) that interact via a short-range attraction which dictates the bond strength through the attractive well of depth, ε and a three body term which limits the bond angles and introduces a bending stiffness[15–18].

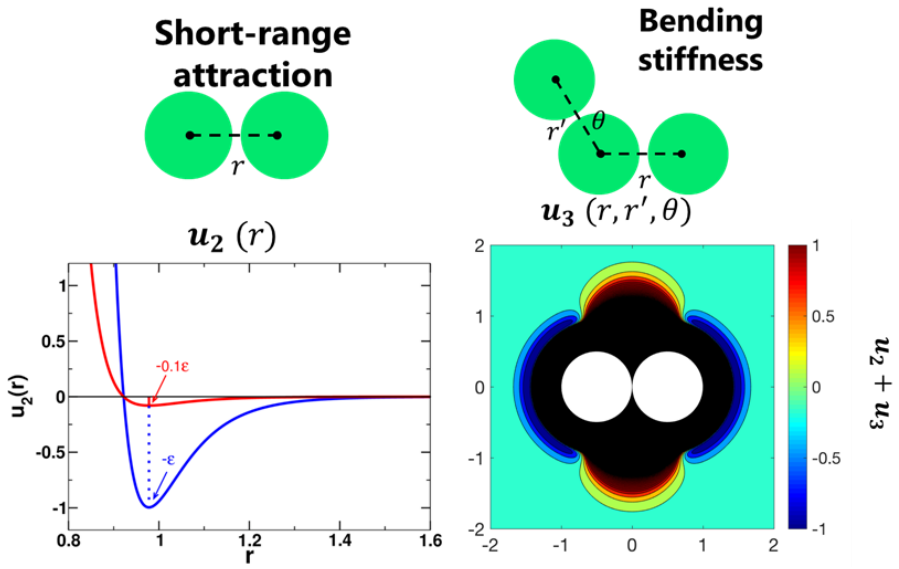

Figure S21: On the left hand-side the Lennard-Jones type potential u_2 that dictates the association strength is shown, while on the right hand-side ($u_2 + u_3$), dictating the bond angle as well as the bond distance, is shown. The plot shows that potential energy contour $(u_2 + u_3)(r)$ that an incoming particle sees when it approaches, at a distance r, two other particles (white spheres) that are already bonded. The incoming particle can form a new bond (and remain bonded) only in the region in blue, where the potential is attractive.

The model is studied through coarse-grained Molecular Dynamics (MD) simulations and for N particles with position vectors $\{\boldsymbol{r}_i\},\ i = 1 \ldots N$, the total potential energy is[17]:

$$U(\boldsymbol{r}_1, \ldots, \boldsymbol{r}_N) = \varepsilon \left[\sum_{i>j} u_2 \left(\frac{\boldsymbol{r}_{ij}}{d} \right) + \sum_{i} \sum_{j>k}^{j,k \neq i} u_3 \left(\frac{\boldsymbol{r}_{ij}}{d}, \frac{\boldsymbol{r}_{ik}}{d} \right) \right] \quad (4)$$

where $\boldsymbol{r}_{ij} = \boldsymbol{r}_j - \boldsymbol{r}_i$, ε sets the energy scale and d the unit length scale, representing the particle diameter. The two-body term u_2 is a Lennard-Jones like potential which consists of a repulsive core and a narrow attractive well that can be expressed in the following dimensionless (and computationally convenient) form

$$u_2(r) = A(ar^{-18} - r^{-16}) \tag{5}$$

where r is the distance rescaled by the particle diameter d, while a and A are dimensionless parameters that control, respectively, the width and the depth of the potential well. The three body term u_3 limits the coordination number and confers angular rigidity to the inter-particle bonds. For two particles both bonded to a third one and whose relative positions with respect to it are represented by the vectors $\boldsymbol{r}$ and $\boldsymbol{r}'$ departing from the same particle (also rescaled by the particle diameter):

$$u_3(r, r') = B\Lambda(r)\Lambda(r') \exp\left[-\left(\frac{\boldsymbol{r}\cdot\boldsymbol{r}'}{rr'} - \cos\bar{\theta}\right)^2 / w^2\right] \tag{6}$$

Where $B, w, \bar{\theta}$ are dimensionless parameters. The range of three-body interaction is set to two particle diameters, as ensured by the radial modulation:

$$\Lambda(r) = r^{-10}\left[1 - \left(\frac{r}{2}\right)^{10}\right]^2 H(2 - r) \tag{7}$$

Where r is the distance rescaled by the particle diameter d. $H(r)$ is the Heaviside function, ensuring that u_3 vanishes beyond the diameter of two particles.

The potential energy (4) depends parametrically on the dimensionless quantities $A, a, B, w, \bar{\theta}$. For all data discussed here we have fixed $a = 0.85, B = 67.27, w = 0.3, \bar{\theta} = 65^\circ$ as already done in[16,18,19]. We then consider two different values of A to describe the two components in the experimental systems. The choice $A = 6.27$ allows us to obtain, by decreasing the ratio

k_BT/ε in the simulations, a percolated network of semiflexible fibers, where the association energy of the particles in the fibers is $+\varepsilon$ and each fiber is composed by particles with coordination number 2. While the term u_2 in the potential energy drives the self-assembly, the term u_3 and its strength relative to u_2 limit the self-assembly of the initially free particle units to fibers and allow for the presence of branching points (or crosslinks, i.e., particles with coordination number 3) among them to form a percolated network. The coordination number is defined by counting the number of neighbors, for a given particle, within a distance close to the minimum of the attractive well ($1.3d$). The linear rheology of this network well matches the experimental rheology of the BTA fibrillar network, as discussed in the following, in the range of frequencies where the entanglements can be considered comparable to the branching points, as also shown in Figure 5a. Hence, we use the choice $A = 6.27$ to model the first component (BTA). We model the second component by keeping the other parameters constant and changing instead $A = 0.5$, which changes the depth of the potential well to 0.1ε as shown in Figure S20 (left). With this choice of A, upon decreasing the ratio k_BT/ε in the simulations, the particles spontaneously self-assemble into small aggregates between which bonds can break and reform easily, whose structure is shown in Figure 5d. We therefore use $A = 0.5$ to model the BTA-PEG-BTA component of the experimental system. We then consider various compositions by mixing the two species into various network structures for different mixing ratios (see snapshots in Figures 5b and c).

In all calculations discussed here, we start from network configurations of N particles initially prepared at $\frac{k_BT}{\varepsilon} = 5 \cdot 10^{-3}$ and quench them to $\frac{k_BT}{\varepsilon} \simeq 0$ by using the dissipative dynamics:

$$m\frac{d^2\boldsymbol{r}_i}{dt^2} = -\eta_f\frac{d\boldsymbol{r}_i}{dt} - \nabla_{r_i}U \qquad (8)$$

where m is the unit mass and η_f the coefficient of friction of each particle in the given solvent, until the kinetic energy drops to a negligible fraction (less than 10^{-10}) of its initial value. This procedure has been optimized to produce stable self-assembled structures and has been extensively tested in various works[18,19].

In all simulations discussed here, we have used $\frac{m}{\eta_f} = 1.0\tau_0$ where, $\tau_0 = \sqrt{md^2/\varepsilon}$ is the unit MD time and the time step used for integrating the equation of motion is $5 \cdot 10^{-3}\tau_0$. The configurations quenched to $\frac{k_B T}{\varepsilon} \simeq 0$ are mechanically stable and represent the gel structures at a local minimum of potential energy, or *inherent structure*. The mechanical tests are performed on these configurations. All the data refer to gel networks consisting of $N = 32000 - 64000$ particles in a cubic simulation box of size $L = 54\,d$. All simulations have been performed using a version of LAMMPS[20] suitably modified by us to include the interaction potential given by equation 4. For each data point, we have run simulations over 5 independently generated samples and used sample-to-sample fluctuations to obtain error bars. In all plots, error bars are smaller than the symbol size used.

VIII.A Mixed systems and conversion of fraction of each component into approximate weight fractions in the experiment

In the simulations we study various mixtures of the particles that represent the BTA fibrillar network (component-I) and the BTA-PEG-BTA (component-II) components as in the experiments. Each of the two components in the numerical model, however, is made of particles (coarse-grained units) of same size (diameter) d and the mixture composition can be at first just characterized in terms of the fraction of each particle type used, $f = \frac{N_2}{N_1+N_2}$, where N_1 indicates the number of particles used for the BTA component and N_2 the number of

particles used for the BTA-PEG-BTA component. This corresponds to volume fractions ϕ_1 and ϕ_2, where for each species $\phi_i = \frac{N_i \pi d^3}{6(Ld)^3}$, having considered our particles as spheres, d as our unit length and Ld the simulation box size.

To convert the compositions used in the simulations to the mixture compositions used in the experiments, we consider that the self-assembling units of the pure component-II are heavier and have a bigger linear size (≈4 times bigger). To understand to which value of $w_{BTA-PEG-BTA}$ our f may correspond to, and compare it to the experimental weight fractions (Figures 2, S14, S15), we first consider that the same ϕ_2 can be thought of as made of N_2' particles that have the right size ratio with respect to pure component-I ($d_2 \approx 4d$). Then we use N_2' to compute the corresponding weight fraction. That is,

$$\phi_2 = \frac{N_2 \pi d^3}{6(Ld)^3} = \frac{N_2' \pi {d_2}^3}{6(Ld)^3} \tag{9}$$

which for $d_2 \approx 4d$ gives us $N_2' = N_2/64$.

Considering that pure component-II has also a bigger mass (m_2) compared to the pure component-I (m_1), we obtain the conversion of f in terms of weight fraction of component-II:

$$w_{II} = \frac{N_2' m_2}{N_2' m_2 + N_1 m_1} = \frac{\frac{m_2}{m_1}\frac{f}{64(1-f)}}{1 + \frac{m_2}{m_1}\frac{f}{64(1-f)}} \tag{10}$$

If we use this relationship, varying f in the range 0.1 - 0.9 and using $m_2 \approx 20 m_1$ (as in the experiment) corresponds to w_{II} varying in the range 0.03 - 0.76 in the experiment. We use this conversion scheme when comparing the simulations data to experiments throughout the paper, in Figures 6b, 7a and 7b.

VIII.B Mechanical Tests (linear viscoelasticity)

For each of the samples with various mixing ratios, prepared by following the procedure just described above, we use a computational scheme, inspired by a recently developed experimental technique[21], to obtain the full linear viscoelastic spectrum by applying an optimally windowed chirp (OWCh) signal[19]. We employ this method over the traditional discrete frequency sweeps because it is computationally faster and has relatively higher signal-to-noise ratio, making the measurement more accurate at low frequencies. The computational details of the method can be found in the Ref. 14. The optimally windowed chirp signal $\gamma(t)$[19] is used to impose an oscillatory strain in the xy plane through the equation:

$$m\frac{d^2\boldsymbol{r}_i}{dt^2} = -\nabla_{\boldsymbol{r}_i}U - \eta_f\left(\frac{d\boldsymbol{r}_i}{dt} - \dot{\gamma}\,(t)y_i\boldsymbol{e}_x\right) + \boldsymbol{F}_r^i(t) \qquad (11)$$

which is solved for each self-assembled unit and where we use Lees-Edwards boundary conditions, $\boldsymbol{e}_x$ is a unit vector along the x axis. $\boldsymbol{F}_r^i(t)$ is a random force that introduces the thermal fluctuations and is related to the coefficient of friction, η_f, and to the temperature T by the equation: $\langle \boldsymbol{F}_r^i(t)\boldsymbol{F}_r^j(t')\rangle = 2\eta_f k_B T\delta_{ij}\delta(t-t')$. Here we choose $\eta_f = 10\,\varepsilon\tau_0/d^2$ to make sure we are well in the overdamped limit of the dynamics and set the thermal fluctuations to be much smaller than the physical interactions in the fibers of component-I, $\frac{k_BT}{\varepsilon} = 10^{-4}$. We monitor the evolution of shear stresses generated over time, $\sigma_{xy}(t)$, by computing the interaction part of the global stress tensor through the standard virial equation[22]:

$$\sigma_{\alpha\beta} = \frac{1}{V}\sum_{i=1}^{N}\frac{\partial U}{\partial r_i^{\alpha}}r_i^{\beta} \qquad (12)$$

Where V represents the volume of the system and α, β stand for the cartesian components $\{x, y, z\}$. Since the velocities of the particles are small ($v_i \lesssim 10^{-5} d/\tau_0$), we ignore the kinetic term $m v_i^{\alpha} v_i^{\beta}$ in the calculation of the stress tensor, as well as any contribution due to the viscous forces appearing in the equation (11). The complex viscoelastic modulus (G^*) is then extracted from the Fourier transform of stress ($\tilde{\sigma}$) and strain ($\tilde{\gamma}$) signals as $G^*(\omega_i) = \tilde{\sigma}(\omega_i)/\tilde{\gamma}(\omega_i)$, whose real and imaginary parts represent the storage modulus (G') and loss modulus (G''), respectively.

References

(1) Leenders, C. M. A.; Albertazzi, L.; Mes, T.; Koenigs, M. M. E.; Palmans, A. R. A.; Meijer, E. W. Supramolecular Polymerization in Water Harnessing Both Hydrophobic Effects and Hydrogen Bond Formation. *Chem. Commun.* **2013**, *49* (19), 1963. https://doi.org/10.1039/c3cc38949a.

(2) Ferry, J. D. *Viscoelastic Properties of Polymers*; Wiley: New York: NY, 1980.

(3) Rubinstein, M.; Colby, R. H. *Polymer Physics*; OUP Oxford, 2003.

(4) Schärtl, W. *Light Scattering from Polymer Solutions and Nanoparticle Dispersions*; Springer Laboratory; Springer Berlin Heidelberg: Berlin, Heidelberg, 2007. https://doi.org/10.1007/978-3-540-71951-9.

(5) Cross, M. M. Rheology of Non-Newtonian Fluids: A New Flow Equation for Pseudoplastic Systems. *J. Colloid Sci.* **1965**, *20* (5), 417–437. https://doi.org/10.1016/0095-8522(65)90022-X.

(6) Irving, J. B. *Viscosities of Binary Liquid Mixtures: A Survey of Mixture Equations; Report No. 630*; National Engineering Laboratory: East Kilbridge, Glasgow, U.K., 1977.

(7) Vlassopoulos, D.; Cloitre, M. Tunable Rheology of Dense Soft Deformable Colloids. *Curr. Opin. Colloid Interface Sci.* **2014**, *19* (6), 561–574. https://doi.org/10.1016/j.cocis.2014.09.007.

(8) Moghimi, E.; Jacob, A. R.; Koumakis, N.; Petekidis, G. Colloidal Gels Tuned by Oscillatory Shear. *Soft Matter* **2017**, *13* (12), 2371–2383. https://doi.org/10.1039/C6SM02508K.

(9) Granek, R.; Cates, M. E. Stress Relaxation in Living Polymers: Results from a Poisson Renewal Model. *J. Chem. Phys.* **1992**, *96* (6), 4758–4767. https://doi.org/10.1063/1.462787.

(10) MacKintosh, F. C.; Käs, J.; Janmey, P. A. Elasticity of Semiflexible Biopolymer Networks. *Phys. Rev. Lett.* **1995**, *75* (24), 4425–4428. https://doi.org/10.1103/PhysRevLett.75.4425.

(11) Baker, M. B.; Albertazzi, L.; Voets, I. K.; Leenders, C. M. A.; Palmans, A. R. A.; Pavan, G. M.; Meijer, E. W. Consequences of Chirality on the Dynamics of a Water-

Soluble Supramolecular Polymer. *Nat. Commun.* **2015**, *6* (1). https://doi.org/10.1038/ncomms7234.
(12) Beuwer, M. A.; Knopper, M. F.; Albertazzi, L.; van der Zwaag, D.; Ellenbroek, W. G.; Meijer, E. W.; Prins, M. W. J.; Zijlstra, P. Mechanical Properties of Single Supramolecular Polymers from Correlative AFM and Fluorescence Microscopy. *Polym. Chem.* **2016**, *7* (47), 7260–7268. https://doi.org/10.1039/C6PY01656A.
(13) Schindelin, J.; Arganda-Carreras, I.; Frise, E.; Kaynig, V.; Longair, M.; Pietzsch, T.; Preibisch, S.; Rueden, C.; Saalfeld, S.; Schmid, B.; Tinevez, J.-Y.; White, D. J.; Hartenstein, V.; Eliceiri, K.; Tomancak, P.; Cardona, A. Fiji: An Open-Source Platform for Biological-Image Analysis. *Nat. Methods* **2012**, *9* (7), 676–682. https://doi.org/10.1038/nmeth.2019.
(14) Lou, X.; Lafleur, R. P. M.; Leenders, C. M. A.; Schoenmakers, S. M. C.; Matsumoto, N. M.; Baker, M. B.; van Dongen, J. L. J.; Palmans, A. R. A.; Meijer, E. W. Dynamic Diversity of Synthetic Supramolecular Polymers in Water as Revealed by Hydrogen/Deuterium Exchange. *Nat. Commun.* **2017**, *8* (1), 15420. https://doi.org/10.1038/ncomms15420.
(15) Del Gado, E.; Kob, W. A Microscopic Model for Colloidal Gels with Directional Effective Interactions: Network Induced Glassy Dynamics. *Soft Matter* **2010**, *6* (7), 1547–1558. https://doi.org/10.1039/B916813C.
(16) Colombo, J.; Del Gado, E. Self-Assembly and Cooperative Dynamics of a Model Colloidal Gel Network. *Soft Matter* **2014**, *10* (22), 4003. https://doi.org/10.1039/c4sm00219a.
(17) Bouzid, M.; Gado, E. D. Mechanics of Soft Gels: Linear and Nonlinear Response. In *Handbook of Materials Modeling: Applications: Current and Emerging Materials*; Andreoni, W., Yip, S., Eds.; Springer International Publishing: Cham, 2018; pp 1–29. https://doi.org/10.1007/978-3-319-50257-1_129-1.
(18) Colombo, J.; Del Gado, E. Stress Localization, Stiffening, and Yielding in a Model Colloidal Gel. *J. Rheol.* **2014**, *58* (5), 1089–1116. https://doi.org/10.1122/1.4882021.
(19) Bouzid, M.; Keshavarz, B.; Geri, M.; Divoux, T.; Del Gado, E.; McKinley, G. H. Computing the Linear Viscoelastic Properties of Soft Gels Using an Optimally Windowed Chirp Protocol. *J. Rheol.* **2018**, *62* (4), 1037–1050. https://doi.org/10.1122/1.5018715.
(20) Plimpton, S. Fast Parallel Algorithms for Short-Range Molecular Dynamics. *J. Comput. Phys.* **1995**, *117* (1), 1–19. https://doi.org/10.1006/jcph.1995.1039.
(21) Geri, M.; Keshavarz, B.; Divoux, T.; Clasen, C.; Curtis, D. J.; McKinley, G. H. Time-Resolved Mechanical Spectroscopy of Soft Materials via Optimally Windowed Chirps. *Phys Rev X* **2018**, *8* (4), 041042. https://doi.org/10.1103/PhysRevX.8.041042.
(22) Thompson, A. P.; Plimpton, S. J.; Mattson, W. General Formulation of Pressure and Stress Tensor for Arbitrary Many-Body Interaction Potentials under Periodic Boundary Conditions. *J. Chem. Phys.* **2009**, *131* (15), 154107. https://doi.org/10.1063/1.3245303.